

Orbital

The Electronic Journal of Chemistry

JULY-SEPTEMBER
2012
VOLUME 4
NUMBER 3

Estudo das degradações de pesticidas usados na região de Dourados-MS



Published by the
Department of Chemistry of the Federal
University of Mato Grosso do Sul,
Campo Grande, BRAZIL.

Orbital - Vol. 4 No. 3 - July-September 2012

Table of Contents

EDITORIAL

<u>Chemistry or Hua-Shue?</u>	
<i>Grégoire Jean-François Demets</i>	

FULL PAPERS

<u>Degradation study of pesticides used in Dourados-MS</u>	
<i>Virgilio Vieira de Olival, Rozanna Marques Muzzi, Jéssica Alves Nogueira, Fábio Gozzi, Anderson Teodoro, Dirce Martins de Oliveira, Dayana Doffinger Ramos, Ana Paula Pereira da Rosa, Marly Eiko Osugi, Paula Loureiro Paulo, Silvio Cesar de Oliveira, Valdir Souza Ferreira, Lincoln Carlos Silva de Oliveira, Amilcar Machulek Junior</i>	146-158
<u>Synthesis, characterization and applications of some novel mordent and heterocyclic disperse dyes on polyester and wool fibers</u>	
<i>Hitendra Mangubhai Patel</i>	159-170
<u>The synthesis, characterization and theoretical study of nano tetrabutylammonium trichloroiodoaluminate (III)</u>	
<i>shahriar Ghammamy</i>	171-177
<u>Theoretical study of structural and electronic properties of poly(vinyl chloride) nanotube inclusions</u>	
<i>Assad Kareen Edaan</i>	178-186
<u>Equilibrium adsorption of rhodamine B on used black tea leaves from acidic aqueous solution</u>	
<i>Mohammad Abul Hossain, M. Atiqur Rahman</i>	187-201
<u>Alum promoted synthesis of 2H-indazolo[2,1-b]phthalazinetrione derivatives in water</u>	
<i>Balaji Rajendra Madje, Jagdish V. Bharad, Milind B. Ubale, Murlidhar S. Shingare</i>	202-208

REVIEWS

<u>Chalcones: compounds possessing a diversity in applications</u>	
<i>Urmila Berar</i>	209-221

TECHNICAL NOTES

<u>A tutorial for molecular dynamics simulations using Amber package</u>	
<i>Marcos Vinícius Rifon Garcia, Wivirkins N. Marciela, Roberto da Silva Gomes, Marcos Serrou do Amaral</i>	222-234



This work is licensed under a [Creative Commons Attribution 3.0 License](https://creativecommons.org/licenses/by/3.0/).

Editorial

Chemistry or Hua-Shue?

Presently, 10 to 18% of the world's population speaks traditional Chinese or Mandarin [1]. One of the consequences of Chinese economic growth during the last decades is a growing number of papers from that region in high impact chemistry journals. This obvious process drives us to a reflexion on the fate of the English language as *lingua franca* and as the scientific language in a near future. As it happened with other languages such as classical Greek, Latin, and French, English language may be bound to gradual substitution in a short period of time.

During the early 90s, the presence of Chinese speaking authors in those journals was almost inexpressive, rarely exceeding 1% of the published papers [2]. Nowadays this number is close to 10% or more if one only considers the papers produced in the PRC, and everything indicates that this fraction will grow.

In spite of being spoken by many people, the Mandarin language should find several obstacles to its eventual implementation as an international language. The first of them is referred to its complexity. It is extremely rich phonetically, and employs a very subtle and complicated tonal system. It uses a rich grammar, and very complicated ideograms, which can be counted in thousands.

English, on the other hand, is phonetically simple and quite flexible. It is spoken by about 5% of the world's population as mother tongue and it is the official language of 54 nations [1]. It is the third in the number of speakers after Mandarin and Spanish. Such a number of anglophones may be explained by the extension of the British Empire during the nineteenth century, which was known as the Empire where the sun never sets down. Beyond its relative simplicity, since it does not use accents for example, English is also spoken by machines once everything involving communication between men and machines, especially programming languages, is based on English. It allows the utilization of short words to express what it is wanted in this context. It has to be mentioned that several protocols as for example the aviation communication system are also based on this language and, it is unlikely that they will be totally replaced at a time: this would be technically impracticable...

Unless otherwise Mandarin becomes extremely simplified, I mean, much more than the actual "simplified Chinese", and the calligraphy system be totally replaced, it is quite unlikely that Chinese will dethrone English as the *lingua franca*. At least for the next 50 years.

Chemistry ou Hua-Shue?

Atualmente de 10 a 18% da população mundial fala o chinês tradicional ou Mandarim [1]. O crescimento econômico da China nas últimas décadas teve por consequência direta um crescimento expressivo do número de artigos oriundos daquela região em revistas de química de alto impacto. Este processo evidente nos leva fatalmente à reflexão sobre o destino do Inglês como língua franca e idioma científico num futuro próximo. A exemplo do que aconteceu com outros idiomas como o grego clássico, o latim, e o francês, o inglês pode estar fadado à gradativa substituição em um curto intervalo de tempo.

No início dos anos 90, a presença de autores de língua chinesa nestas revistas era praticamente inexpressiva, passando raramente de 1% do número de artigos publicados, hoje em dia este número beira os 10% se contarmos somente artigos produzidos na RPC [2], fração esta que ao que tudo indica só tende a crescer.

Apesar de muito falado, o idioma Mandarim há de encontrar muitos obstáculos à sua eventual implantação como idioma internacional. O primeiro deles é sua dificuldade. Extremamente rico foneticamente, envolvendo um sistema tonal bastante sutil e complicado, possui uma rica gramática, isto sem contar a complexidade de seus ideogramas que podem ser contados aos milhares.

O inglês, por sua vez, é foneticamente simples e bastante flexível. É falado por aproximadamente 5% da população mundial como primeiro ou segundo idioma e é oficial em 54 nações [1]. E é o terceiro em número de falantes ficando atrás do Mandarim e do Espanhol. Essa cifra de anglófonos pode ser explicada pela extensão do Império Britânico do século XIX, que era conhecido como o Império onde o sol nunca se põe. Além de relativamente simples, já que não conta com acentos, por exemplo, o inglês é hoje falado também pelas máquinas, uma vez que tudo envolvendo comunicação entre homem e máquina, especialmente linguagens de programação, é baseado no inglês já que este idioma permite a utilização de verbetes curtos para expressar o que se deseja neste contexto. Temos que contar também que diversos protocolos a exemplo do sistema de comunicação em aviação também são baseados naquele idioma, sendo pouco provável que se queira substituir tudo de uma só vez: seria inviável tecnicamente...

A menos que o Mandarim seja simplificado ao extremo, digo muito mais do que o atual "chinês simplificado" e o sistema de ideogramas totalmente substituído, será muito improvável que consiga destronar o inglês. Pelo menos nos próximos 50 anos.

Grégoire Jean-Fançois Demets (FFCLRP-USP)

Associate Editor, Orbital

References and Notes

- [1] Source: Wikipedia
- [2] Based on Journal the American Chemical Society and Angewandte Chemie Int. Ed. - first volumes of 1990

Estudo das degradações de pesticidas usados na região de Dourados-MS

Virgílio Vieira de Olival^a, Rozanna Marques Muzzi^a, Jéssica Alves Nogueira^b, Fábio Gozzi^{b*}, Anderson Teodoro^b, Dirce Martins de Oliveira^b, Dayana Doffinger Ramos^b, Ana Paula Pereira da Rosa^b, Marly Eiko Osugi^b, Paula Loureiro Paulo^b, Silvio Cesar de Oliveira^b, Valdir Souza Ferreira^b, Lincoln Carlos Silva de Oliveira^b, Amilcar Machulek Junior^b

^aPrograma de Pós-Graduação em Ciência e Tecnologia Ambiental – FACET, Universidade Federal da Grande Dourados. CEP 79825-070, Dourados, MS, Brazil.

^bCentro de Ciências Exatas e Tecnologia, Universidade Federal de Mato Grosso do Sul. Av. Senador Filinto Muller, 1555, CEP 79074-460, Campo Grande, MS, Brazil.

Received: 12 June 2012; revised: 30 July 2012; accepted: 01 August 2012. Available online: 02 September 2012.

ABSTRACT: *The intensive use and irregular disposal of pesticides in agriculture has caused serious environmental and health problems. In this work was evaluated the efficiency of UV and some advanced oxidation processes involving photo-Fenton reaction, O₃ and O₃/UV for the treatment of aqueous solutions containing commercial and standard pesticides. The results showed that the combination of UV radiation in alkaline means with O₃ significantly increased the efficiency of the process of degradation and the photo-Fenton system is a promising alternative for the treatment of effluents containing pesticides.*

Keywords: *degradation; pesticides; ozonation; photo-Fenton*

Introdução

Os pesticidas são substâncias utilizadas no controle de diversas pragas na agricultura, entretanto, o uso frequente, e muitas vezes incorreto, oferece riscos para o meio ambiente, principalmente por apresentarem elevada toxicidade e, geralmente, serem persistentes, podendo permanecer por vários meses ou anos no ambiente [1]. No Estado de Mato Grosso do Sul, os municípios de Dourados e São Gabriel D'Oeste são as regiões onde se consomem mais pesticidas. A consequência direta dessa atividade são os inúmeros casos de intoxicações por pesticidas, ocasionando sérios problemas ambientais

* Corresponding author. E-mail: fabiogozzi@gmail.com

e de saúde [2].

A maior parte dos pesticidas utilizados atinge as fontes de águas naturais, principalmente pela deriva na aplicação, resíduos de embalagens vazias, lavagens de equipamentos e efluentes de indústrias de pesticidas [3]. Estimativas indicam que apenas 0,1% dos pesticidas efetivamente aplicados alcançam as pragas, logo, 99,9% deles estão disponíveis para afetar o ambiente ao seu redor [4]. Os efluentes de pesticidas gerados na agricultura atingem a concentração em torno de $10 \mu\text{gL}^{-1}$ de carbono orgânico total (COT), enquanto o das indústrias que fabricam os pesticidas chega a 1000mgL^{-1} de COT. Até os frascos vazios de pesticidas, quando retornam às empresas para serem reciclados, geram um efluente da água de lavagem de 10 a 100mgL^{-1} de COT, que necessitam de tratamento adequado [5].

Em geral, o desempenho dos processos convencionais para o tratamento de efluentes desta natureza, destacando-se aqueles que envolvem a oxidação por via biológica, que são os métodos de mais baixo custo, depende muito do grau de toxicidade do efluente, pois a oxidação é promovida por microrganismos. Logo, o estudo de novas técnicas para o tratamento de efluentes de elevada toxicidade são imprescindíveis.

Nos últimos anos, observou-se uma evolução crescente no número de trabalhos científicos publicados envolvendo os processos oxidativos avançados (POAs) como técnicas promissoras e eficazes na destruição de poluentes refratários [6-10]. Nas reações envolvendo os POAs, são formados os radicais hidroxila, que apresentam alto potencial padrão de redução, cerca de 2,8 V, menor apenas do que o do flúor, que é de 3,03 V, sendo capazes de reagir com praticamente todas as classes de compostos orgânicos, degradando-os e resultando em sua completa mineralização, obtendo como produtos CO_2 e H_2O e íons inorgânicos provenientes de heteroátomos ou ainda, levando a formação de produtos orgânicos menos complexos e mais biodegradáveis [11].

Um dos POAs mais investigados atualmente é o processo foto-Fenton que tem atraído grande interesse devido à sua alta eficiência em gerar radicais hidroxilas durante a decomposição de H_2O_2 catalisada por Fe^{2+} em meio ácido e irradiação UV-visível [12, 13].

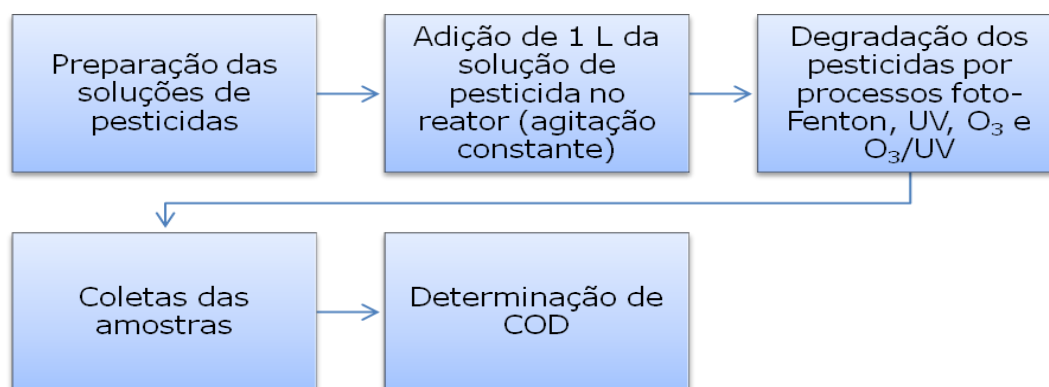
Outro processo que tem atraído interesse de pesquisadores são os sistemas utilizando ozônio [14], devido ao seu alto potencial de oxidação que sob condições apropriadas também leva à formação de radicais hidroxilas. O ozônio combinado com irradiação UV se torna interessante à medida que coexistem três processos de degradação: a fotólise direta, a ozonização direta e a oxidação por radicais hidroxilas, que geram reações rápidas e não seletivas, sendo amplamente estudada por vários autores [15, 16].

Como alternativa para o tratamento de resíduos de pesticida, o Ministério da Agricultura, Pecuária e Abastecimento (MAPA) através da Instrução Normativa Nº 2 de 3 de Janeiro de 2008 regulamentou as práticas para tratamento de efluentes gerados por empresas de aviação agrícola. Ele recomenda o uso de ozonizador com capacidade mínima para produzir um grama de ozônio por hora funcionando por um período mínimo de seis horas, para cada carga de quatrocentos e cinquenta litros de restos e sobras de agrotóxicos remanescentes da lavagem e limpeza das aeronaves e equipamentos [17]. Algumas técnicas usando fotólise direta [18], Fenton e foto-Fenton [19-21], O₃ [18, 22-23], e O₃/UV [14, 18, 22-23] têm sido estudadas para o tratamento de águas contendo pesticidas.

O presente trabalho teve como propósito aplicar os processos foto-Fenton, UV, O₃ e O₃/UV para a degradação dos pesticidas comerciais Positron Duo[®], Censor[®], Consentó[®], Ridomil Gold MZ[®], DMA[®] 806 BR e o ácido 2,4-diclorofenoxiacético (2,4-D) padrão, utilizados na aviação agrícola na região de Dourados/MS.

Materiais e Métodos

Os experimentos foram realizados seguindo o fluxograma abaixo.



Fluxograma 1. Metodologia.

Reagente e preparo das soluções

As soluções dos pesticidas Positron Duo[®] (Iprovalicarbe e Propinebe), Censor[®] (Fenamidona), Consentó[®] (Cloridrato de Propamocarbe e Fluopicolide), Ridomil Gold MZ[®] (Metalaxil-M e Mancozebe), DMA[®] 806 BR (2,4-D e Sal Dimetilamina), tabelas 1 e 2, e o pesticida 2,4-D padrão foram preparadas de acordo com as concentrações utilizadas para aplicação em campo recomendada pelo MAPA. Devido os pesticidas apresentarem baixa solubilidade em água, exceto o 2,4-D, os mesmos, após a saturação, foram filtrados com o auxílio de uma bomba a vácuo passando por uma membrana de 0,2 µm, após a filtração obteve-se uma solução homogênea com a carga orgânica dissolvida. Em seguida foram retiradas amostras para análise do teor de carbono orgânico total (COT) expressa

em teor de carbono orgânico dissolvido (COD). A concentração das soluções para a realização dos experimentos foi estabelecida em torno de 100 mgL^{-1} de COD.

A solução padrão de 2,4-D foi preparada para a concentração de 100 mgL^{-1} de COD utilizando padrão 2,4-D (Fluka Analytical 97%). Os demais reagentes utilizados foram de grau analítico.

Tabela 1 – Informações dos pesticidas comerciais

Nome Comercial	Classe	Princípio Ativo	Fórmula Química	Grupo Químico	Perigo Ambiental (Classe)
Positron Duo®	Fungicida	Iprovalicarbe	$\text{C}_{18}\text{H}_{28}\text{N}_2\text{O}_3$	Carbamato	Classe II
		Propinebe	$(\text{C}_5\text{H}_8\text{N}_2\text{S}_4\text{Zn})_x$	Ditiocarbamato	
Censor®	Fungicida	Fenamidona	$\text{C}_{17}\text{H}_{17}\text{N}_3\text{OS}$	Imidazolinona	Classe II
Consento®	Fungicida	Cloridrato de Propamocarbe	$\text{C}_9\text{H}_{21}\text{ClN}_2\text{O}_2$	Carbamato	Classe II
Ridomil Gold® MZ	Fungicida	Metalaxil-M	$\text{C}_{15}\text{H}_{21}\text{NO}_4$	Fenilamidas	Classe II
		Mancozebe	$(\text{C}_4\text{H}_6\text{N}_2\text{S}_4\text{Mn})_x \cdot (\text{Zn})_y$	ditiocarbamatos	
DMA® 806 BR	Herbicida	2,4-D	$\text{C}_8\text{H}_6\text{Cl}_2\text{O}_3$	ácido ariloxialcanóico	Classe III

Determinação de carbono orgânico dissolvido (COD)

A mineralização dos pesticidas foi acompanhada por análise de COT utilizando um analisador multi N/C 2100, Analytikjena com valores expressos em COD. A concentração de COD foi expressa como uma concentração relativa (COD/COD_0).

Degradação utilizando o sistema foto-Fenton

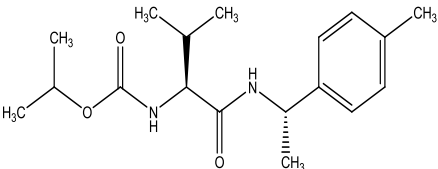
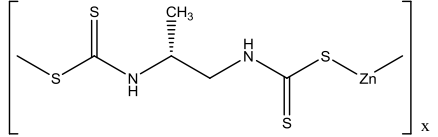
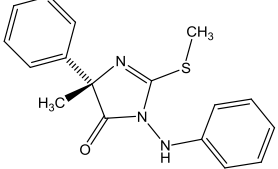
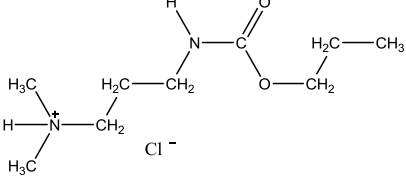
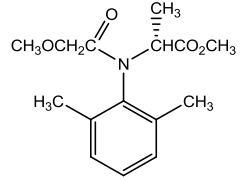
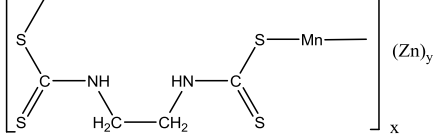
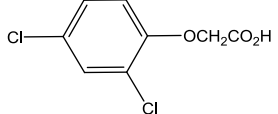
Utilizou-se um reator fotoquímico de geometria anular de 1,0 L (volume irradiado). A fonte de radiação empregada foi uma lâmpada de vapor de mercúrio de 125 W (sem o bulbo de proteção) de alta pressão com máximo de emissão em 254 nm (fluxo de fótons de 2×10^{19} fótons s^{-1}) [12] posicionada no eixo longitudinal do reator no interior de um cilindro constituído de quartzo. Para o controle da temperatura foi utilizado um banho termostático (MARCONI, MA-184) e o efluente dentro do reator permaneceu em constante agitação com o auxílio de um agitador magnético, Figura 1.

As condições experimentais adotadas foram: $[\text{Fe}^{2+}] = 0,5 \text{ mM}$, $[\text{H}_2\text{O}_2] = 50 \text{ mM}$ e $\text{pH} = 3,0$, sabendo que a faixa de pH de melhor eficiência é entre 2,5 e 3,0 [11, 24]. A fonte de ferro utilizada foi de $\text{FeSO}_4 \cdot 7\text{H}_2\text{O}$ (Vetec, 99%), a solução de H_2O_2 foi preparada a partir de uma concentrada (Vetec, 35% v/v), diluindo $5,0 \cdot 10^{-4}$ mols de H_2O_2 em 60 mL de H_2O ultra pura e adicionada lentamente por meio de uma bomba peristáltica com vazão de 1 mL min^{-1} junto com o acionamento do cronômetro e a contagem do tempo de reação (120 min). Foram realizadas coletas nos tempos de 0, 5, 10, 15, 20, 30, 45, 60, 75, 90 e 120 minutos para acompanhar a reação. Logo após a coleta, foram adicionadas 3 gotas de solução de KOH com concentração de 10 molL^{-1} a fim de precipitar o Fe e

cessar a reação de Fenton.

Cabe ressaltar, que apesar da concentração de ferro utilizada nos experimentos estar acima do padrão de lançamento de efluentes ($15,0 \text{ mgL}^{-1} \text{ Fe}$) estipulado pela Resolução CONAMA Nº 357, [17], o mesmo pode ser facilmente recuperado por precipitação, conforme um teste de recuperação do ferro realizado por Teixeira & Canela [25].

Tabela 2 – Informações dos pesticidas comerciais

Nome Comercial	Nome Químico	Fórmula Química	Estrutura Química
Positron Duo®	isopropil 2-metil-1-[(1-p-toliletil) carbamoil]-(S)-propilcarbamato	$\text{C}_{18}\text{H}_{28}\text{N}_2\text{O}_3$	
	polímero propileno bis ditiocarbamato de zinco	$(\text{C}_5\text{H}_8\text{N}_2\text{S}_4\text{Zn})_x$	
Censor®	(S)-1-anilino-4-metil-2-metiltio-4-penilimidazolin-5-ona	$\text{C}_{17}\text{H}_{17}\text{N}_3\text{OS}$	
Consento®	hidrocloreto de propil 3-(dimetilamino)propil-carbamato	$\text{C}_9\text{H}_{21}\text{ClN}_2\text{O}_2$	
Ridomil Gold® MZ	Metil N-metóxiacetil-N-2,6-xilil-D-alaninato	$\text{C}_{15}\text{H}_{21}\text{NO}_4$	
	etileno-bis-ditiocarbamato de manganês e íon zinco	$(\text{C}_4\text{H}_6\text{N}_2\text{S}_4\text{Mn})_x \cdot (\text{Zn})_y$	
DMA® 806 BR	Ácido 2,4-diclorofenóxiacético	$\text{C}_8\text{H}_6\text{Cl}_2\text{O}_3$	

Degradação utilizando os sistemas UV, O_3 e O_3/UV

Utilizou-se um reator fotoquímico de geometria cilíndrica de 1,0 L, encamisado,

por onde recircula água para controle da temperatura com a utilização do banho termostático. No interior do reator foi fixado o eletrodo do medidor de pH para monitoramento *in situ* do pH e um tubo de quartzo onde a lâmpada (vapor de mercúrio de 125 W - fluxo de fótons de 2×10^{19} fótons s^{-1}) [12] foi introduzida, Figura 2.

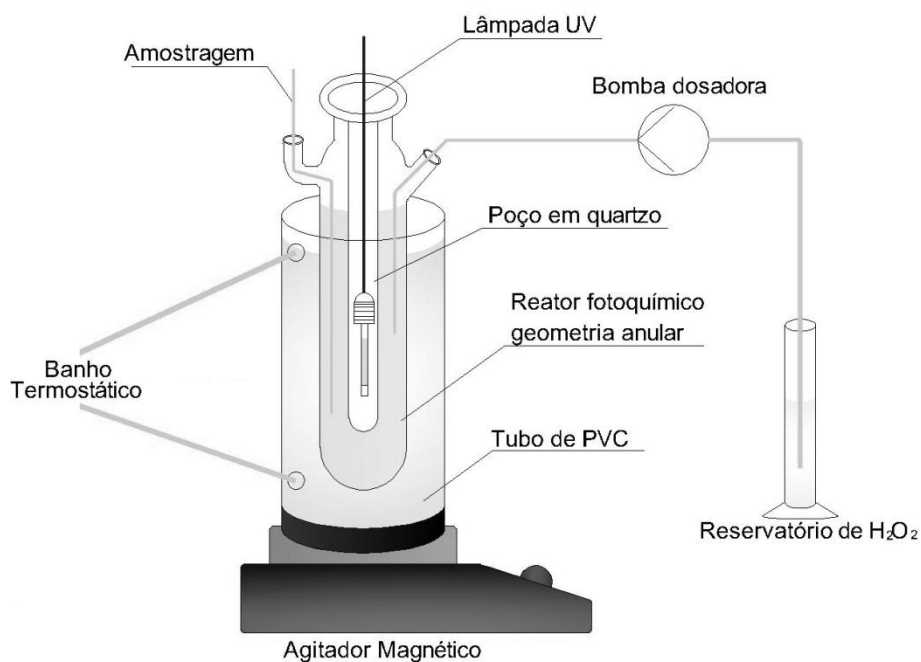


Figura 1. Esquema do reator fotoquímico de geometria anular.

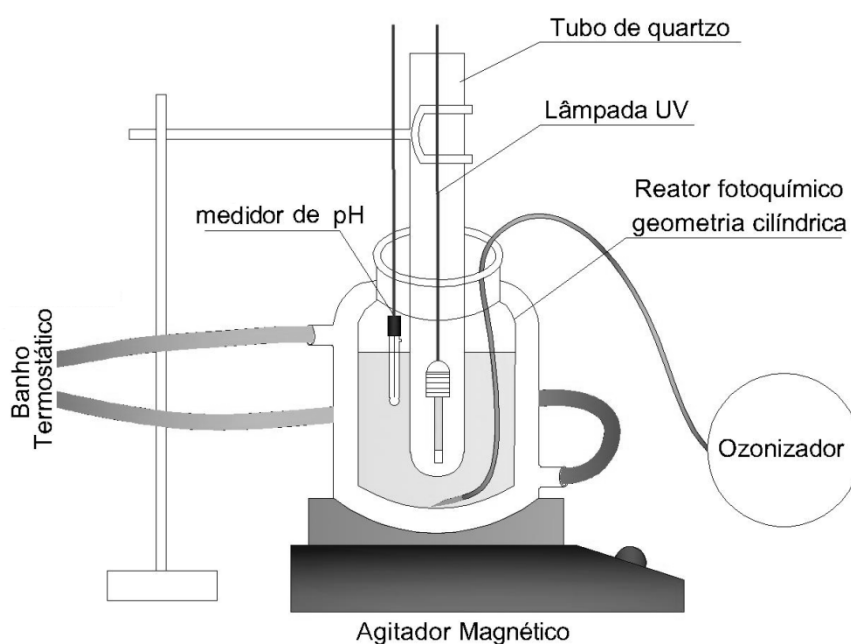


Figura 2. Esquema do reator fotoquímico de geometria cilíndrica.

Para a produção de ozônio foi utilizado o gerador MG5 da Philozon conectado a um cilindro de O_2 (99,99%) com fluxo de 1 Lmin^{-1} da mistura oxigênio e ozônio, fornecendo concentrações de O_3 de $5 \mu\text{g mL}^{-1}$ à $60 \mu\text{g mL}^{-1}$. Nos experimentos, o ozônio foi borbulhado na base interna do reator, dispersando-se por todo o efluente, na concentração de $30 \mu\text{g mL}^{-1}$ que equivale a produção de $1,8 \text{ gh}^{-1}$. Ao iniciar a aplicação do O_3 foi acionado o cronômetro para controle do tempo de reação (120 min). Foram realizadas coletas nos tempos de 0, 5, 10, 15, 20, 30, 45, 60, 90 e 120 minutos para análise de COT.

Inicialmente foram realizados alguns testes com o pesticida 2,4-D padrão utilizando o sistema O_3 e O_3/UV com pH inicial da solução em 10,0, 7,0 e 3,0, mantido ao longo da reação, para verificação da influência do pH na geração de radicais hidroxilas e assim na degradação do pesticida.

Resultados e Discussão

Sistema foto-Fenton

Os experimentos utilizando o processo foto-Fenton com as mesmas concentrações de íons ferrosos e de peróxido de hidrogênio foram mantidos em uma faixa de pH de $3,0 \pm 0,2$ e temperatura entre $30 \pm 2^\circ\text{C}$. A mineralização dos pesticidas é observada na Figura 3, onde os pesticidas Censor[®], Ridomil Gold[®] MZ, Consentto[®] e Positron Duo[®] foram totalmente mineralizados em 30, 45, 60 e 90 minutos de reação, respectivamente, e os pesticidas DMA 806 BR (2,4-D comercial) e 2,4-D padrão tiveram a mineralização de 95% e 98,3%, respectivamente, após 120 minutos de reação.

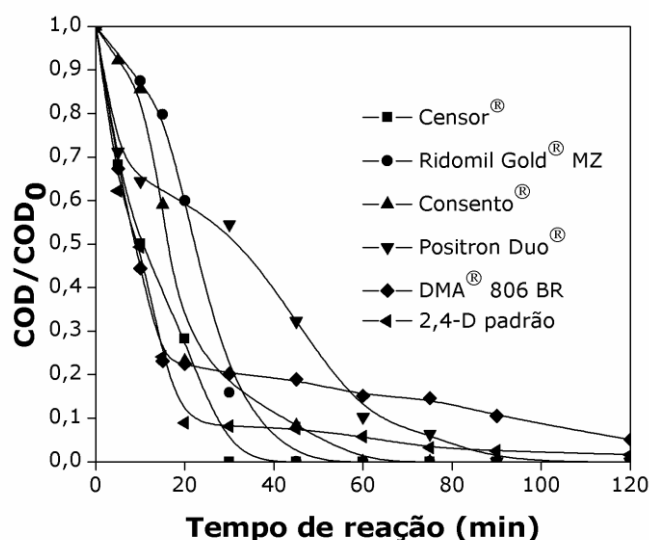


Figura 3. Mineralização dos pesticidas comerciais (A) e comparação entre o pesticida 2,4-D comercial e padrão (B) por processo foto-Fenton. pH = 3, $[\text{Fe}^{2+}] = 0,5 \text{ mM}$, $[\text{H}_2\text{O}_2] = 50 \text{ mM}$ e $\text{COD}_0 = 100 \text{ mg L}^{-1}$

Como as condições de reações foram iguais a todos os pesticidas (concentrações de H_2O_2 e Fe^{2+}), esta diferença no tempo e no percentual de mineralização dos pesticidas demonstra que compostos diferentes necessitam de diferentes concentrações de reagentes para alcançar uma eficiência satisfatória [26]. A mineralização do pesticida 2,4-D padrão e comercial tiveram comportamento distinto, Figura 3, provavelmente ocasionado pela presença de substâncias presentes na formulação comercial. A mineralização após 20 minutos de reação foi maior para o 2,4-D padrão em relação ao comercial, 91% e 77,5% respectivamente.

Sistemas UV, O_3 e O_3/UV

A mineralização do pesticida 2,4-D padrão pelo sistema O_3 e O_3/UV com pH inicial da solução em 10,0, 7,0 e 3,0 foi avaliada como parâmetro para os demais pesticidas, Figura 4. Observa-se que em meio alcalino, mantendo o pH constante, obtêm-se uma melhor porcentagem de mineralização utilizando O_3 (Figura 2A) 33,4%, e O_3/UV (Figura 2B) 52%, respectivamente.

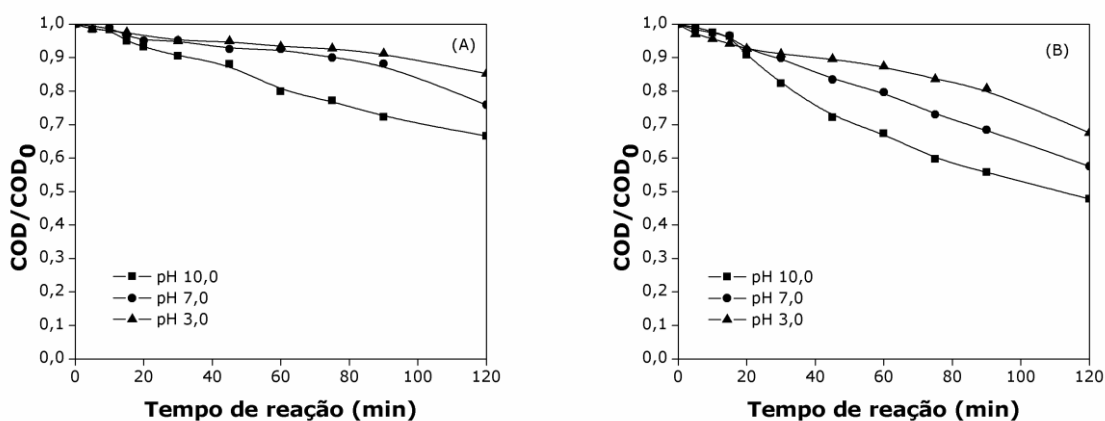
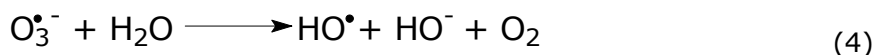
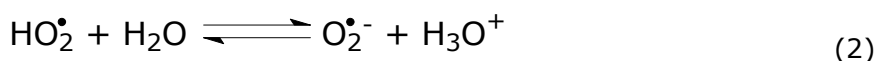
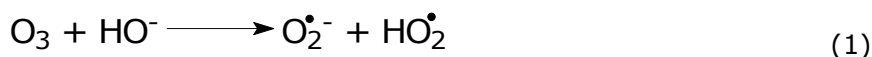


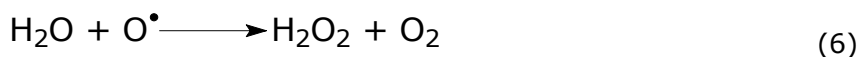
Figura 4. Estudo da influência do pH na degradação do pesticida 2,4-D padrão no sistema O_3 (A) e O_3/UV (B). $\text{COD}_0 = 100 \text{ mgL}^{-1}$.

Em um sistema utilizando ozônio, a oxidação da matriz orgânica pode ocorrer de maneira direta ou indireta [27, 28]. Em meio ácido, pH 4, o ozônio não se decompõe em radicais mais reativos, diminuindo a eficiência na remoção de COT [3] como mostra o resultado para pH 3, com percentual de mineralização em 14,8% para 2,4-D padrão, Figura 4A.

Observa-se um aumento na eficiência do método quando o ozônio se encontra em meio alcalino, pois, ocorre a formação de radicais hidroxilas, espécies altamente reativas e não seletivas, pela decomposição do ozônio através do íon hidroxila, Equações 1-4 [29, 30].



Combinando o ozônio com radiação UV há a influência da fótólise direta, reações radicalares e ozonização direta da matriz orgânica, Equações 5-7 [15], aumentando ainda mais a mineralização.



Após a verificação dos sistemas em diferentes pH, mantendo-os constantes, utilizando o 2,4-D padrão como modelo, Figura 5, os sistemas utilizando O_3 , combinado ou não com UV, com pH inicial em 10 foram aplicados no tratamento de água contendo os demais pesticidas comerciais. A fotodegradação utilizando apenas a radiação UV, mostrou uma baixa mineralização, percentual inferior a 12%, Figura 5A. Os experimentos utilizando somente O_3 , também apresentaram uma baixa mineralização, 21,8%, para o pesticida comercial Ridomil Gold[®] com sistema sem controle de pH, Figura 5B. A combinação de O_3 e UV, Figura 5C, mostrou os melhores resultados, provavelmente devido a uma maior eficiência na formação de radicais hidroxilas do que o processo O_3 (Equações 5-7).

Entre os pesticidas comerciais, o Censor[®], apresentou a maior taxa de mineralização, remoção de carbono orgânico total de 50,0%. Os sistemas utilizando UV, O_3 e O_3/UV sem controle de pH apresentaram uma queda considerável de pH, variando de 10,0 a 3,0, exceto para o sistema UV onde o pH teve pequena variação, 10,0 a 9,3. Esta queda no pH indica que compostos ácidos foram formados durante o processo de oxidação, provavelmente ácidos orgânicos como produtos finais da degradação dos pesticidas em estudo [12,23,31].

Comparação entre os sistemas

Dentre os POAs estudados, a eficiência obtida pelo sistema foto-Fenton revelou valores superiores aos demais, com constante de velocidade de mineralização de $0,115 \text{ min}^{-1}$ e mineralização de 98% para o pesticida 2,4-D padrão, vide Figura 6 e Tabela 3.

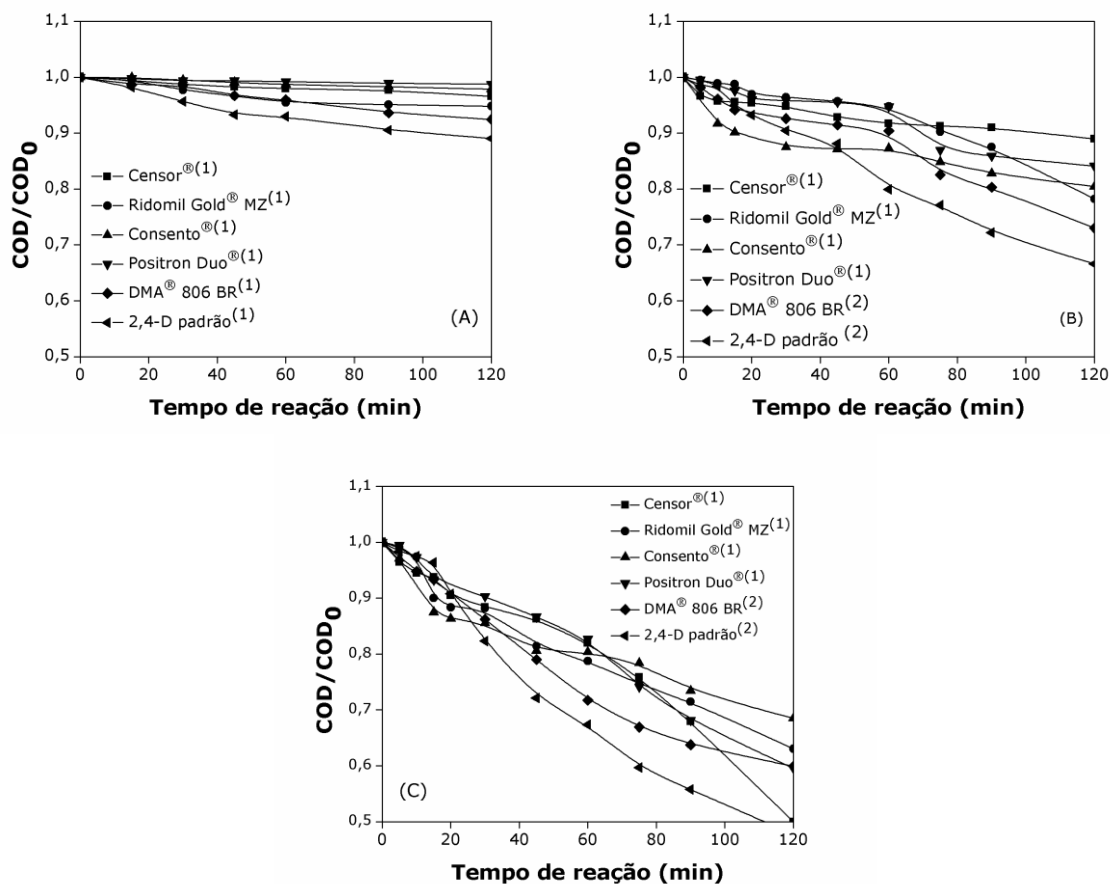


Figura 5. Mineralização dos pesticidas utilizando o sistema UV (A), O_3 (B) e O_3/UV . (C).
⁽¹⁾Experimentos realizados sem controle de pH. ⁽²⁾Experimentos realizados mantendo pH constante. pH inicial $10 \pm 0,3$ e $COD_0 = 100 \text{ mg L}^{-1}$.

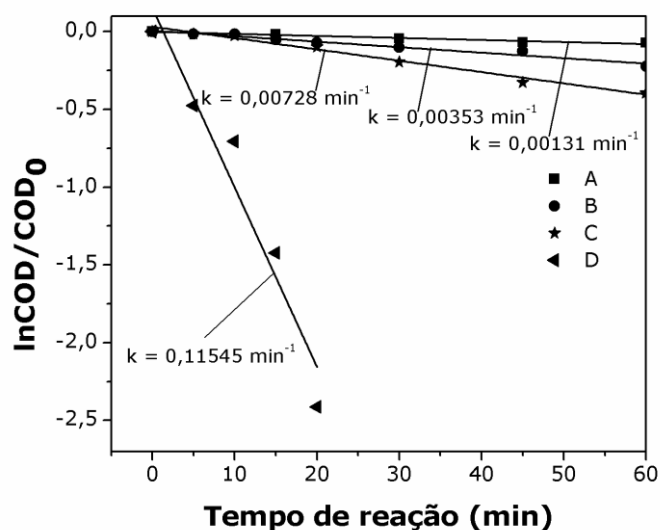


Figura 6. Constante de velocidade de mineralização de uma reação de pseudo primeira ordem para os sistemas UV (A), O_3 (B), O_3/UV (C) e foto-Fenton (D). pH = 3 (foto-Fenton), pH = 10 (demais sistemas) $COD_0 = 100 \text{ mg L}^{-1}$.

Tabela 3. Comparação entre os sistemas estudados. pH = 3,0±0,3 para foto-Fenton, pH inicial em 10 para os demais sistemas. COT₀ = 100 mg L⁻¹

Pesticidas	Mineralização (%)			
	foto-Fenton	UV	O ₃	O ₃ /UV
Censor [®]	100 (30 min)	3,4	11,0	50,0
Ridomil Gold [®] MZ	100 (45 min)	5,2	21,8	37,0
Consento [®]	100 (60 min)	2,1	19,6	31,5
Positron Duo [®]	100 (90 min)	1,2	15,9	40,4
DMA [®] 806 BR	95	7,5	27,0*	40,0*
2,4-D padrão	98	10,9	33,4*	52,3*

* Experimentos realizados com pH em 10±0,3 constante durante a reação

Os sistemas UV e O₃ apresentaram baixa eficiência, porém, quando associados, obtiveram um aumento considerável na mineralização dos pesticidas em todos os testes realizados conforme os resultados demonstrados na Tabela 3. De acordo com Wu e colaboradores [32], a combinação da radiação UV com outros sistemas, favorece a geração de radicais hidroxilas, resultando em reações mais rápidas e não seletivas, aumentando assim a eficiência do processo de degradação. Como Dourados está entre os municípios que mais consomem pesticidas no Estado de Mato Grosso do Sul, observa-se diversos casos de intoxicação além de problemas ambientais e de saúde. Desta forma, a necessidade de desenvolver e aprimorar técnicas de manejo e métodos de tratamento de resíduos contendo pesticidas se faz necessário.

Conclusão

Foram estudados sistemas baseados na ozonização e no processo foto-Fenton. Os resultados obtidos na mineralização dos pesticidas mostraram que todos os métodos são capazes de mineralizar os pesticidas, embora com diferentes eficiências. A mineralização dos pesticidas foi afetada por fatores como pH e a composição comercial. O sistema foto-Fenton apresentou os melhores resultados quando comparado aos demais sistemas estudados, alcançando taxas de mineralização superiores a 95%. Isto credencia esta técnica para o tratamento de águas residuais contendo pesticidas. Entretanto, a IN n° 2 de 2008 (MAPA) recomenda a utilização da ozonólise (sem radiação UV) para o tratamento de efluentes contendo pesticidas de aeronaves de pulverização agrícola. No entanto, os resultados demonstraram que é importante considerar o pH do meio, pois, uma vez que com a ozonólise não se obtém a mineralização total dos pesticidas, pode ocorrer a formação de subprodutos de oxidação mais tóxicos.

Agradecimentos

Os autores agradecem à FUNDECT-MS, PROPP-UFMS, CAPES, CNPq, INCT-EMA pelo auxílio financeiro e bolsas concedidas.

Referências

- [1] Rodrigues, B. N.; Almeida F. S. *Guia de Herbicidas*, 5ª ed., Londrina: Grafmarke, 2005.
- [2] Pires, D. X.; Caldas, E. D.; Recena, M. C. P. *Cad. Saúde Pública*. **2005**, *21*, 598. [[CrossRef](#)]
- [3] Malato, S.; Cáceres, J.; Aguera, A.; Mezcua, M.; Hernando, D.; Vial, J.; Fernández-Alba, A. R. *Environ. Sci. Technol.* **2001**, *35*, 4359. [[CrossRef](#)]
- [4] Sabik, H.; Jeanot, R.; Roundeau, B.; *J. Chromatogr. A*. **2000**, *885*, 217. [[CrossRef](#)]
- [5] Malato, S.; Blanco, J.; Richter, C.; Maldonado, M. I. *App. Catal. B*. **2000**, *25*, 31. [[CrossRef](#)]
- [6] Machulek, A. J.; Quina, F. H.; Gozzi, F.; Silva, V. O.; Friedrich, L. C.; Moraes, J. E. F. In: *Organic Pollutants Ten Years After the Stockholm Convention – Environmental and Analytical Update*; Puzyn, T. and Mostrag-Szlichtyng, A. (Org). *Croatia: In: Tech*, 2012, chap. 11.
- [7] Rizzo, L. *Water Res.* **2011**, *45*, 4311. [[CrossRef](#)]
- [8] González, O.; Esplugas, M.; Sans, C.; Torres, A.; Esplugas, S. *Water Res.* **2009**, *43*, 2149. [[CrossRef](#)]
- [9] Oller, I.; Malato, S.; Sánchez-Pérez, J. A. *Sci. Total Environ.* **2011**, *409*, 4141. [[CrossRef](#)]
- [10] Navarro, S.; Fenoll, J.; Vela, N.; Ruiz, E.; Navarro, G. *Chem. Eng. J.* **2011**, *167*, 42. [[CrossRef](#)]
- [11] Pignatello, J. J. *Environ. Sci. Technol.* **1992**, *26*, 944. [[CrossRef](#)]
- [12] Machulek, A. J.; Moraes, J. E. F.; Giongo, C. V.; Silverio, C. A.; Friedrich, L. C.; Nascimento, C. A. O.; Gonzalez, M. C.; Quina, F. H. *Environ. Sci. Technol.* **2007**, *41*, 8459. [[CrossRef](#)]
- [13] Trovó, A. G.; Villa, R. D.; Nogueira, R. F. P. *Quim. Nova*. **2005**, *28*, 847. [[CrossRef](#)]
- [14] Machulek, A.; Gogritchain, E.; Moraes, J. E.; Quina, F. H.; Oliveros, E., Braun, A. M. *Sep. Purif. Technol.* **2009**, *67*, 141. [[CrossRef](#)]
- [15] Beltrán, F. J.; García-Araya, J. F.; Acedo, B. *Wat. Res.* **1994**, *28*, 2165. [[CrossRef](#)]
- [16] Benitez, F. J.; Beltrán-Heredia, J.; Gonzales, T. *Ozone: Sci. Eng.* **1994**, *16*, 213. [[CrossRef](#)]
- [17] Disponível em: <http://www.agricultura.gov.br>. Acesso em Julho de 2012.
- [18] Rao, Y. F.; Chu, W. *Chemosphere*. **2009**, *74*, 1444. [[CrossRef](#)]
- [19] Oturan, M. A.; Oturan, N.; Edelah, M. C.; Podvorica, F. I.; Kacemi, K. E. *Chem. Eng. J.* **2011**, *171*, 127. [[CrossRef](#)]
- [20] Bensalah, N.; Khodary, A.; Wahab, A. A. *J. Hazard. Mater.* **2011**, *189*, 479. [[CrossRef](#)]
- [21] Jiménez, M.; Oller, I.; Maldonado, M. I.; Malato, S.; Ramírez, A. H.; Zapata, A.; Peralta-Hernández, J. M. *Catal. Today*. **2011**, *161*, 214. [[CrossRef](#)]
- [22] Chelme-Ayala, P.; El-Din, M. G.; Smith, D. W.; Adams, C. D. *Wat. Res.* **2011**, *45*, 2517. [[CrossRef](#)]

- [23] Lucas, M.S.; Peresa, J. A.; Puma, G. Li. *Sep. Purif. Technol.* **2010**, 72, 235. [[CrossRef](#)]
- [24] Nogueira, R. F.; Trovó, A. G.; Silva, M. R. A.; Villa, R. D. *Quim. Nova.* **2007**, 30, 400. [[CrossRef](#)]
- [25] Teixeira, S. C. G.; Canela, M. C. *Quim. Nova.* **2007**, 30, 1830. [[CrossRef](#)]
- [26] Paterlini, W. C.; Nogueira, R. F. P. *Chemosphere.* **2005**, 58, 1107. [[CrossRef](#)]
- [27] Zhao, L.; Ma, J.; Sun, Z.; Liu, Z.; Yang, Y. *Front. Environ. Sci. Engin.* **2008**, 2, 44. [[CrossRef](#)]
- [28] Kuns, A.; Peralta-Zamora, P. *Quim. Nova.* **2002**, 25, 78. [[CrossRef](#)]
- [29] Uslu, M.Ö.; Balcioglu, I. A. *Sci. Total Environ.* **2009**, 407, 3450. [[CrossRef](#)]
- [30] Huang, C. P.; Dong, C.; Tang, Z. *Waste Management.* **1993**, 13, 361. [[CrossRef](#)]
- [31] Coelho, A. D.; Sans, C.; Agüera, A.; Gómez, M. J.; Esplugas, S.; Dezotti, M. *Sci. Total Environ.* **2009**, 407, 3572. [[CrossRef](#)]
- [32] Wu, J. J.; Wu, C-C.; Ma, H-W.; Chang, C-C. *Chemosphere.* **2004**, 54, 997. [[CrossRef](#)]

Full Paper

Synthesis, characterization and applications of some novel mordent and heterocyclic disperse dyes on polyester and wool fibers

Hitendra M. Patel*

Department of Chemistry, V. P. and R. P. T. P Science College, Vallabh Vidyanagar-388 120. Gujarat, India.

Received: 28 October 2011; revised: 27 December 2011; accepted: 30 July 2012.
Available online: 05 September 2012.

ABSTRACT: The novel mordent and disperse heterocyclic dyes were prepared by coupling of various diazo solution of aromatic amines with 1-[(2-butyl-2,3-dihydrobenzofuran-3-yl)]-1-(4-hydroxyphenyl)methanone. The resultant mordent and disperse heterocyclic dyes were characterized by elemental analyses, IR and $^1\text{H-NMR}$ and $^{13}\text{C-NMR}$ spectral studies. The UV-visible spectral data have also been discussed in terms of structural property relationship. The dyeing assessment of all the mordent and disperse heterocyclic dyes was evaluated on wool and polyester textile fibers. The results of antibacterial studies of chrome pretreated fabrics revealed that the toxicity of mordented dyes against *Escherichia coli*, *Staphylococcus aureus*, *Salmonella typhi*, *Bacillus subtilis* bacteria was fairly good.

Keywords: heterocyclic dyes; UV absorber; fastness property; microbial activity

Introduction

In the field of dyes, the heterocyclic compounds play the important role for the most of commercial dyes [1-6]. Most of the heterocyclic dyes [7] are marketed in the form of azo disperse, azo-vat, azo-acid dyes etc. All these have part of phenols and naphthols having hydroxyl group as auxochrome group. One of the hydroxy compound i.e. 1-[(2-butyl-2,3-dihydrobenzofuran-3-yl)]-1-(4-hydroxyphenyl)methanone having hydroxy (as auxochrome) groups and a keto (chromophore) group. This compound has wide applications as an excellent UV absorber [8, 9] which prevents the photo degradability of most of vinyl polymers [10]. The area in which the azo dye formation based on this compound has not been developed except of few patents [11, 12]. The

* Corresponding author. E-mail: shreeniketan71@yahoo.in

formation of dyes based on this heterocyclic compounds may yield with good hue properties.

Hence, in continuation of earlier work [13-15], the present communication comprises the studies on novel mordent and disperse heterocyclic dyes based on 1-[(2-butyl-2,3-dihydrobenzofuran-3-yl)]-1-(4-hydroxyphenyl)methanone

Material and Methods

All the chemicals used were of commercial grade and were further purified by crystallization. Melting points were determined by open capillary method and are uncorrected. The visible absorption spectra were measured on a Carl Zeiss UV/VIS Specord spectrometer, elemental analysis were carried out on Perkin elmer CHNS/O Analyzer 2400 Series II, Infrared spectra were recorded in KBr pellets on a Perkin-elmer Spectrum GX FT-IR model, NMR were recorded on Hitachi R-1500, ^{13}C - NMR spectra were recorded on Bruker Avance DPX 100 spectrometer, TLC (Thin layer chromatography) was run on a glass plate using methanol-water-acetic acid (12:3:7) solvent system. A spot color was visualized by U.V. chamber. The equipment used for dyeing purpose was done by using HTHP dyeing machine (model – LL).

Preparation of azo disperse dyes

Diazotization

Diazotization of various aromatic amines 1(a-j) was carried out by the method reported in literature [16].

Coupling procedure

The coupling of above mentioned diazotized aromatic amines was carried out in the similar manner. The general procedure adopted is given below:

1-[(2-butyl-2,3-dihydrobenzofuran-3-yl)]-1-(4-hydroxyphenyl)methanone 2.64 g (0.02 mol) was dissolved in 16 mL sodium hydroxide (0.02 M) solution. The clear solution was cooled in ice-bath and diazonium solution of amine was added drop wise over 30 minutes with vigorous stirring. The pH was maintained between 7.5 to 8 by simultaneous addition of 10% w/v sodium carbonate solution. Stirring was continued for 2 hours, allowing the temperature to rise to ambient. The dye was then filtered off, washed with warm water and with cold water until it becomes acid free, and was dried at 50 °C in an oven. The dyes were designated as dye (D₁₁₋₂₀) re-precipitated from DMF.

Disperse dyeing method

Dyeing of polyester fiber [17] is convenient at 90-135 °C and at high pressure (24-30 psi) in the laboratory. A model glycerin-bath high-temperature beaker and HTHP-

LL dyeing machine was used. For this purpose a paste of finely powdered dye (50 g) was prepared with dispersing agent dodamol (90 g) wetting agent Tween-80 (5 g) and water (5 g) in a ball mill. To this paste, water (99 mL) was added with stirring and the pH was adjusted to 4.5 - 5 using acetic acid, the previously mentioned dye suspension (100 mL) was added to a beaker provided with a lid and a screw cap. Before closing the lid and lightening the metal cap over the beaker a wetted pattern of polyester was rolled in to the beaker, and then placed vertically on the rotatory carrier inside the tank and the clamp plate was firmly tightened. The rotatory carrier was then allowed to rotate in the glycerin-bath and the temperature was raised to 90 °C at the rate of 2° C/min. The dyeing was continued for 1 hour under pressure. After cooling for 1 hour, the beaker was removed from the bath and washed with distilled water. The dyed pattern was thoroughly washed with hot water at 50 °C and then with cold water and dried at room temperature.

Mordent dyeing method

The heterocyclic dye pattern of wool obtained as mentioned above was treated with potassium dichromate solution equal to half of the weight of dye was allowed to rolled in to the beaker and again beaker was then placed vertically on the rotatory carrier inside the tank and the dyeing was continue for 1 hour under the pressure. After cooling for 1 hour, the beaker was removed from the bath and wash with distilled water. The dyed pattern was thoroughly washed with warm water and then with cold water and air dried at room temperature.

Characteristic data of dyes

1-(2-butyl-2,3-dihydrobenzofuran-3-yl)-1-[4-hydroxy-3-(2-nitrophenyl)diazenyl-phenyl]-methanone (D₁₁). Calculated for C₂₅H₂₃N₃O₅: m.wt.: 445, % yield 77, m.p. : 230-231⁰ C, Rf. value: 0.81; C , 67.41%; H, 5.20% ; N, 9.43%. Found: C, 67.38%; H, 5.17%; N, 9.38%. IR : 3460 cm⁻¹(-OH); 3077 cm⁻¹(=CH. aromatic); 1630 cm⁻¹ (C=O, diaryl), 1525 cm⁻¹ (N=N); 1484 cm⁻¹(C=C aromatic); 1338 cm⁻¹ (C-N), 1123 cm⁻¹ (C-O); 737 cm⁻¹, 586 cm⁻¹, 480 cm⁻¹. ¹H-NMR : 7.3-8.4 δ (Ar-H, multiplet), 5.35 δ (Ar-OH, singlet), 4.77 δ(β, C-H, for benzofuran), 4.60 δ(α, C-H, for benzofuran), 1.31 to 2.40 δ (-CH₂-, multiplet), 0.90 δ (-CH₃, triplet). ¹³C-NMR: 59.5 (C₃) (CH, Aliphatic), 73.7 (C₂) (CH, Aliphatic), 34.4 (CH₂, Butyl), 27.3 (CH₂, Butyl), 23.0 (CH₂, Butyl), 14.1 (CH₃, Butyl), 199.3 (C₁, Methanone), 156.6 (C₄, Phenolic -OH), 143.9 (C-NO₂), 125.0 (C-N=N), 147.6 (N=N-C), C-Ph. of benzofuran: 128.9 (C₁), 128.7 (C₂), 120.1 (C₃), 126.5 (C₄), 112.2 (C₅), 160.9 (C₆), O=C-Ph. of benzene: 129.6 (C₁), 122.9 (C₂), 125.0 (C₃), 156.6 (C₄), 119.0 (C₅), 132.4 (C₆), -N=N-Ph. of benzene: 147.6 (C₁), 143.9 (C₂), 124.2 (C₃), 131.8 (C₄), 135.1 (C₅), 123.9 (C₆).

1-[2-butyl-2,3-dihydrobenzofuran-3-yl]-1-[4-hydroxy-3-(4-nitrophenyl)diazenyl-phenyl]-methanone (D₁₂). Calculated for C₂₅H₂₃N₃O₅: m.wt.: 445, %yield : 72, m.p. : 217-218⁰

C, Rf. value: 0.85; C, 67.71%; H, 4.77%; N, 9.48%. Found : C, 67.65%; H, 4.72%; N, 9.41%. IR : 3453 cm^{-1} (-OH); 3087 cm^{-1} (=CH aromatic); 1628 cm^{-1} (C=O, diaryl), 1528 cm^{-1} (N=N); 1490 cm^{-1} (C=C. aromatic); 1348 cm^{-1} (C-N), 1100 cm^{-1} (C-O); 740 cm^{-1} , 568 cm^{-1} , 479 cm^{-1} . $^1\text{H-NMR}$: 7.3-8.4 δ (Ar-H, multiplet), 5.35 δ (Ar-OH, singlet), 4.77 δ (β , C-H, for benzofuran), 4.60 δ (α , C-H, for benzofuran), 1.31 to 2.40 δ (-CH₂-, multiplet), 0.90 δ (-CH₃, triplet). $^{13}\text{C-NMR}$: 59.5 (C₃) (CH, Aliphatic), 73.7 (C₂) (CH, Aliphatic), 34.4 (CH₂, Butyl), 27.3 (CH₂, Butyl), 23.0 (CH₂, Butyl), 14.1 (CH₃, Butyl), 199.3 (C₁, Methanone), 156.6 (C₄, Phenolic -OH), 143.9 (C-NO₂), 125.0 (C-N=N), 147.6 (N=N-C), C-Ph. of benzofuran: 128.9 (C₁), 128.7 (C₂), 120.1 (C₃), 126.5 (C₄), 112.2 (C₅), 160.9 (C₆), O=C-Ph. of benzene: 129.6 (C₁), 122.9 (C₂), 125.0 (C₃), 156.6 (C₄), 119.0 (C₅), 132.4 (C₆), -N=N-Ph. of benzene: 147.6 (C₁), 143.9 (C₂), 131.7 (C₃), 131.8 (C₄), 143.9 (C₅), 123.9 (C₆).

1-[2-butyl-2,3-dihydrobenzofuran-3-yl]-1-[4-hydroxy-3-(3-nitrophenyl)diazenyl-phenyl]-methanone (D₁₃). Calculated for C₂₅H₂₃N₃O₅ : m.wt. : 445, %yield : 75, m.p. : 212-213⁰ C, Rf. value: 0.77; C, 67.71%; H, 4.77%; N, 9.48%. Found: C, 67.69%; H, 4.75%; N, 9.43%. IR : 3480 cm^{-1} (-OH); 3072 cm^{-1} (=CH aromatic), 1631 cm^{-1} (C=O, diaryl), 1540 cm^{-1} (N=N), 1480 cm^{-1} (C=C aromatic), 1339 cm^{-1} (C-N), 1104 cm^{-1} (C-O), 738 cm^{-1} , 560 cm^{-1} , 470 cm^{-1} . $^1\text{H-NMR}$: 7.3-8.4 δ (Ar-H, multiplet), 5.35 δ (Ar-OH, singlet), 4.77 δ (β , C-H, for benzofuran), 4.60 δ (α , C-H, for benzofuran), 1.31 to 2.40 δ (-CH₂-, multiplet), 0.90 δ (-CH₃, triplet). $^{13}\text{C-NMR}$: 59.5 (C₃) (CH, Aliphatic), 73.7 (C₂) (CH, Aliphatic), 34.4 (CH₂, Butyl), 27.3 (CH₂, Butyl), 23.0 (CH₂, Butyl), 14.1 (CH₃, Butyl), 199.3 (C₁, Methanone), 156.6 (C₄, Phenolic -OH), 143.9 (C-NO₂), 125.0 (C-N=N), 147.6 (N=N-C), C-Ph. of benzofuran: 128.9 (C₁), 128.7 (C₂), 120.1 (C₃), 126.5 (C₄), 112.2 (C₅), 160.9 (C₆), O=C-Ph. of benzene: 129.6 (C₁), 122.9 (C₂), 125.0 (C₃), 156.6 (C₄), 119.0 (C₅), 132.4 (C₆), -N=N-Ph. of benzene: 147.6 (C₁), 143.9 (C₂), 124.2 (C₃), 131.8 (C₄), 135.1 (C₅), 123.9 (C₆).

1-[2-butyl-2,3-dihydrobenzofuran-3-yl]-1-[4-hydroxy-3-(2,6-dichloro-4-nitrophenyl)diazenyl-phenyl]-methanone (D₁₄). Calculated for C₂₅H₂₁O₅N₃Cl₂ : m.wt. : 514, % yield: 70, m.p. : 256-262⁰ C, Rf. value : 0.78; C, 58.38%; H, 4.12%; N, 8.17%. Found: C, 58.32%; H, 4.09.71%; N, 8.14%. IR : 3636 cm^{-1} (-OH), 3080 cm^{-1} (=CH aromatic); 1658 cm^{-1} (C=O, diaryl), 1531 cm^{-1} (N=N); 1478 cm^{-1} (C=C aromatic); 1343 cm^{-1} (C-N), 1103 cm^{-1} (C-O); 780 cm^{-1} , 741 cm^{-1} , 584 cm^{-1} , 489 cm^{-1} . $^1\text{H-NMR}$: 7.3-8.4 δ (Ar-H, multiplet), 5.35 δ (Ar-OH, singlet), 4.77 δ (β , C-H, for benzofuran), 4.60 δ (α , C-H, for benzofuran), 1.31 to 2.40 δ (-CH₂-, multiplet), 0.90 δ (-CH₃, triplet). $^{13}\text{C-NMR}$: 59.5 (C₃) (CH, Aliphatic), 73.7 (C₂) (CH, Aliphatic), 34.4 (CH₂, Butyl), 27.3 (CH₂, Butyl), 23.0 (CH₂, Butyl), 14.1 (CH₃, Butyl), 199.3 (C₁, Methanone), 156.6 (C₄, Phenolic -OH), 143.9 (C-NO₂), 125.0 (C-N=N), 147.6 (N=N-C), C-Ph. of benzofuran: 128.9 (C₁), 128.7 (C₂), 120.1 (C₃), 126.5 (C₄), 112.2 (C₅), 160.9 (C₆), O=C-Ph. of benzene: 129.6 (C₁), 122.9

(C₂), 125.0 (C₃), 156.6 (C₄), 119.0 (C₅), 132.4 (C₆), -N=N-Ph. of benzene: 149.4 (C₁), 130.8 (C₂), 122.6 (C₃), 150.5 (C₄), 122.6 (C₅), 130.9 (C₆).

1-[2-butyl-2,3-dihydrobenzofuran-3-yl]-1-[4-hydroxy-3-(2,4-dimethylphenyl)diazenyl-phenyl]-methanone (D₁₅). Calculated for C₂₇H₂₈O₃N₂ : m.wt. : 429, % yield : 81, m.p. : 202-204^oC, Rf. value : 0.86 ; C, 75.68%; H, 6.59%; N, 6.54%. Found: C, 75.62%; H, 6.56%; N, 6.50%. IR : 3573 cm⁻¹ (-OH); 3075 cm⁻¹(= CH aromatic); 1620 cm⁻¹ (C=O, diaryl), 1534 cm⁻¹ (N = N); 1484 cm⁻¹ (C=C aromatic); 1463 cm⁻¹ (C-N), 1343 cm⁻¹ (C-O); 1100 cm⁻¹, 736 cm⁻¹, 570 cm⁻¹, 469 cm⁻¹. ¹H-NMR: 7.3-8.4 δ (Ar-H, multiplet), 5.35 δ (Ar-OH, singlet), 4.77 δ (β, C-H, for benzofuran), 4.60 δ (α, C-H, for benzofuran), 2.34 δ (-CH₃, multiplet), 1.31 to 2.40 δ (-CH₂-, multiplet), 0.90 δ (-CH₃, triplet). ¹³C-NMR: 59.5 (C₃) (CH, Aliphatic), 73.7 (C₂) (CH, Aliphatic), 34.4 (CH₂, Butyl), 27.3 (CH₂, Butyl), 23.0 (CH₂, Butyl), 14.1 (CH₃, Butyl), 199.3 (C₁, Methanone), 156.6 (C₄, Phenolic -OH), 143.9 (C-NO₂), 125.0 (C-N=N), 147.6 (N=N-C), C-Ph. of benzofuran: 128.9 (C₁), 128.7 (C₂), 120.1 (C₃), 126.5 (C₄), 112.2 (C₅), 160.9 (C₆), O=C-Ph. of benzene: 129.6 (C₁), 122.9 (C₂), 125.0 (C₃), 156.6 (C₄), 119.0 (C₅), 132.4 (C₆), -N=N-Ph. of benzene: 149.0 (C₁), 131.1 (C₂), 131.2 (C₃), 132.4 (C₄), 126.3 (C₅), 122.8 (C₆).

1-[2-butyl-2,3-dihydrobenzofuran-3-yl]-1-[4-hydroxy-3-(3-chlorophenyl)diazenyl-phenyl]-methanone (D₁₆). Calculated for C₂₅H₂₃O₃N₂Cl : m.wt. : 435, %yield : 85, m.p. : 161-164^oC, R.f. value : 0.90, C, 69.04%; H, 5.33%; N, 6.44% Found C, 69.01%; H, 5.28%; N, 6.40%. IR : 3430 cm⁻¹(-OH); 3066 cm⁻¹(=CH aromatic); 1630 cm⁻¹ (C=O, diaryl), 1584 cm⁻¹ (N=N); 1482 cm⁻¹(C=C aromatic); 1350 cm⁻¹(C-N), 1104 cm⁻¹ (C-O); 786 cm⁻¹, 740 cm⁻¹, 586 cm⁻¹, 489 cm⁻¹. ¹H-NMR : 7.3-8.4 δ (Ar-H, multiplet), 5.35 δ (Ar-OH, singlet), 4.77 δ(β, C-H, for benzofuran), 4.60 δ(α, C-H, for benzofuran), 1.31 to 2.40 δ (-CH₂-, multiplet), 0.90 δ (-CH₃, triplet). ¹³C-NMR: 59.5 (C₃) (CH, Aliphatic), 73.7 (C₂) (CH, Aliphatic), 34.4 (CH₂, Butyl), 27.3 (CH₂, Butyl), 23.0 (CH₂, Butyl), 14.1 (CH₃, Butyl), 199.3 (C₁, Methanone), 156.6 (C₄, Phenolic -OH), 143.9 (C-NO₂), 125.0 (C-N=N), 147.6 (N=N-C), C-Ph. of benzofuran: 128.9 (C₁), 128.7 (C₂), 120.1 (C₃), 126.5 (C₄), 112.2 (C₅), 160.9 (C₆), O=C-Ph. of benzene: 129.6 (C₁), 122.9 (C₂), 125.0 (C₃), 156.6 (C₄), 119.0 (C₅), 132.4 (C₆), -N=N-Ph. of benzene: 154.1 (C₁), 123.3 (C₂), 133.0 (C₃), 131.0 (C₄), 130.4 (C₅), 121.1 (C₆).

1-[2-butyl-2,3-dihydrobenzofuran-3-yl]-1-[4-hydroxy-3-(4-chlorophenyl)diazenyl-phenyl]-methanone (D₁₇). Calculated for C₂₅H₂₃O₃N₂Cl : m.wt. : 435, %yield : 84, m.p.: 118-120^o C, R.f. value : 0.84, C, 69.04%; H, 5.33%; N, 6.44%. Found : C, 68.98%; H, 5.31%; N, 6.39%. IR : 3591 cm⁻¹(-OH); 3060 cm⁻¹(=CH aromatic); 1629 cm⁻¹ (C=O, diaryl), 1532 cm⁻¹. (N=N); 1470 cm⁻¹ (C=C aromatic); 1323 cm⁻¹ (C-N), 1104 cm⁻¹ (C-O); 780 cm⁻¹, 737 cm⁻¹, 581 cm⁻¹, 470 cm⁻¹. ¹H-NMR : 7.3-8.4 δ (Ar-H, multiplet), 5.35 δ (Ar-OH, singlet), 4.77 δ(β, C-H, for benzofuran), 4.60 δ(α, C-H, for benzofuran), 1.31 to

2.40 δ (-CH₂-, multiplet), 0.90 δ (-CH₃, triplet). ¹³C-NMR: 59.5 (C₃) (CH, Aliphatic), 73.7 (C₂) (CH, Aliphatic), 34.4 (CH₂, Butyl), 27.3 (CH₂, Butyl), 23.0 (CH₂, Butyl), 14.1 (CH₃, Butyl), 199.3 (C₁, Methanone), 156.6 (C₄, Phenolic -OH), 143.9 (C-NO₂), 125.0 (C-N=N), 147.6 (N=N-C), C-Ph. of benzofuran: 128.9 (C₁), 128.7 (C₂), 120.1 (C₃), 126.5 (C₄), 112.2 (C₅), 160.9 (C₆), O=C-Ph. of benzene: 129.6 (C₁), 122.9 (C₂), 125.0 (C₃), 156.6 (C₄), 119.0 (C₅), 132.4 (C₆), -N=N-Ph. of benzene: 147.6 (C₁), 143.9 (C₂), 124.2 (C₃), 130.4 (C₄), 133.0 (C₅), 123.9 (C₆).

1-[2-butyl-2,3-dihydrobenzofuran-3-yl]-1-[4-hydroxy-3-(4-hydroxyphenyl)diazenyl-phenyl]-methanone (D₁₈). Calculated for C₂₅H₂₄O₄N₂ : m.wt. : 416, %yield : 78, m.p.: 133-136^oC, R.f. value : 0.80; C, 72.10%; H, 5.81%; N, 6.73%. Found: C, 72.07%; H, 5.98%; N, 6.70. IR : 3580 cm⁻¹(-OH); 3056 cm⁻¹ (=CH aromatic); 1635 cm⁻¹ (C=O, diaryl), 1523 cm⁻¹ (N=N); 1475 cm⁻¹ (C=C aromatic); 1327 cm⁻¹ (C-N), 1101 cm⁻¹ (C-O); 742 cm⁻¹, 578 cm⁻¹, 470 cm⁻¹, ¹H-NMR : 7.3-8.4 δ (Ar-H, multiplet), 5.35 δ (2,Ar-OH, singlet), 4.77 δ (β , C-H, for benzofuran), 4.60 δ (α , C-H, for benzofuran), 1.31 to 2.40 δ (-CH₂-, multiplet), 0.90 δ (-CH₃, triplet). ¹³C-NMR: 59.5 (C₃) (CH, Aliphatic), 73.7 (C₂) (CH, Aliphatic), 34.4 (CH₂, Butyl), 27.3 (CH₂, Butyl), 23.0 (CH₂, Butyl), 14.1 (CH₃, Butyl), 199.3 (C₁, Methanone), 156.6 (C₄, Phenolic -OH), 143.9 (C-NO₂), 125.0 (C-N=N), 147.6 (N=N-C), C-Ph. of benzofuran: 128.9 (C₁), 128.7 (C₂), 120.1 (C₃), 126.5 (C₄), 112.2 (C₅), 160.9 (C₆), O=C-Ph. of benzene: 129.6 (C₁), 122.9 (C₂), 125.0 (C₃), 156.6 (C₄), 119.0 (C₅), 132.4 (C₆), -N=N-Ph. of benzene: 145.3 (C₁), 124.4 (C₂), 116.2 (C₃), 160.7 (C₄), 116.2 (C₅), 124.4 (C₆).

1-[2-butyl-2,3-dihydrobenzofuran-3-yl]-1-[4-hydroxy-3-(4-methylphenyl)diazenyl-phenyl]-methanone (D₁₉). Calculated for C₂₆H₂₆O₃N₂ : m.wt.: 414, % yield : 77, m.p. : 106-108^o C , Rf. value : 0.84 ; C, 75.34 %; H, 6.32 %; N, 6.76%. Found: C, 75.28 %; H, 6.26 %; N, 6.72%. IR : 3630 cm⁻¹(-OH); 3024 cm⁻¹ (=CH aromatic); 1626 cm⁻¹ (C = O, diaryl), 1527 cm⁻¹ (N=N); 1468 cm⁻¹ (C=C aromatic); 1446 cm⁻¹ (CH₃), 1351 cm⁻¹ (C-N); 1111 cm⁻¹ (C-O); 744 cm⁻¹, 580 cm⁻¹, 473 cm⁻¹. ¹H-NMR: 7.3-8.4 δ (Ar-H, multiplet), 5.35 δ (Ar-OH, singlet), 4.77 δ (β , C-H, for benzofuran), 4.60 δ (α , C-H, for benzofuran), 2.34 δ (-CH₃, singlet), 1.31 to 2.40 δ (-CH₂-, multiplet) 0.90 δ (-CH₃, triplet). ¹³C-NMR: 59.5 (C₃) (CH, Aliphatic), 73.7 (C₂) (CH, Aliphatic), 34.4 (CH₂, Butyl), 27.3 (CH₂, Butyl), 23.0 (CH₂, Butyl), 14.1 (CH₃, Butyl), 199.3 (C₁, Methanone), 156.6 (C₄, Phenolic -OH), 143.9 (C-NO₂), 125.0 (C-N=N), 147.6 (N=N-C), C-Ph. of benzofuran: 128.9 (C₁), 128.7 (C₂), 120.1 (C₃), 126.5 (C₄), 112.2 (C₅), 160.9 (C₆), O=C-Ph. of benzene: 129.6 (C₁), 122.9 (C₂), 125.0 (C₃), 156.6 (C₄), 119.0 (C₅), 132.4 (C₆), -N=N-Ph. of benzene: 149.7 (C₁), 122.9 (C₂), 129.3 (C₃), 140.6 (C₄), 129.3 (C₅), 122.9 (C₆).

1-[2-butyl-2,3-dihydrobenzofuran-3-yl]-1-[4-hydroxy-3-(2-methylphenyl)diazenyl-phenyl]-methanone (D₂₀). Calculated for C₂₆H₂₆O₃N₂ : m.wt.: 414, %yield : 73, m.p. :

120-124⁰ C , Rf. value : 0.841; C, 75.34 %; H, 6.32 %; N, 6.76%. Found: C, 75.30 %; H, 6.30 %; N, 6.70%. IR : 3503 cm⁻¹ (-OH); 3053 cm⁻¹ (=CH aromatic); 1630 cm⁻¹ (C=O, diaryl), 1535 cm⁻¹ (N=N); 1478 cm⁻¹ (C=C aromatic); 1450 cm⁻¹ (CH₃), 1320 cm⁻¹ (C-N); 1109 cm⁻¹ (C-O); 747cm⁻¹, 579 cm⁻¹, 468 cm⁻¹. ¹H-NMR: 7.3-8.4 δ (Ar-H, multiplet), 5.35 δ (Ar-OH, singlet), 4.77 δ (β, C-H, for benzofuran), 4.60 δ (α, C-H, for benzofuran), 2.34 δ (-CH₃, singlet), 1.31 to 2.40 δ (-CH₂-, multiplet) 0.90 δ (-CH₃, triplet). ¹³C-NMR: 59.5 (C₃) (CH, Aliphatic), 73.7 (C₂) (CH, Aliphatic), 34.4 (CH₂, Butyl), 27.3 (CH₂, Butyl), 23.0 (CH₂, Butyl), 14.1 (CH₃, Butyl), 199.3 (C₁, Methanone), 156.6 (C₄, Phenolic -OH), 143.9 (C-NO₂), 125.0 (C-N=N), 147.6 (N=N-C), C-Ph. of benzofuran: 128.9 (C₁), 128.7 (C₂), 120.1 (C₃), 126.5 (C₄), 112.2 (C₅), 160.9 (C₆), O=C-Ph. of benzene: 129.6 (C₁), 122.9 (C₂), 125.0 (C₃), 156.6 (C₄), 119.0 (C₅), 132.4 (C₆), -N=N- Ph. of benzene: 147.6 (C₁), 140.6 (C₂), 124.2 (C₃), 131.8 (C₄), 130.2 (C₅), 123.9 (C₆).

Fastness property

The fastness to light, sublimation and perspiration of dye pattern was assessed according to British standard: 1006-1978 and the wash fastness test according to Indian standard: IS: 765-1979. The rubbing fastness was tested by using Crock meter (Atlas) AATCC-1961, shown in Table1 and Table 2.

Table1. Result of dyeing and various fastness properties of heterocyclic dyes onto polyester

Dyes No.	Color shades on wool	Light fastness	Wash fastness	Perspiration fastness		Sublimation fastness	Rubbing fastness	
				Acid	Alkaline		Dry	Wet
D ₁₁	Dark-brown	5	5	5	5	5	4	4
D ₁₂	Yellowish brown	5	4	5	5	5	4	4
D ₁₃	Reddish Brown	5	5	5	5	5	5	4
D ₁₄	Dark-Brown	4	5	4	5	4	4	4
D ₁₅	Green	5	4	5	5	5	5	4
D ₁₆	Yellowish Orange	5	5	5	5	5	5	3
D ₁₇	Yellowish Orange	5	4	5	5	5	5	4
D ₁₈	chocolate brown	5	4	4	4	5	5	4
D ₁₉	Lemon Yellow	5	5	5	5	5	5	4
D ₂₀	Yellowish Orange	5	5	4	5	5	5	4

Table2. Results of mordent heterocyclic dyeing and various fastness properties of heterocyclic dyes onto wool

Dyes No.	Color shades on wool	Light fastness	Wash fastness	Perspiration fastness		Sublimation fastness	Rubbing fastness	
				Acid	Alkaline		Dry	Wet
D ₁₁	Dark-brown	5	5	4	5	5	4	3
D ₁₂	Yellowish brown	5	4	4	5	4	4	4
D ₁₃	Reddish Brown	5	4	4	5	5	4	3
D ₁₄	Dark-Brown	5	4	4	5	4	4	4
D ₁₅	Green	4	4	4	4	4	5	4
D ₁₆	Yellowish Orange	4	4	4	4	5	5	4
D ₁₇	Yellowish Orange	5	4	4	4	5	5	3
D ₁₈	chocolate brown	5	4	4	5	4	4	3
D ₁₉	Lemon Yellow	4	4	4	5	5	5	4
D ₂₀	Yellowish Orange	5	4	4	5	5	5	4

Determination of the percentage exhaustion and fixation

The dye bath percentage exhaustion and fixation of the dyed fabric was determined according to the known method [18] shown in Table 3.

Antimicrobial activity

The *in vitro* antimicrobial activities [19, 20] of the heterocyclic chrome dyes were tested against *Escherichia coli*, *Staphylococcus aureus*, *Salmonella typhi* and *Bacillus subtilis* bacteria using agar nutrient as the medium. A stock solution of 250 ppm was prepared by dissolving the compounds in 20 % DMSO solution. The antimicrobial activity was performed at a concentration 100 µg/ mL, using the agar-cup method in which the well diameter was 4 mm [21]. Benzyl penicillin was used as a standard drug for antibacterial screening and solvent DMSO was used as a control. Antimicrobial activities of the heterocyclic chrome dyes are shown in Table 4.

Table 3. Absorption maxima, exhaustion (E) and fixation (F) of heterocyclic dyes on polyester/wool

Dyes No.	Absorption maxima λ_{max}/nm in DMF	Log ϵ	Mordent dyeing on wool		Disperse dyeing on Polyester	
			%E	%F	%E	%F
D ₁₁	431	4.3	81	90	72	91
D ₁₂	425	4.2	71	94	73	82
D ₁₃	432	4.3	75	91	84	90
D ₁₄	450	4.4	82	93	72	81
D ₁₅	434	4.4	78	90	76	85
D ₁₆	442	4.4	76	89	71	91
D ₁₇	440	4.3	85	92	77	92
D ₁₈	416	4.1	82	88	70	80
D ₁₉	431	4.3	74	90	72	89
D ₂₀	425	4.3	71	91	75	87

Table 4. Antibacterial activity of heterocyclic chrome dyes (100 µg/mL) of (D₁₁-D₂₀)

Dye No.	Zone of inhibition (mm)			
	<i>E. coli</i>	<i>S. aureus</i>	<i>S. typhi</i>	<i>B. subtilis</i>
D ₁₁	21	20	19	21
D ₁₂	19	19	14	22
D ₁₃	24	23	21	20
D ₁₄	22	22	22	25
D ₁₅	13	14	15	18
D ₁₆	20	18	22	20
D ₁₇	23	21	17	23
D ₁₈	14	17	19	19
D ₁₉	12	15	17	14
D ₂₀	13	17	18	16
Benzyl penicillin	28	26	27	29

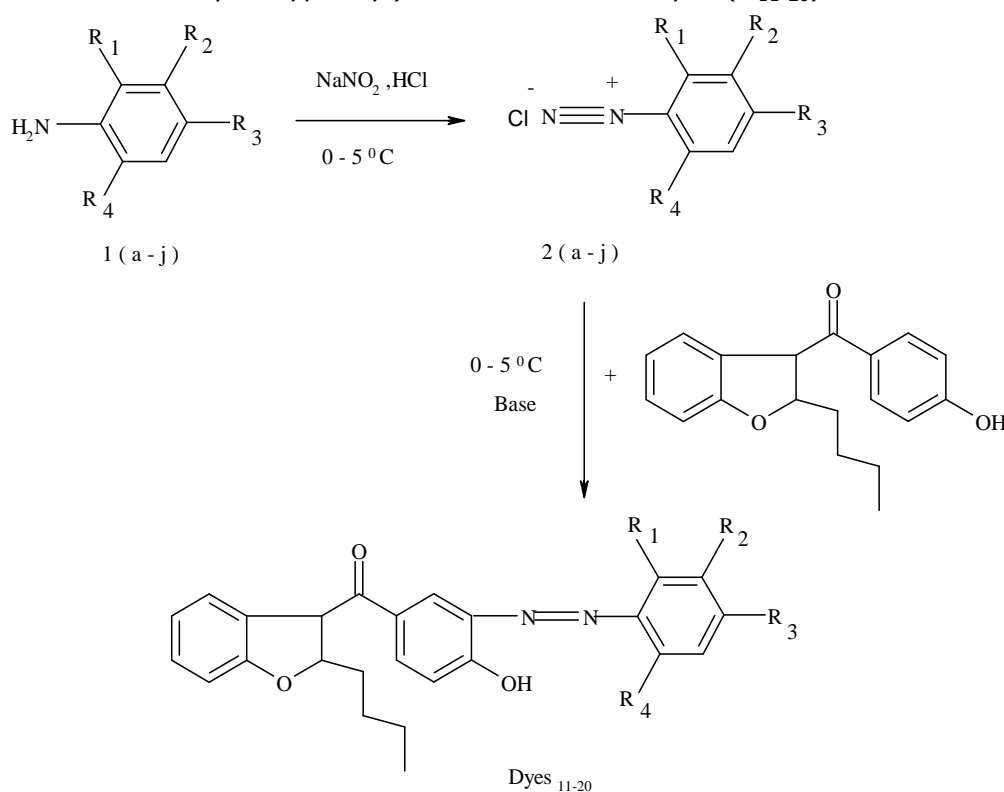
Results and Discussion

Physical properties of dyes

All the dyes are obtained as amorphous powder ranging from yellow to reddish brown in colour. The purity of the dyes were checked by TLC using methanol-water-acetic acid (12:3:7) solvent system. The TLC results show that only single spot observed for each dye. The purified dyes have melting points measured by open capillary tube. The melting points were uncorrected.

The results of elemental analysis content of each dye are consistent with the predicted structure as shown in Scheme 1.

Scheme 1. Synthesis of 1-[(2-butyl-2,3-dihydrobenzofuran-3-yl)]-1-(4-hydroxyphenyl)methanone based dyes (D₁₁₋₂₀)



Dyes No	R ₁	R ₂	R ₃	R ₄	Amines 1(a-j)
D ₁₁	NO ₂	H	H	H	2- Nitroaniline
D ₁₂	H	H	NO ₂	H	4- Nitroaniline
D ₁₃	H	NO ₂	H	H	3 -Nitroaniline
D ₁₄	Cl	H	NO ₂	Cl	2,6 -Dichloro-4-nitroaniline
D ₁₅	CH ₃	H	CH ₃	H	2,4-Dimethylaniline
D ₁₆	H	Cl	H	H	3-Chloroaniline
D ₁₇	H	H	Cl	H	4-Chloroaniline
D ₁₈	H	H	OH	H	4-hydroxyaniline
D ₁₉	H	H	CH ₃	H	4-Methylaniline
D ₂₀	CH ₃	H	H	H	2-Methylaniline

The number of azo group is almost one for each dye. The nitrogen content and

number of azo group for each dye are co-related with each other. The IR spectrum of each dye comprises the important features (shown above) of aromatic, azo, hydroxyl and keto groups. The NMR spectra also giving important signals at their respective positions. All diazo compounds based on the well known structure of 1-[(2-butyl-2,3-dihydrobenzofuran-3-yl)]-1-(4-hydroxyphenyl)methanone and reactive site for azo coupling, the structure of azo dyes shown in Scheme 1 are confirmed.

The visible absorption spectroscopic properties of dye were recorded in DMF solution. The absorption maxima (λ_{\max}) of all dyes fall into the range of 416-450 nm in DMF, as shown in Table- I. The value of the logarithm of molar extinction coefficient ($\log \epsilon$) of all the dyes were in the range of 4.1–4.4 consistent with their high intensity of absorption.

More ever the presence of electron donating or electron attracting groups did not bring about any marked increase or decreased in λ_{\max} in the visible region and that $\log \epsilon$ remained nearly constant. However electron attracting substituents like -Cl and -NO₂ in the substituent group of the coupler increase polarizability, and will result in bathochromic shifts. This leads to decrease in energy between the highest occupied molecular orbital and lowest unoccupied molecular orbital and thus $\pi \rightarrow \pi^*$ electron transition takes place at lower frequency photon resulting in the bathochromic shift of the visible absorption band.

Dyeing properties of dyes

The mordent and dispersed heterocyclic dyes were applied at 2% depth on wool and polyester fabric respectively. Their dyeing properties are given in Table II and Table III. These heterocyclic dyes gave a wide range of colour varying from yellowish brown to reddish brown shades with good levelness, brightness and depth on the fabric. The variations in the shades of the heterocyclic dyes fabric result from both the nature and position of the substituent present on the diazotized compound. The light fastness values of the heterocyclic dyes are more consistent (as shown in Table III). The dyeing showed an excellent fastness to light, with very good to excellent fastness to washing, perspiration and sublimation and it shows poor rubbing fastness.

A remarkable degree of levelness after washing is observed. This may be attributed to good penetration and affinity of the heterocyclic dyes in to fiber structure. The most prominent features of these heterocyclic dyes are that, the dye pattern treated with Cr (III) salt solution affords excellent shining shade of dyes. This might be the chrome complex formation on fiber. The bacterial activity of chrome complexes of heterocyclic dyes was monitored against the plant pathogens. The results (Table IV) show that these heterocyclic dyes are inhibiting the bacteria about 70%. The dye pattern of chrome treated heterocyclic dyes may be affordable for human body.

Conclusion

Produced heterocyclic dyes have good fastness to light, sublimation and perspiration but show poor rubbing fastness properties. The nature of the substituent in the coupling components has a little influence on the visible absorption and shade of the dyeing. Comparison of above two heterocyclic dyes reveals that mordent heterocyclic dyes have good shades than heterocyclic disperse dyes.

Acknowledgments

The Author is also thankful to Mr. Ashok C. Kapadia of Colortax (Pvt) Ltd., for characterization of heterocyclic dyes and Shashikant Patel of sumit-mill, pandesara, surat for providing standard of analysis work.

References and Notes

- [1] Kosolia, C. T.; Tsatsaroni, E. G. *J. Appl. Polym. Sci.* **2010**, *116*, 1422. [[CrossRef](#)]
- [2] Schwander, H. R. *Dyes and Pigments*, **1982**, *3*, 133. [[CrossRef](#)]
- [3] Towns, A. D. *Dyes and Pigments*, **1999**, *42*, 3. [[CrossRef](#)]
- [4] Sarayu, K.; Swaminathan, K.; Sandhya S. *Dyes and Pigments*, **2007**, *75*, 362. [[CrossRef](#)]
- [5] Agbo, S. I.; Hallas, G.; Towns, A. D. *Dyes and Pigments* **2000**, *47*, 33. [[CrossRef](#)]
- [6] Mehta, P.; Surana, M.; Mehta R.; Kabra, B. V. *Der Chemica Sinica*, **2011**, *2*, 37. [[link](#)]
- [7] Dawane, B. S.; Chobe, S. S.; Mandawad, G. G.; Shaikh, B. M.; Konda S. G.; Patil, S. D. *Der Pharmacia Sinica*, **2010**, *1*, 140. [[Link](#)]
- [8] Pu, S.; Wang, R.; Liu, G.; Liu, W.; Cui, S.; Yan, P. *Dyes and Pigments*, **2012**, *94*, 195. [[CrossRef](#)]
- [9] Tamura, M.; Ohishi, T.; Sakurai, H.; US Patent. 4, 298, 522 **1981**.
- [10] Farouqui, F. I; Hossain, I. *Textile Dyer Printer* **1990**, *23*, 15.
- [11] Layer, R. W.; US Patent. 4, 133,799 **1979**.
- [12] Seto, N., Morigaki, M.; US Patent. 4, 864,039 **1989**.
- [13] Patel, H. M. *Der Chemica Sinica* **2011**, *2*, 89. [[Link](#)]
- [14] Patel, H. M. *Der Chemica Sinica* **2012**, *3*, 175. [[Link](#)]
- [15] Patel, H. M. *Advances in Applied Science Research* **2012**, *3*, 235. [[Link](#)]
- [16] David, F.; Blengy, H. E. *Fundamental process of Dye chemistry*, New York: Willy, 1949, 241.
- [17] Malik, G. M.; Zadafiya, S. K. *Der Chemica Sinica* **2010**, *1*, 15. [[Link](#)]
- [18] Shishtawy, R. M. E.; Youssef, Y. A. ; Ahmed, N. S. E.; Mousa, A. A. *Dyes and Pigments* **2007**, *72*, 57. [[CrossRef](#)]
- [19] Ampati, S.; Jukanti, R.; Sagar, V.; Ganta, R.; Manda, S. *Der Chemica Sinica* **2010**, *1*, 157. [[Link](#)]
- [20] Valarmathi, R.; Akilandeswari, S.; Indu latha, V. N.; Umadevi, G. *Der Pharmacia*

Sinica **2011**, 2, 64. [[Link](#)]

- [21] Pelzar, M. J.; Chan, E. C. S.; Krieg, N. R. Antibiotics and Other Chemotherapeutic Agents in Microbiology, 5th ed. New York: Blackwell Science, 1998.

The synthesis, characterization and theoretical study of nano tetrabutylammonium trichloroiodoaluminate (III)

Shahriar Ghammamy

Department of Chemistry, Faculty of Science, Islamic Azad University, Malard Branch, Po Box 34146-16818, Malard, Iran.

Received: 27 February 2012; revised: 02 July 2012; accepted: 27 July 2012. Available online: 07 September 2012.

ABSTRACT: There is provided a nano aluminate complex that has a quaternary ammonium cation. This nano system has an equal molar ratio of Al to N that has been prepared by reaction of an organic salt R^+X^- such as $[(CH_3)_4NBr]$, and a Lewis acid such as $AlCl_3$, compounds. The synthesized compound was characterized by IR, Mass, X-Ray diffraction measurements. In addition, the structure of synthesized compound was optimized at the theoretical level of the Moller-Plesser perturbations of the second order (MP2), with LanL2DZ basis set and molecular specifications such as bond length and angle were extracted using Gaussian 98 program. Theoretical data show good agreement with the experimental result.

Keywords: nanoparticles; aluminate complex; XRD; theoretical calculation

Introduction

Many of complex compounds are formed by at least two components. The first component is contained an organic salt or mixture of salts such as phosphonium, sulfonium, or quaternary ammonium halides including one or more alkyl moieties. The second component is contained a Lewis acid (metal halide) such as $ZnCl_2$, $GaCl_3$, $InBr_3$, $AlCl_3$, $HfCl_4$, $ZrCl_4$, $GeCl_4$, $SiCl_4$, WCl_6 , $SbCl_3$ and $RuCl_3$ [1-2]. The properties of these complexes can be varied by changing the constituent ions.

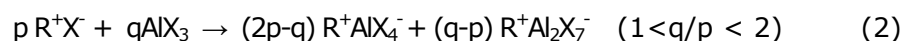
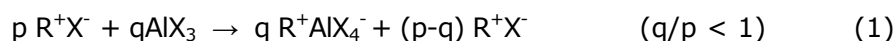
Whereas symmetric R_4NX have been studied by different experimental techniques and they have special characteristics, we focus our attention on tetra-alkyl-ammonium

* Corresponding author. E-mail: shghamami@yahoo.com

halides [3-5].

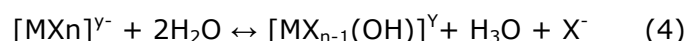
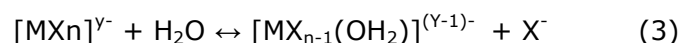
In order to make a complex compound, reaction of metal halide with organic salt such as quaternary ammonium halide solution may be performed at -10 to 100 °C and the 2 to 9 Al/N molar ratio [1-2].

Of course in the literature were found the mole ratio less than 2 according to the following reactions [6]:



It is noteworthy that if the molar ratio, q/p , is less than 1, reaction consist of $R^+AlX_4^-$ and $R^+Al_2X_7^-$ [7-9]. When q/p is greater than 1 but less than 2, reaction products consist of R^+X^- and $R^+AlX_4^-$ [7-9]. Those compound for which $q/p=1$ contain only $R^+AlX_4^-$.

Furthermore the solution chemistry of these complexes has been studied in some molecular solvents. It was found that some metal halide complexes undergo the following hydration and hydrolysis reactions in aqueous solution [6, 10].



Therefore, in order to avoid hydrolysis reaction, some nonaqueous molecular solvent, such as acetonitrile, can be used in place of water.

These reactions and complex compounds can be employed in a very wide range of applications such as alkylation, isomerization, hydrocracking, polymerization, dimerization, oligomerization, acylation, acetylation, metathesis, copolymerization, hydroformylation, dehalogenation etc [11-15]. For example, an isobutane-butene alkylation catalyzed with butyl pyridinium chloroaluminate, and co-catalyzed with t-butyl chloride, in literature has been mentioned [1].

Special series of mentioned complex compounds are called aluminates complex which are produce by reaction of alkyl-ammonium salts and aluminum chloride according to a reported general procedure [16]. Some of the chloroaluminate complexes are used for alkylation of benzene instead of $AlCl_3$ as a catalyst. These compounds solve problems such as the formation of aluminate waste, low yield, cumbersome product recovery, and non-reuse of the catalyst.

An advantage of the chloroaluminate compounds is their adjustable Lewis acidity. Acidity can be altered by varying the molar ratio of the two components and can be used to produce specific catalysts or compounds [17].

Extended practical applications of these materials have motivated us to improve

our knowledge. In this direction, in order to gain insight into neoteric material, a nano quaternary ammonium haloaluminate complex was synthesized by using an equal molar ratio of a quaternary ammonium salt and aluminum chloride compounds and then was identified by different experimental methods and finally was determined stable configuration of complex via an *ab initio* calculations.

Material and Methods

Tetrabutylammonium iodide and aluminum chloride were purchased from Merck Corporation. In this study all the chemical solvents were of analytical grade and were used as received without purification. Fourier transform infrared (FT-IR) spectra were recorded on a Bruker Tensor 27 (420 models) FT-IR spectrometer, using the pressing potassium bromide disk. The ranges of DTGS were 4000–400 cm^{-1} . The nanoparticles were characterized by X-ray diffraction (XRD; PMD-3000).

Mass spectrum was recorded by mass spectroscopy (Mass; Agilent Technology (HP), 5973 Network Mass Selection Detector).

2.0 mmol (0.27 g) aluminum chlorides was placed in a round flask and in this flask, 5 mL CH_3CN (without water) was added. The mixture was stirred at room temperature for ~ten minutes until the solution became yellow. Then 2.0 mmol (0.73 g) tetrabutylammonium iodide (dried) was mixed with 5 mL CH_3CN (without water) in other round flask and stirred for 1 h until solution became milky and was then added to first flask. The resulting solution was then kept for 3 h at room temperature with stirring. Reaction was exothermic and the resultant became orange.

The nanoparticles were centrifuged at 5000 rpm for 20 min and the precipitates were collected and redispersed in diethyl ether. The precipitate was centrifuged again at 5000 rpm for 20 min and the precipitates were redispersed in hexane. At the end of the solution was centrifuged at 5000 rpm for 20 min once more, and the precipitates were collected and redispersed in CH_3CN . The light orange precipitate was extracted in ceramic dish, dried in sand-bath and kept in desiccator. Weight and yield of dried nanoparticles was 0.80 g and 80%, respectively. These washed and dried nanoparticles were used for spectroscopic, SEM and XRD measurement. Spectroscopic data of synthesized aluminates complex are reported as IR (KBr): 3380, 3315, 3225, 3010, 2958, 2874, 2735, 2360, 1950, 1475, 1382, 1158, 463, 453, 1061, 879, 885 cm^{-1} ; MS, $m/z=360$ (M^+), 353, 333, 313, 290, 279, 254, 239, 203, 184, 167, 142, 133, 121, 98, 85, 63, 50.

The *ab initio* calculations were carried by means of the Gaussian 98 software. The structure of anionic segment $[\text{AlCl}_3\text{I}]^-$, and synthesized compound $[(\text{C}_4\text{H}_9)_4\text{N}]^+[\text{AlCl}_3\text{I}]^-$ was optimized at the theoretical level of the Moller-Plesser perturbations of the second order (MP2) with LanL2DZ basis set. Calculations were done in the gas phase.

Optimization procedures and frequency calculations were done in order to extract most stable structure, bond length and angle, vibratory frequencies and finally results checked for more confidence and theoretical data were compared with experimental results.

Results and Discussion

Fist of all, it was synthesized with an equal molar ratio of Al to I in order to synthesize only one product, $[(C_4H_9)_4N]^+[AlCl_3I]^-$, without impurity. Non-aqueous molecular solvent, acetonitrile, was used with initial substances in order to avoid hydrolysis reaction. Then the resultant nano aluminate complex after purification was characterized by IR, Mass, X-Ray diffraction measurements.

The solubility of synthesized ionic liquid was verified in common solvents. The results of solvation shows that soluble in solvents such as methanol, water, slightly soluble in ethanol and dimethyl sulfoxide and insoluble in toluene, acetonitrile, chloroform and hexane.

The cationic segment and synthesized structure of $[(C_4H_9)_4N]^+[AlCl_3I]^-$ were optimized by MP2 method using LanL2DZ basis set in the gas phase (Figure 1). Structure formation energy ($E(HF)$), RMS force and displacement, maximum force and displacement demonstrate stability of structures (global minimum). Also Table 1 consists of calculated molecular parameters (bond length and angle), anionic segments and synthesized $[(C_4H_9)_4N]^+[AlCl_3I]^-$ in sequence. Results of Table 1 for $[(C_4H_9)_4N]^+[AlCl_3I]^-$ show, Al-I bond length is 2.826 Å, Al-Cl(2) bond length is 1.875 Å, Al-Cl(3) bond length is 1.875 Å, Al-Cl(4) bond length is 1.930 Å, I-Al-Cl(2) bond angels are 106.5°, and I-Al-Cl(3) bond angel is 106.5°, Cl(3)-Al-Cl(2) bond angel is 120.5° Cl(4)-Al-Cl(2) bond angle is 118.9°, Cl(4)-Al-Cl(3) 109.505°. Table 2 show calculated IR frequencies (theoretical) in 1-4000 cm^{-1} without correction.

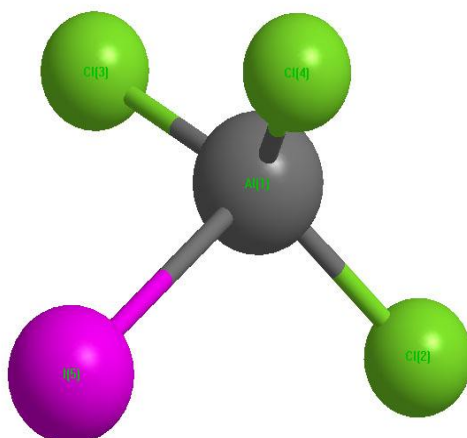
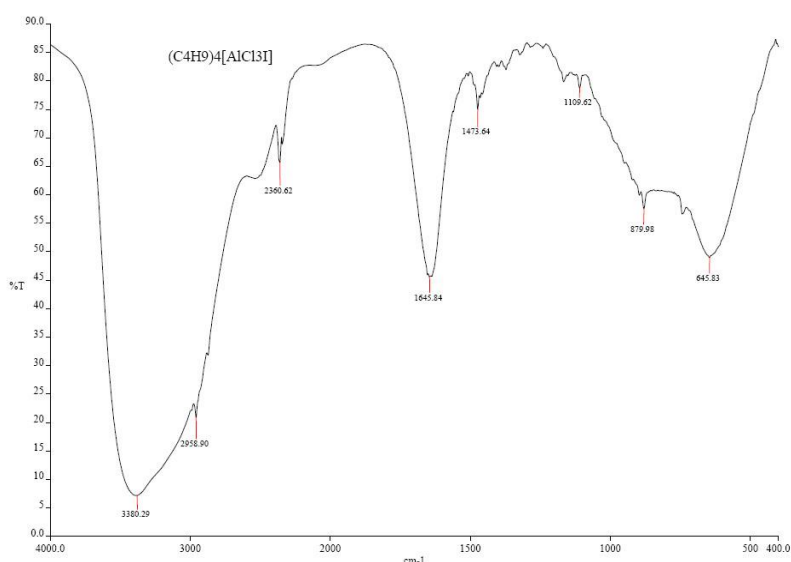


Figure 1. Optimized cationic structure of $[(C_4H_9)_4N]^+$.

Table 1. Optimized parameters of $[(C_4H_9)_4N]^+[AlCl_3I]^-$ based on Gaussian 98 program

Bond	Bond lengths [Å]	angles	Bond angles [°]
Al-I	2.826	I-Al-Cl(2)	106.5
Al-Cl(2)	1.875	I-Al-Cl(3)	106.5
Al-Cl(3)	1.875	Cl(3)-Al-Cl(2)	120.5
Al-Cl(4)	1.930	Cl(4)-Al-Cl(2)	118.9
		Cl(4)-Al-Cl(3)	118.9

FTIR spectrum of $[(C_4H_9)_4N]^+[AlCl_3I]^-$ which were recorded by a Bruker instrument, are shown in Figure 2. The experimental bands and assignments for FTIR spectra of $[(C_4H_9)_4N]^+[AlCl_3I]^-$ are presented in Table 2.

**Figure 2.** FTIR spectrum of $[(C_4H_9)_4N]^+[AlCl_3I]^-$.

X-ray powder diffraction measurement was performed at room temperature and data on crystallite size was obtained. Figure 3 shows typical XRD patterns of the tested sample. Then the crystallite size of $[(C_4H_9)_4N]^+[AlCl_3I]^-$ powders was calculated by classical Debye-Scherrer Eq (1):

$$d = K \cdot \lambda / \beta \cdot \cos \theta \quad (1)$$

Wherein d is the crystallite size, λ is the X-ray wavelength ($\lambda=0.154$ nm), β is the width of the peak (full width at half maximum (FWHM) or integral breadth) after correcting for instrumental peak broadening (β expressed in radians) ($\beta=0.0039^\circ$), θ is the Bragg angle ($2\theta=22.7$) and K is the Scherrer constant ($K=0.9$). Whereas the crystallite size is related to the diffraction peak broadening and this method is applicable to crystallites in the range of 3–100 nm then the value of crystallite size determined from X-ray diffraction for $[(C_4H_9)_4N]^+[AlCl_3I]^-$ powders, ($d=36$ nm).

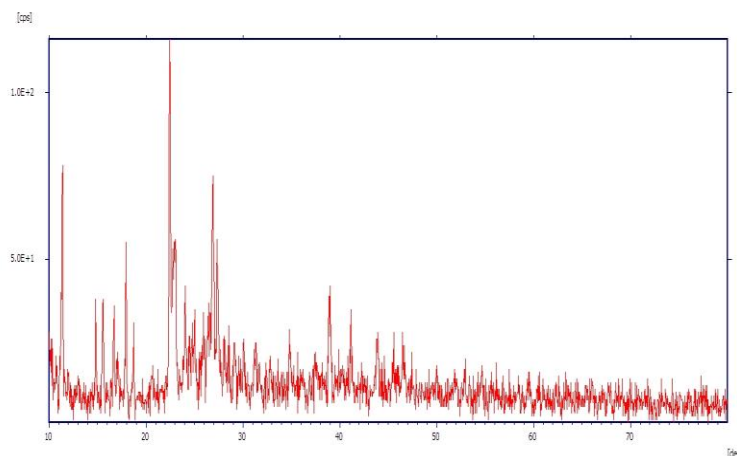


Figure 3. XRD patterns of $[(C_4H_9)_4N]^+[AlCl_3I]^-$.

Table 2. Experimental frequencies of $[(C_4H_9)_4N]^+[AlCl_3I]^-$ (cm^{-1}).

$(cm^{-1})_0$	Vibration	Intensity
	$(C_4H_9)_4N^+$	
3380	$U_{CH_2}+U_{19}$	(m, br)
3315	$U_{CH_2}+U_8$	(w, br)
3225	U_{CH_2} , asym. str	(sh)
3010	$U_{13}.U_{CH_2}$, asym. str	(w,br)
2958	U_{14} . asym. str	(w,br)
2874	$U_{14}.U_{CH_2}$, asym. str	(w,br)
2735	$U_7+ U_{16}$	(w)
2360	$U_3+ U_8+ U_{16}$	(w)
1950	$U_8+ U_{15}$	(w,br)
1475	U_{15},CH_2 ,asym.def	(ms)
1382	U_{16},CH_2 , sym. str	(s)
1158	U_{rock},CH_2 ,roking U_{14}	(m)
463	U_{19} , $U_{C_4,dif}$.	(w,br)
453	U_{19} , $U_{C_4,dif}$.	(w,br)
	$[AlCl_3I]^-$	
1061	Al-Cl	(s)
879	Al-I	(s)
885	B - I	(m)

Mass spectrometry was used to prove the structure of the notified nano aluminate complex (Figure 4.)

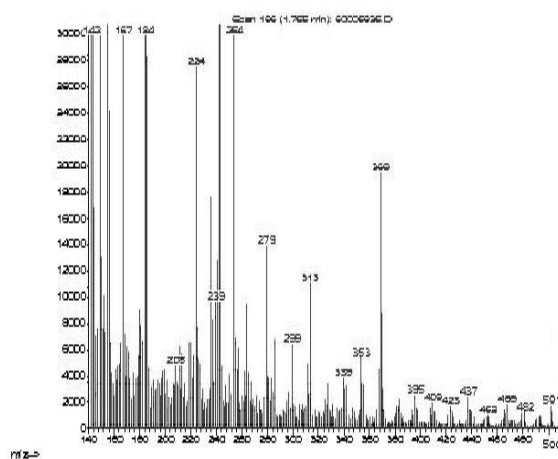


Figure 4. Mass spectra of $[(C_4H_9)_4N]^+[AlCl_3I]^-$.

Conclusion

We present the mentioned results as recommendations in order to increase information with respect to $[(C_4H_9)_4N]^+[AlCl_3I]^-$ and continue the quest for more details.

In summary, the molecular structure of $[(C_4H_9)_4N]^+[AlCl_3I]^-$ is confirmed by presence of functional groups in FTIR spectra and fragment ion in mass spectrometric. Also theoretical data show good agreement with the experimental result.

In addition, the value of crystallite size in nano scale are demonstrated by X-ray diffraction method for $[(C_4H_9)_4N]^+[AlCl_3I]^-$ nano crystalline powders.

References and Notes

- [1] Blanco, L. H.; Gomez, A.; Bermudez, G. *Acta Sud. Quim.* **1981**, *1*, 106.
- [2] Amado, E.; Blanco, L. H. *Phys. Chem. Liq.* **2000**, *38*, 451. [[CrossRef](#)]
- [3] Blanco, L. H.; Vargas, E. F. *J. Sol. Chem.* **2006**, *35*, 21. [[CrossRef](#)]
- [4] Hussey, C. L.; *Pure Appl. Chem.* **1988**, *60*, 1763. [[CrossRef](#)]
- [5] Gale, R. J.; Gilbert, B.; Osteryoung, R. A. *Inorg. Chem.* **1978**, *17*, 2728. [[CrossRef](#)]
- [6] Matsumoto, T.; Ichikawa, K. *J. Am. Chem. Soc.* **1984**, *106*, 4316. [[CrossRef](#)]
- [7] Takahashi, S.; Koura, N.; Murase, M.; Ohno, H. *J. Chem. Soc. Faraday Trans. 2* **1986**, *82*, 49. [[CrossRef](#)]
- [8] Appleby, D.; Hussey, C. L.; Seddon, K. R. *J. E. Turp Nature* **1986**, *323*, 614. [[CrossRef](#)]
- [9] Forsyth, S. A.; Pringle, J. M.; MacFarlane, D. R. *Aust. J. Chem.* **2004**, *57*, 113. [[CrossRef](#)]
- [10] Endres, F. *Chem. Phys. Chem.* **2002**, *3*, 144. [[CrossRef](#)]
- [11] Buzzeo, M. C.; Evans, R. G.; Compton, R. G. *Chem. Phys. Chem.* **2004**, *5*, 1106. [[CrossRef](#)]
- [12] Endres, F.; El Abedin, S. Z. *Phys. Chem. Chem. Phys.* **2006**, *8*, 2101. [[CrossRef](#)]
- [13] Wilkes, J. S. *Green Chemistry* **2002**, *4*, 73. [[CrossRef](#)]
- [14] Hussey, C. L. *Pure Appl. Chem.* **1988**, *60*, 1763. [[CrossRef](#)]
- [15] Verevkin, S. P.; Kozlova, S. A.; Emel'yanenko, V. N.; Goodrich, P. C. *J. Phys. Chem.* **2008**, *112*, 11273. [[CrossRef](#)]
- [16] Sheldon, R. R. *Chem. Common.* **2001**, *413*, 2399. [[CrossRef](#)]
- [17] Verevkin, S. P.; Emel'yanenko, V. N.; Toktonov, A. V.; Goodrich, P.; Hardacre, C. J. *Phys. Chem. B* **2009**, *113*, 12704. [[CrossRef](#)]

Theoretical study of structural and electronic properties of poly(vinyl chloride) nanotube inclusions

Asaad K. Edaan

Polymer Research Center (PRC), University of Basrah, Basrah-16001, Iraq.

Received: 27 February 2012; revised: 02 July 2012; accepted: 27 July 2012. Available online: 07 September 2012.

ABSTRACT: The structural and electronic properties of inclusion or interconnection between NT and PVC were studied by quantum semiempirical approximation method using (PM3) self-consistent field molecular orbital method. The total structural energy, HOMO level energy, LUMO level energy, band gap ($E_g = E_{LUMO} - E_{HOMO}$), and dipole moment of the compounds were calculated. Increasing the distance between NT and PVC led to decline the total energy difference which led to better interconnection between NT and PVC and vice versa when the distant is decreased. Therefore the more stable compound is **f**. The best electronic energies were obtained at the structures 3c and 3b in the first distance respectively. The dipole moments for all structures have the following trend: **b** > **d** > **c** > **e** > **f** > **a** > **g**.

Keywords: nanotube; PVC; PM3; HOMO; LUMO; dipole moment

Introduction

Poly(vinyl chloride) (PVC) is an important commercial thermoplastic, which is widely used as pipes, electric cables, building materials and other civilian products [1, 2]. PVC is used in many domestic and industrial applications in different forms such as composites, copolymers, and blends [3]. Low thermal stability, poor processability and brittleness are the main reasons behind the limitation of using PVC in some applications [4]. Polymer nanocomposites have unique properties over normal composites (short and long fibers) such as nanoparticle inclusion effect on the polymer brush configuration and free energies which depends strongly on inclusion shape, size, and inclusion location in

* Corresponding author. E-mail: asaad_kareem2000@yahoo.com

the brush [5].

PVC is an important for the occurrence of structural defects [6]. PVC has many important applications such as employed in the field of sensors based on their membranes [7], and can be used as a matrix material for low-temperature photochemical studies [8]. Another study indicated that the conversion is depending on defect structures in radical suspension polymerization of vinyl chloride, which proved that the polymer-rich phase becomes extremely dense, making the diffusion coefficient of the monomer much lower than that in the monomer-rich phase, which led to substantial reduction in the propagation rate, thereby allowing the chain-transfer processes to compete more effectively [9]. The physical properties and the morphology of PVC resins are depending on their microstructures, which are function of the distributions and concentrations of internal double bonds, branches, and the relative configurations of the stereogenic centers [10]. The Effect of different feeding methods of the monomers and initiators on the morphology properties of core-shell particles such as the deformation of PVC/MBS2 blend led to absorb massive impact energy, and MBS2 led to enhance the toughness properties of PVC matrix efficiently [11]. The molecular weight and its relationship to the internal double bonds in PVC at various monomer conversions have been studied. The concentration of these defects structure per chain was largely constant as a function of molecular weight [12].

During the recent period, there are number of studies on PVC polymer like nanoclay-fillers [13, 14], dispersing of nano-sized silica (SiO_2) in PVC-blend-based polymer electrolytes which may be a potential candidate for all solid lithium rechargeable batteries [15], to improve the thermal and mechanical properties of PVC. Specific interfacial interactions between the π -electronic system of carbon nanotube CNT and the polymer functional groups (CNT based polyacrylonitrile (PAN) composites), which shown to be effective when stable uniform dispersions of carbon nanotubes were obtained with the aid of surfactants having multiple unsaturated carbon bonds, as a result of the unique set of properties of (CNT) [16]. Glass transition temperature and melting temperature are an increase for the composites of multiwalled carbon nanotube (MWCNT)/PVC with respect to pure PVC, and the modulus of the MWCNT/PVC composites increased while there was a reduction in their tensile strength, pointing out a decrease in polymer toughness [17]. In the same context, for the segregated system PVC/MWNT, it was found that the conductivity and magnetic properties of the system are depending on concentration of the nanotubes in wide temperature and frequency ranges [18]. The use of MWNT-PVC composite coated wire electrode allows the electrochemical detection by potentiometric method [19]. Increasing in glass transition temperature (T_g) of PVC was observed with increasing in the contain of MWCNT [20].

The characterization of defects in (PVC) was investigated theoretical-experimental by combining quantum chemical calculations (DFT) and NMR chemical shifts measurements [10]. However, nano inclusions can be chosen as insulators to lower the thermal conductivity and scatter carriers which reduce the electrical conductivity [21]. One of the important theoretical researches on the nano inclusions is molecular dynamics (MD) simulations of effects of different kinds of nano inclusions (bucky-ball, graphene, single-walled-carbon-nanotube (SWNT), X-shaped SWNT junction and Y-shaped SWNT junction) into polyethylene (PE) matrices on structural and physical properties of PE matrices [22].

The main objective of this study is to investigate the physical properties of different types of nanotube conformations with PVC using computational quantum methods, by semiempirical PM3 (Parameterized Austin Model 3).

Material and Methods

Computational procedure

Semiempirical methods can be defined by the set of approximations used and by the values of the parameters [23]. Calculations on the electronic and structural properties of our model were carried out using (PM3) self-consistent field molecular orbital method [24-26]. All calculations were performed using the Gaussian 09 package [27]. The electronic properties such as highest occupied molecular orbital (E_{HOMO}) energy, lowest unoccupied molecular orbital (E_{LUMO}) energy, and the energy gap ($E_g = E_{\text{LUMO}} - E_{\text{HOMO}}$), the dipole moment (μ) were calculated.

Results and Discussion

Structure determination

Our model consists of five optimized units of Carbon Nanotube (NT) with length (11.065 \AA) and radius (8.135 \AA) as in Figure 1 and five optimized units (monomer) of the PVC as in Figure 2. The electronic and structural properties were calculated without any geometry constraints for full geometry optimizations. First structure was a chain of PVC in the middle of NT by distances ($1.918, 2.416, 2.915, 3.414, \text{ and } 3.913 \text{ \AA}$) between PVC chain and NT as shown in Figure 3a with an increase of 0.5 \AA after each distance. The second structure was a PVC chain parallel to NT with distances ($1.419, 1.919, 2.419, 2.919 \text{ and } 3.419 \text{ \AA}$ respectively) between PVC chain and NT as can be seen in Figure 3b with an increase of 0.5 \AA after each distance. With regard to structures 3c, 3d and 3e, the process and the distance between NT and PVC chain are the same in the second structure, except increasing three, four, and five chains of PVC related to the NT as shown in Figures 3c, 3d and 3e respectively.

Structures, **3f** and **3g**, the chain of PVC are parallel to the ends of NT with distances (2.580, 3.080, 3.533, 3.998, and 4.470Å) between the PVC chain and NT as demonstrated in Figure **3f** and **3g** respectively.

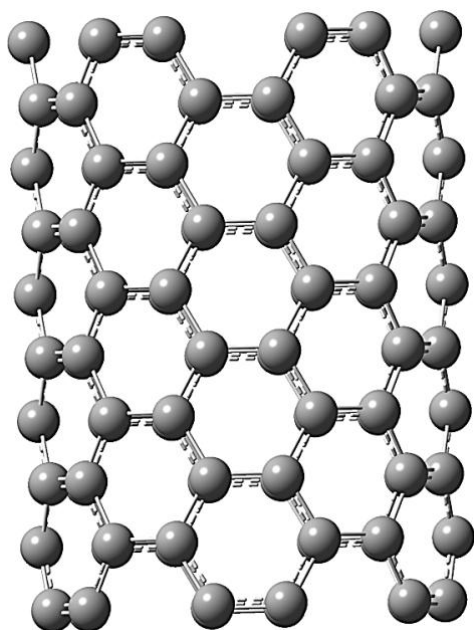


Figure 1: Nanotube structure (NT)

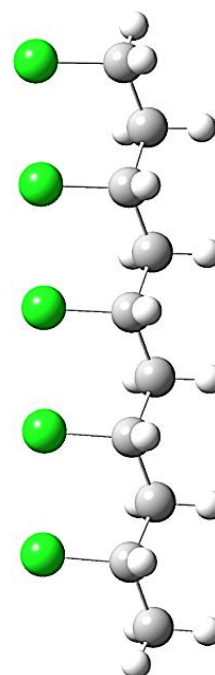


Figure 2: PVC structure

Structural Energy

The results of the total structural energy as a function of distance for all studied structures are shown in the Figure 4. The structural energy in the form of energy difference between the total energy of the system (NT-PVC), total energy of (NT) and total energy of (PVC) was calculated using Equation 1.

$$\Delta E_{Total} = (E_{NT-PVC}) - (E_{NT}) - (E_{PVC}) \quad (1)$$

According to the calculations, the highest energy differences 4.280, and 4.057 a.u were obtained of **3d** and **3e** structures respectively in the distance 1.419Å. The energy difference for **3c**, **3b**, **3a**, **3g**, and **3f** structures decrease in turn to reach the lowest value of 0.0537 a.u was found in the structure **3f** at distance 4.470Å. Generally, energy difference decreases connected with increasing in the distance NT-PVC and contradictory result was found with decreases the distance. As a conclusion, the large energy difference led to more stable structure. However, small energy differences produce more facility of NT-PVC formation.

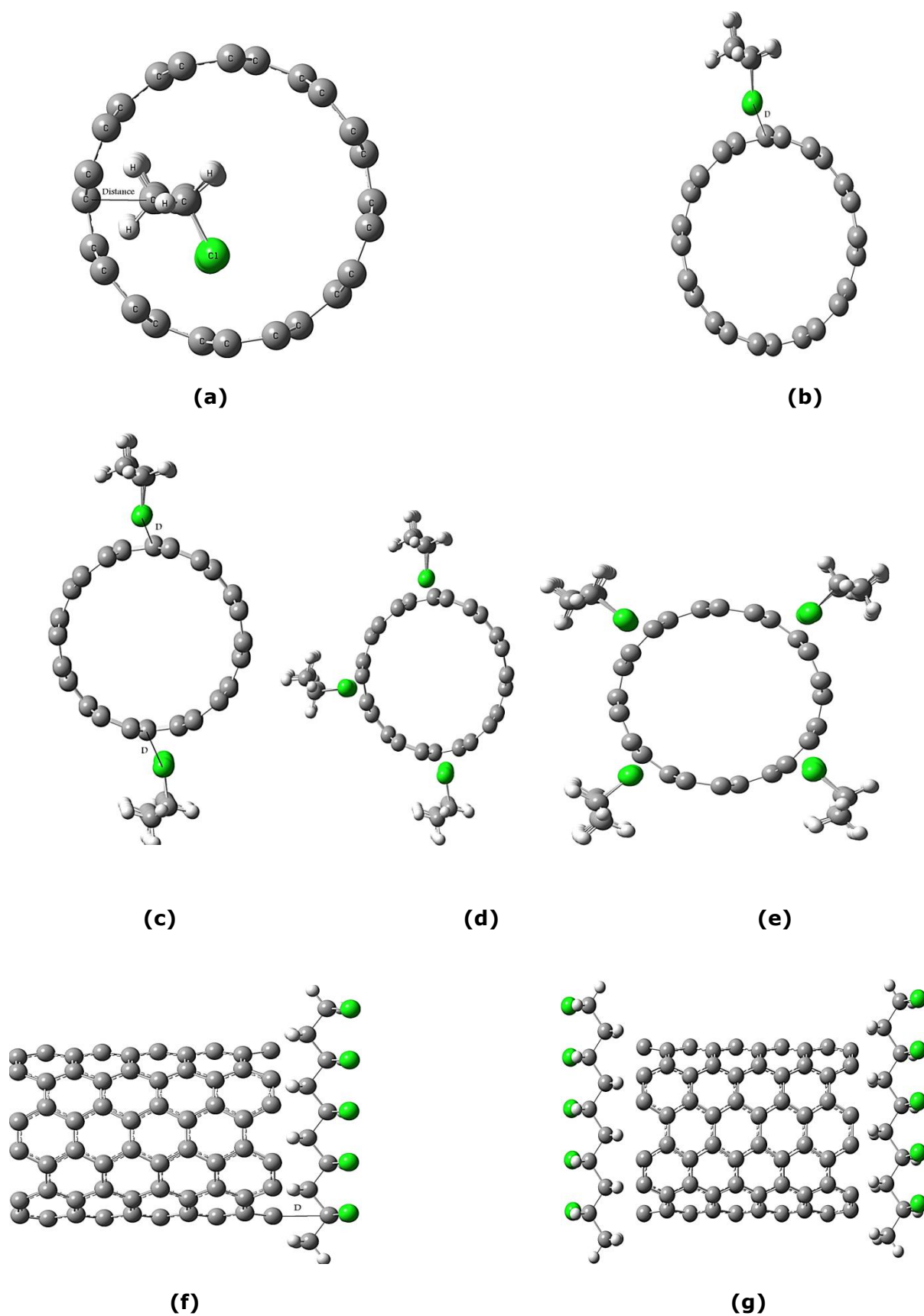


Figure 3. (a) PVC in the middle of nanotube NT with different distances (D), (b) 1 PVC chain parallel to NT, (c) 2 PVC chains parallel to NT, (d) 3 chains of PVC- parallel to NT, (e) 4 chains of PVC parallel to NT, (f) PVC is parallel to the ends of NT, (g) two chains of PVC are parallel to the ends of NT.

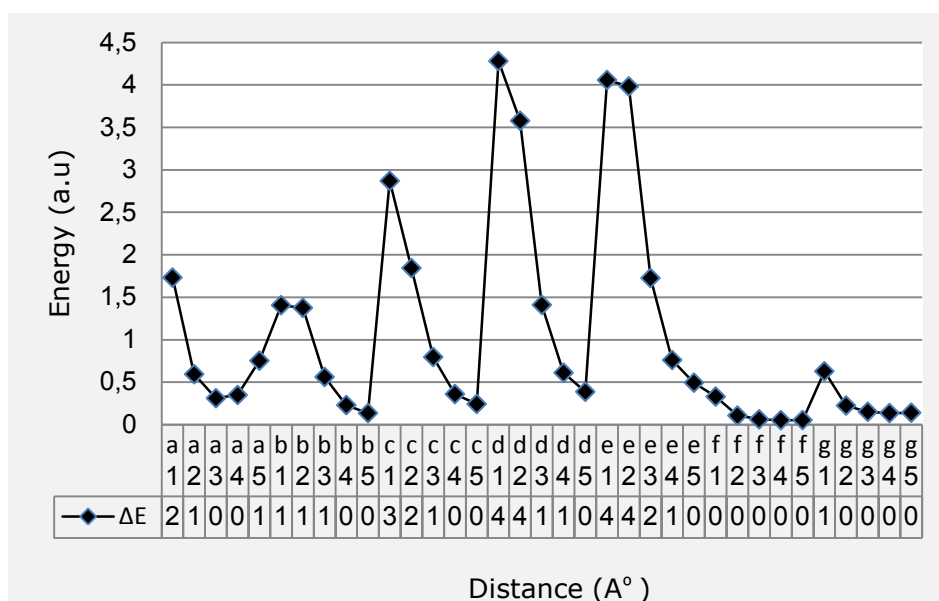


Figure 4. Total energy as a function of distance of NT-PVC inclusions

Electronic Properties

The results of electronic energies of compounds are shown in the Figure 5. The values of occupied molecular orbital (E_{HOMO}) and unoccupied molecular orbital (E_{LUMO}) were discussed with regardless to their sing. The result indicated that the highest E_{HOMO} energy has the highest value of -7.850 eV at **3g-4** (fourth distance) and the lowest value of -6.437 eV at **3d-1** (first distance), while the lowest E_{LUMO} energy has the highest value of -3.752 eV at **4g-4** (fourth distance) and the lowest value of -1.387 eV at **3e-1** (first distance). The energy gap ($E_g = E_{\text{LUMO}} - E_{\text{HOMO}}$) has the highest value of 5.325 eV at **3e-1** (first distance) and the highest value of 2.873 eV at **3d-1** (first distance). This means that the best electronic energies were obtained at the compound **E1** and **3d-1** (first distance). The comparison between these energies with the energies of NT [$(E_{\text{HOMO}} = -7.630 \text{ eV})$, $(E_{\text{LUMO}} = -3.527 \text{ eV})$ and $(E_g = 4.102 \text{ eV})$] and the energies of PVC [$(E_{\text{HOMO}} = -7.9163 \text{ eV})$, $(E_{\text{LUMO}} = 1.324 \text{ eV})$ and $(E_g = 9.241 \text{ eV})$] both separately is leading to find out that NT energies have the greatest influence in the system. Finally was found out that the high energy of LUMO suggests a high stability.

Dipole Moment

The most important parameters affecting the electric charge transport properties of polymers are the Dipole Moments (μ). The electrical conductivity of a polymer chain is altered when its orientation and consequently its symmetry and non-isotropic interactions are changed [28]. It can also be seen in Figure 6 that the dipole moments for all compounds have the following order: **b** > **d** > **c** > **e** > **f** > **a** > **g**. The dipole moment for structures **b** and **d** is greater than other structures. The polarization and

distance are affecting the value of dipole moment. The biggest value of dipole moment of 24.298 Deby was detected with **b** structure specifically in the first distance **3b-1** while the lowest dipole moment of (0.287 Deby was detected with **C** compound in the first distance **c-5**. This effect can be ascribed to quite strong polarization of the structure between the electron donating – electron accepting of NT – PVC. These characteristics increase the efficiency of electrochemical polymerization processes of these compounds [28].

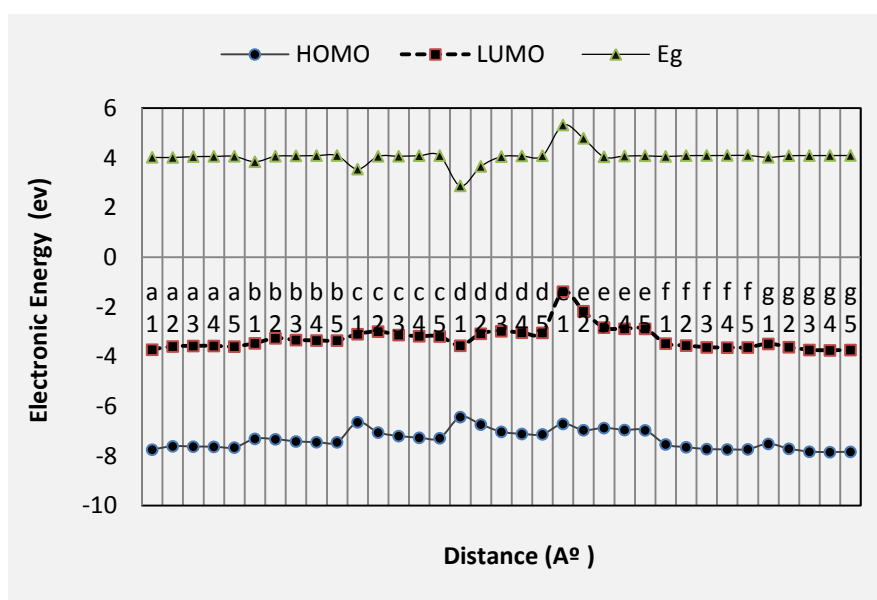


Figure 5. Electronic energies as a function of distance of NT-PVC inclusions

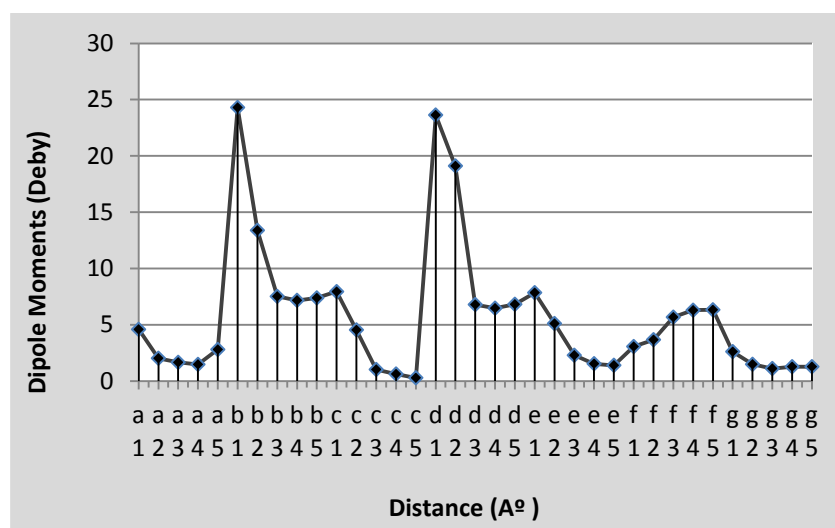


Figure 6. Dipole Moment as a function of distance of NT-PVC inclusions

Conclusion

The inclusion process between NT and PVC and the possible obtaining of new stable structures were studied using quantum mechanical PM3 method. The distances

between NT-PVC interconnections were found to have a direct effect on the system total energy. Comparison with the energies of NT and PVC the best electronic energies were obtained at the compound **e-1** and **d-1**. The strong polarization between the electron donating – electron accepting of NT – PVC led to the biggest value of dipole moment for compound **b** in the first distance **b-1**. In addition, any further characteristics of the structures and the stability of these complexes can be performed by taking into consideration the polarization effect in process calculation.

References and Notes

- [1] Wang, G.; Qu, Z.; Liu, L.; Shi, Q.; Guo, J. *Mater. Sci. Eng., A* **2008**, 472, 136. [[CrossRef](#)]
- [2] Zhonghou, Z.; Yingying, L.; Chunmian, Y.; Guangxiu, C. IEEE International Conference on Consumer Electronics, Communications and Networks (CECNet), **2011**, 1391. [[Link](#)]
- [3] Fakhreia, A.; Zahoor, A. *Sol-Gel Sci. Technol.* **2012**, 61, 229.
- [4] Liu, C.; Luo, Y. F.; Jia, Z. X.; Zhong, B. C.; Li, S. Q.; Guo, B. C.; Jia, D. M. *Express Polymer Letters*, **2011**, 5, 591. [[CrossRef](#)]
- [5] Jaeup, U. K.; Ben, O. *Macromolecules* **2006**, 39, 413. [[CrossRef](#)]
- [6] William, H. S. J. *J. Polym. Sci. Part A: Polym. Chem.* **2005**, 43, 2451. [[CrossRef](#)]
- [7] Siavash, R.; Mir, F. M.; Zahra, S. B.; Mojtaba, S. *Anal. Chim. Acta*, **2005**, 548, 192. [[CrossRef](#)]
- [8] Thomas, E. B. *Inorg. Chim. Acta* **2008**, 361, 1319. [[CrossRef](#)]
- [9] Jindra, P.; Kim, F. D. P.; Wendy, V. Z.; Eltjo, J. V.; Arend, J. S.; Michelle, L. C. *Macromolecules*, **2005**, 38, 6352. [[CrossRef](#)]
- [10] Philippe, D.; Edith, B.; Benoit, C.; Joris, W.; Marie-Francoise, R.; Guy, B. M.; Peter, J. A.; Jan, M. *Chem. Phys. Lett.* **2007**, 436, 388. [[CrossRef](#)]
- [11] Si, Q. B.; Zhou, C.; Yang, H. D.; Zhang, H. X. *Eur. Polym. J.* **2007**, 43, 3060. [[CrossRef](#)]
- [12] Jindra, P.; Kim F. D. P.; Michela, A.; Maarten, B.; Eltjo, J. V.; Arend, J. S.; Michelle, L. C. *Macromolecules*, **2008**, 41, 5527. [[CrossRef](#)]
- [13] Xu, W.; Zhou, Z.; Ge, M.; Pan, W. *Therm. Anal. Calorim.* **2004**, 78, 91. [[CrossRef](#)]
- [14] Gong, F.; Feng, M. H. C.; Shang, S.; Yang, M. *Polym. Degrad. Stab* **2004**, 84, 289. [[CrossRef](#)]
- [15] Ramesh, S. A. K. A. *J. Mater. Sci.* **2009**, 44, 6404. [[CrossRef](#)]
- [16] Linda, V.; Ellen, W.; Daniel, H. W.; Gad, M. *Polymer*, **2007**, 48, 6843. [[CrossRef](#)]
- [17] Mkhabela, V. J.; Mishra, A. K.; Mbianda, X. Y. *Carbon* **2011**, 49, 610. [[CrossRef](#)]
- [18] Mamunya, Y. P.; Levchenko, V. V.; Rybak, A.; Boiteux, G.; Lebedev, E. V.; Ulansk J.; Seytre, G. *J. Non-Cryst. Solids* **2010**, 356, 635.
- [19] Abdolkarim, A.; Anahita, I. *Talanta* **2007**, 71, 887. [[CrossRef](#)]
- [20] Sterzynski, T.; Tomaszewsk, J.; Piszczek, K.; Skórczewska, K. *Composites Science and Technology*, **2010**, 70, 966. [[CrossRef](#)]
- [21] Ting, Z.; Qiushi, Z.; Jun, J.; Zhen, X.; Jianmin, C. *Appl. Phys. Lett.* **2011**, 98,

22104. [[CrossRef](#)]
- [22] Ying, L. *Polymer* **2011**, *52*, 2310. [[CrossRef](#)]
- [23] James, J. P. S. *J. Mol. Model.* **2004**, *10*, 155. [[CrossRef](#)]
- [24] James, J. P. S. *J. Comp. Chem.* **1989**, *10*, 209. [[CrossRef](#)]
- [25] James, J. P. S. *J. Comp. Chem.* **1989**, *10*, 221. [[CrossRef](#)]
- [26] James, J. P. S. *J. Comp. Chem.* **1991**, *12*, 320. [[CrossRef](#)]
- [27] Frisch, M. J.; Trucks, G. W.; Schlegel, H. B.; Scuseria, G. E.; Robb, M. A.; Cheeseman, J. R.; Scalmani, G.; Barone, V.; Mennucci, B.; Petersson, G. A.; Nakatsuji, H.; Caricato, M.; Li, X.; Hratchian, H. P.; zmaylov, A. F.; Bloino, J.; Zheng, G.; Sonnenberg, J. L.; Hada, M.; Ehara, M.; Toyota, K.; Fukuda, R.; Hasegawa, J.; Ishida, M.; Nakajima, T.; Honda, Y.; Kitao, O.; Nakai, H.; Vreven, T.; Montgomery, Jr., J. A.; Peralta, J. E.; Ogliaro, F.; Bearpark, M.; Heyd, J. J.; Brothers, E.; Kudin, K. N.; Staroverov, V. N.; Kobayashi, R.; Normand, J.; Raghavachari, K.; Rendell, A.; Burant, J. C.; Iyengar, S. S.; Tomasi, J.; Cossi, M.; Rega, N.; Millam, J. M.; Klene, M.; Knox, J. E.; Cross, J. B.; Bakken, V.; Adamo, C.; Jaramillo, J.; Gomperts, R.; Stratmann, R. E.; Yazyev, O.; Austin, A. J.; Cammi, R.; Pomelli, C.; Ochterski, J. W.; Martin, R.L.; Morokuma, K.; Zakrzewski, V. G.; Voth, G. A.; Salvador, P.; Dannenberg, J. J.; Dapprich, S.; Daniels, A. D.; Farkas, O.; Foresman, J. B.; Ortiz, J. V.; Cioslowski, J.; Fox, D. J. Gaussian, Inc., Wallingford CT, 2009.
- [28] Hossein, S. I. B.; Saeed, J. *Chemistry Central Journal*, **2011**, *5*, 13. [[CrossRef](#)]

Equilibrium adsorption of rhodamine B on used black tea leaves from acidic aqueous solution

M. Abul Hossain* and M. Atiqur Rahman

Department of Chemistry, University of Dhaka, Dhaka-1000, Bangladesh.

Received: 03 August 2012; revised: 24 August 2012; accepted: 30 August 2012.
Available online: 14 September 2012.

ABSTRACT: The presence of carcinogenic dye like rhodamine B (Rh-B) in textile wastewater affects the quality of water to consumers. The adsorption of Rh-B on used black tea leaves (UBTL) was studied in batch process to investigate its removal efficiency. The effects of contact time, concentration, temperature, pH etc. on adsorption have been investigated. The UV-visible spectrophotometer was used for analysis of Rh-B at constant pH. The adsorption isotherms were constructed for different temperatures using acidic solution of pH 2.0. Freundlich, Langmuir and Dubinin–Raduskevich (D-R) equations were used to analyze the equilibrium adsorption data. The experimental data follows Freundlich equation more precisely compare with the Langmuir one. The maximum amount adsorbed calculated from Langmuir equation is 72.5 mg/g at 30 °C which is increased with increasing temperature. Separation factor and thermodynamic parameters revealed that the process is favorable, spontaneous and endothermic nature. Possible mechanism of the process was elucidated from the effect of solution pH on amount adsorbed. The endothermic nature of the adsorption might be due to the fragmentation of Rh-B molecules during the adsorption process.

Keywords: rhodamin B; adsorption; tea leaves; isotherms; pH; thermodynamics; mechanism

Introduction

Removal of dyes from textiles effluents is very important for their strong aromatic forms containing trace alkali, acid and carcinogenic metals. Rhodamine B (Rh-B) is a fluorone dye which is used as a dye and as a dye laser gain medium [1]. It is often used as a tracer dye within water to determine the rate and direction of flow and transport. Rh-B is suspected to be carcinogenic and thus products containing it must contain a warning on its label [2]. Thus the existence of Rh-B in waste water leads to a serious

* Corresponding author. E-mail: hossainabul@yahoo.com

environmental problem.

Different methods of color removal from industrial effluents are biological treatment, coagulation, floatation, adsorption, oxidation and filtration etc [3]. Among the treatment options, adsorption appears to have considerable potential for the removal of color from industrial effluents due to its fewer amounts of sludge and clean operation. The removal of color by various adsorbents has been the subject of several recent researches. Activated carbon is perhaps the most widely used adsorbent for the removal of many organic contaminants which are biologically resistant. But activated carbon is prohibitively expensive. Consequently, the high cost of activated carbon, coupled with the problems associated with regeneration, has necessitated the search for alternative adsorbents. Agricultural waste materials such as baggage pith, saw dust, pine bark, maize cob, rice hull, coconut husk fibers, nut shells, soyabean and cotton seed hulls [3, 4] have been evaluated as low cost adsorbents for removal of dyes and other toxic heavy metals. But their adsorption capacities (less than 40 mg/g-adsorbent), however, are far smaller than activated carbon. Therefore, there is a need for the development of low cost, highly efficient and easily available materials, which can adsorb high amount of dye from aqueous solution.

Used black tea leaves (UBTL) is considered as a low cost adsorbents for removal process because of its high adsorption capacity [5]. It has been observed that for the removal of Cr(VI) from aqueous solution at low pH (1.5-2.0), the maximum adsorption capacity (454 mg/g) of UBTL, is nearly equal to that of activated carbons (350-460 mg/g) [6]. Again, used tea leaves are available as a byproduct of tea industry. Another important fact is that after adsorption, UBTL can easily be destroyed and the adsorbed adsorbate can be recollected from solution [5]. As a result, no secondary pollutant is produced. That is why in our laboratory, UBTL was used previously as an adsorbent for removal of Cr(VI) and Pb(II) from aqueous solutions [5, 7]. In the present study we were interested to remove Rh-B from aqueous acidic solution using used black tea leaves (UBTL) as a low cost adsorbent. Keeping this in mind, the adsorptive characteristics of Rh-B on UBTL was studied by investigating optimum pH, equilibrium time, and the effects of concentration, temperature and solution pH on adsorption.

Material and Methods

Materials

All chemicals used in this study were of analytical grade. Double distilled water was used for preparing different reagents. Commercial grade Rhodamine B (Rh-B) was collected from local market in Dhaka. The chemical formula of the Rh-B is $C_{28}H_{31}N_2O_3Cl$ and molecular mass is 479.02 g. IUPAC name of Rh-B is [9-(2-carboxyphenyl)-6-

diethylamino-3-xanthenylidene]-diethyl ammonium chloride and CAS number is 81-88-9. Synonyms of Rh-B are Rhodamine O, Tetraethyl rhodamine and Rhodamine 610. C. I. Name and number of Rh-B are Basic Violet 10 and 45170, respectively. The structural formula of Rh-B is shown in Figure 1. Rh-B is an amphoteric dye and is highly soluble in acidic media. Since Rh-B adsorb to plastics, solutions were kept in glass bottles [8]. Fresh black tea leaves were collected from Islampur market, Dhaka, Bangladesh.

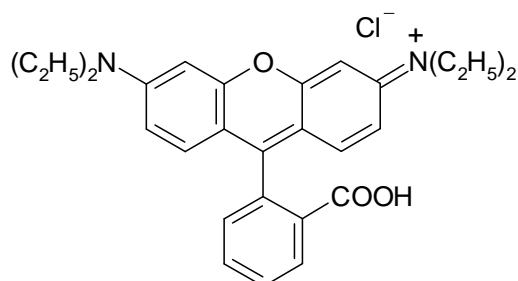


Figure 1. Structure of Rhodamine B.

Preparation of adsorbent

About 200 g of fresh black tea leaves were boiled in 700 mL of distilled water for 2 hours. Boiled tea leaves were washed 3 times with hot distilled water followed by cold distilled water in several times until the tea liquor was completely disappeared. After washing, tea leaves were initially dried at room temperature and then were dried in an oven (NDO-450, EYELA, Japan) at 103 °C for 10 hours. Prepared used black tea leaves (UBTL) were sieved through the metallic sieve with different particle sizes and different particle sizes was kept in an air-tight bottle. The surface morphology of prepared UBTL (425-500 μm) was investigated by a Scanning Electron Microscope (JSM-6490LA, JEOL, Japan), at 25 kV acceleration voltages. Before analysis, UBTL was platinum coated using a Pt-coated Auto system (JFC-1600, JEOL, Japan) to improve electron conductivity and image quality. Figure 2 shows the SEM micrograph of UBTL with 2000 \times image magnification.

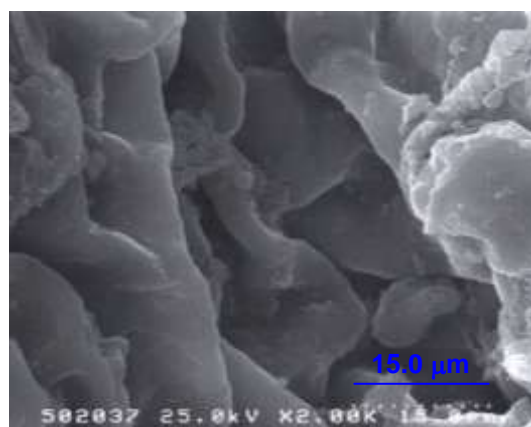


Figure 2. SEM micrograph of prepared UBTL with 2000 \times magnification.

Analysis of adsorbate

A stock solution of 500 mg/L Rh-B solution was prepared by dissolving required amount of commercial grade Rhodamine-B in distilled water. Quantitative analysis of Rh-B in solutions was performed using UV-visible spectrophotometer (Model-1650 PC, Shimadzu, Japan). For construction of calibration curve, a series of different concentrated Rh-B solutions were prepared by required dilution of stock solution and the pH of each solution was adjusted at a definite value of 2.0 using 0.1 mol/L HNO₃ or 0.1 mol/L NaOH solution. The absorbance of different concentrated Rh-B solutions at pH 2.0 was measured at the predetermined wavelength of absorption maxima (λ_{\max}) of 554.0 nm. Beer-Lambert law was verified by plotting the measure absorbance against the concentration of Rh-B within the range of 0.06 to 9 mg/L (figure not shown). The calibration curve at pH 2.0 was used to determine the concentration of Rh-B in different solutions of before and after adsorption.

Adsorption experiments**Selection of solution pH**

For the selection of solution pH, 0.1 g of UBTL was taken in each of the six reagent bottles. 50 mL of 9.1 mg/L Rh-B solutions was taken in each of 6 bottles. The bottles were placed in a thermostatic mechanical shaker (SW B-20, Fisons Ltd. Germany), maintained at 30 °C and were shaking continuously for four hours. The reagent bottles were withdrawn from the shaker and the solutions in bottles were separated from UBTL by centrifuged. After centrifuge, the pH of supernatants was measured. The difference of pH from the initial values was estimated as ΔpH . A plot of ΔpH vs initial pH produces a curve, which intersects the X-axis at two points as shown in Figure 3.

Determination of equilibrium time

To determine the equilibrium time, 0.1g of UBTL was taken in 50 mL of 9.5 mg/L Rh-B solution in each of the series of adsorption bottles. Before addition of UBTL, pH of Rh-B solution was adjusted at selected pH 2.0 by drop-wise addition of 0.1 mol/L HNO₃ or 0.1 mol/L NaOH solution. All bottles were shaken in a thermostated mechanical shaker (SW B-20, Fions Ltd. Germany). The bottles were individually taken out from the shaker after different time of interval such as 15, 45, 60, 120, 240 and 480 minutes of shaking. After adsorption, the UBTL was separated from solutions and the final pH of each solutions was checked, which showed that the pH of the solution did not change. The separated solutions were diluted as required concentration in calibration limit and pH of the diluted solutions were adjusted at 2.0 before measuring their absorbance at 554.0 nm, due to the construction of calibration curve at pH 2.0. The experiment was

performed at the temperature of 30°C. The amounts of Rh-B adsorbed on to UBTL at different contact times were calculated using the following Eq: (1)

$$q_t = (C_i - C_t) \times \frac{V}{W} \quad (1)$$

where C_i and C_t are the concentrations of Rh-B (mg/L) at zero time and at time t , respectively. V is the volume of solution in liter and W is the mass of the dry UBTL in g. The amount adsorbed is plotted against the contact time as shown in Figure 4.

Adsorption isotherms at different temperatures

For the determination of adsorption isotherm at pH 2.0, 7 adsorption bottles containing each of 0.1 g UBTL into 50 mL Rh-B solution of various concentrations ranging from 10 to 500 mg/L have been shaken at 30 ± 0.5 °C for 240 minutes which was equilibrium time as described in last section. After equilibrium adsorption, the residual concentrations of Rh-B in each bottles, were analyzed by UV-vis spectrophotometric method. The equilibrium concentrations were determined for different initial concentrations of Rh-B, and respective amounts adsorbed were calculated from adsorption data. To obtain adsorption isotherms at different temperatures, similar experiments were repeated at temperatures 40 and 50 °C. Each temperature was controlled within ± 0.5 °C. Adsorption isotherms at different temperatures are shown in Figure 5. Standard thermodynamic parameters for the adsorption of Rh-B on UBTL were determined from the adsorption isotherms at different temperatures.

Effect of pH on adsorption

To determine the effect of pH on the adsorption of Rh-B on UBTL, 0.1g UBTL was taken in each of the four adsorption bottles. 50 mL of about 100 mg/L Rh-B solution, whose pH was maintained at 2.0, 4.0, 6.0 and 8.0 by addition of 0.1 mol/L HNO₃ or 0.1 mol/L NaOH solution, was added to each of the four bottles. All bottles were shaken in a thermostated mechanical shaker at 30 °C for 4 hours. After adsorption, the UBTL was separated from each solution. The separated solutions were diluted as required concentration within calibration limits and pH of the diluted solutions were adjusted at 2.0 before measuring their absorbance at 554.0 nm, due to the construction of calibration curve at pH 2.0. In similar way, the concentrations of initial solutions prepared at different pH were determined by measuring the absorbance at pH 2.0 with proper dilution. The amounts adsorbed of Rh-B on UBTL for different initial pH of solutions were determined using equation (1). The amounts adsorbed are plotted against the initial pH of solutions.

Results and Discussion

Characteristics of adsorbent

Used black tea leaves (UBTL) was selected as a low cost adsorbent for the adsorption of Rhodamine B. The constituents of black tea leaves are polyphenones, flavones, polysaccharides, cellulose and hemicelluloses, protein, lipids, lignin, caffeine, etc [9]. The continuous treatment of black tea leaves by boiling water brings a considerable change in composition while preparing used black tea leaves (UBTL). Cellulose, hemicelluloses and lignin are the main composition of prepared UBTL [5]. The SEM microgram of UBTL shows in Figure 2 is a heterogeneous surface indicating the possibility to adsorb Rh-B on different parts of UBTL surface.

Selection of solution pH

It is very important to select the solution pH at a suitable value to use for adsorption experiments. Since adsorption is a surface phenomenon, pH of the solution should be change due to the protonation or deprotonation of surface in acidic or basic media. Again, the nature of adsorbate also changes with solution pH. Therefore, the initial pH of solution should be change during adsorption process. Minimum change of pH is required for investigating the adsorption mechanism. Figure 3, a plot of change of pH as a function initial pH, shows the minimum change of pH is at 2.0 and 6.0, which are considered as the optimum pH for this adsorption. Previous studies had been reported that the UBTL is highly stable and acts as good adsorbent in acidic media [5]. For this reason, pH 2.0 was selected for the adsorption Rh-B from aqueous solution on UBTL.

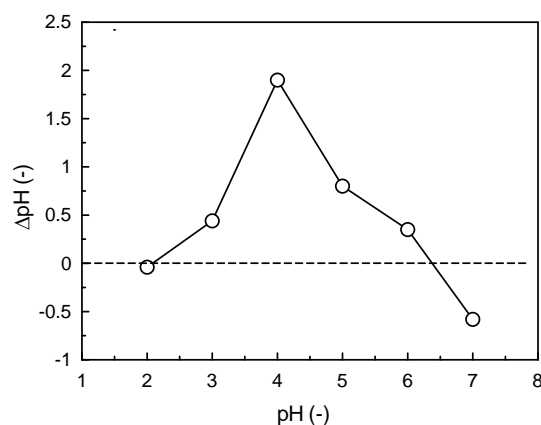


Figure 3. A plot of ΔpH vs. initial pH for determination of optimum pH at 30.0 ± 0.5 °C.

Estimation of equilibrium time

Equilibrium time is another important parameter for adsorption study which is indicated the adsorption and desorption became steady. For the determination of equilibrium time, the adsorption kinetic experiment was carried out for four hours at 30 °C. Maximum concentration of Rh-B solution was considered to be 500 mg/L at pH 2.0

and the amount of UBTL was taken for this experiment was 0.1 g for 50 mL Rh-B solution. Under these conditions the equilibrium time for the adsorption of Rh-B on UBTL was not found to be four hours (Figure 4). This was because after four hours the change of concentration with time was small but not steady. To confirm the fact that Rh-B adsorbed on UBTL after four hours, the adsorption experiment was continued for eight hours (Figure 4) but still equilibrium has not been achieved. It has been reported that the equilibrium time for the adsorption of Cr (VI) on UBTL is 15 days [10]. So for the present system four hours was taken as contact time where most of adsorption taken place, which was considered as pre-equilibrium time.

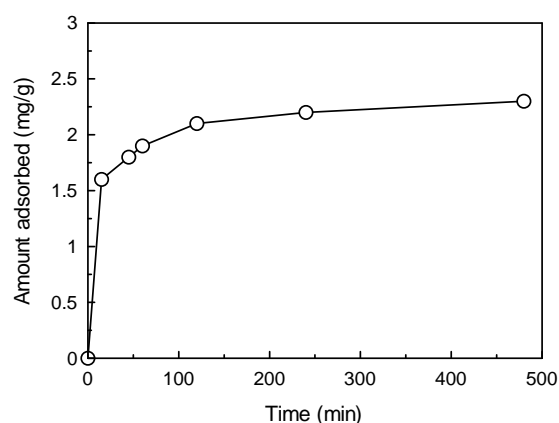


Figure 4. Change of amount adsorbed with time for the adsorption of Rh-B on UBTLs at pH 2.0 and 30.0 ± 0.5 °C.

Analysis of adsorption isotherms at different temperatures

Adsorption isotherm is the most important criteria for understanding an adsorption process. The adsorption isotherm was determined using four hours of equilibrium time and solution pH was at 2.0. Figure 5 shows the adsorption isotherms of Rh-B on UBTL at three different temperatures of 30, 40 and 50 °C. In all cases, the amount adsorbed increases with the increase of equilibrium concentration. To analyze the adsorption isotherms, the most commonly used equilibrium relations, Freundlich and Langmuir equations, were applied to the equilibrium data at different temperatures [11, 12]. The linearized form of Freundlich (2) and Langmuir (3) isotherm can be written as follows:

$$\log \frac{x}{m} = \log k_F + \frac{1}{n} \log C_e \quad (2)$$

$$\frac{C_e}{q_t} = \frac{1}{q_m b} + \frac{C_e}{q_m} \quad (3)$$

where, $q_e = x/m$ = amount adsorbed at equilibrium time (mg/g), k_F = proportionality

constant, C_e = equilibrium concentration of adsorbate in solution (mg/L) and n = Freundlich constant, referred to the intensity of adsorption (for favorable adsorption, n value falling in the range of 1-10), q_m (mg/g) and b (L/mol or L/mg) are the Langmuir constants related to the complete monolayer or maximum adsorption capacity and the energy (or enthalpy) of adsorption, respectively [13]. Figures 6 and 7 show the linear plots of $\log(x/m)$ versus $\log C_e$ and C_e/q_e versus C_e to evaluate the applicability of Freundlich and Langmuir model equations, respectively, for the adsorption of Rh-B on UBTL at different temperatures. The calculated Freundlich and Langmuir constants and their corresponding linear regression correlation coefficient values (R^2) from experimental results at different temperatures are given in Table 1.

Table 1 Freundlich, Langmuir and Dubinin-Radushkevich parameters for the adsorption of Rh-B on UBTL at pH 2.0 for different temperatures

T (°C)	Freundlich parameters			Langmuir parameters			Dubinin-Radushkevich (D-R) Parameters			
	k_f	$1/n$	R^2	q_m (mg/g)	b (L/mg)	R^2	$q_m \times 10^4$ (mol/g)	β (mol ² /kJ ²)	E (kJ/mol)	R^2
30	4.41	0.455	0.992	72.46	0.0138	0.956	4.14	36.8	0.1166	0.997
40	4.88	0.492	0.968	92.59	0.0108	0.970	6.36	37.4	0.1156	0.984
50	6.95	0.592	0.977	185.18	0.0054	0.971	7.82	39.9	0.1120	0.993

The results show that the adsorption isotherms at pH 2.0 for different temperatures are well fit with Freundlich model compared with the Langmuir one within the used concentration range. The maximum adsorption capacity, q_m obtained from Langmuir isotherm is 72.46 mg/g at 30 °C which is increased to 185.2 mg/g with increasing temperature to 50 °C but the adsorption intensity constant, b decreases with increasing adsorption temperature. Generally, in case of chemical interaction: the amount adsorbed increases with increasing temperature and the adsorption intensity also increase with increasing temperature. But the experimental value of b decreases with increasing adsorption temperature which indicated other than chemical interaction might be occurred in the process. However, the higher adsorption efficiencies at increased temperature indicate that the adsorption of Rh-B dye molecules onto the UBTL is endothermic in nature [13-15].

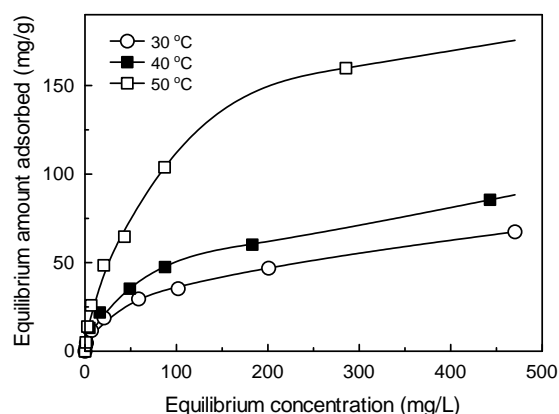


Figure 5. Adsorption isotherms of Rh-B on UBTL at pH 2.0 for different temperatures.

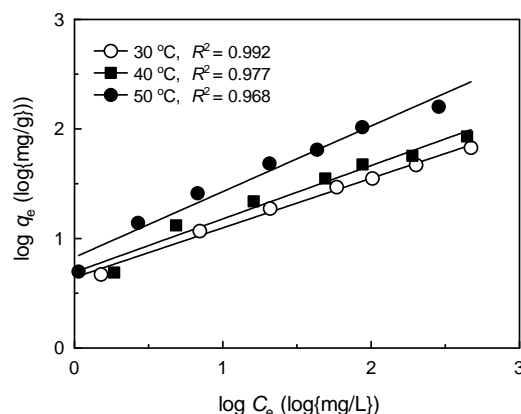


Figure 6. Freundlich isotherms for the adsorption of Rh-B on UBTL at pH 2.0 and different temperatures.

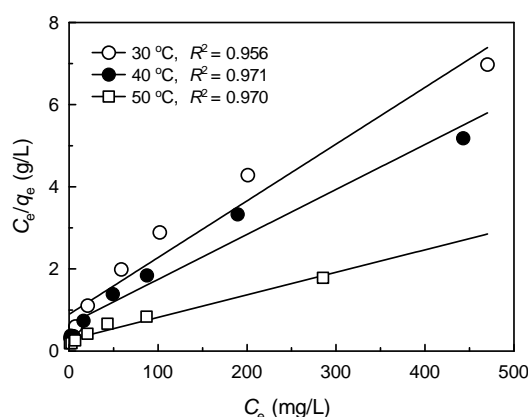


Figure 7. Langmuir isotherms for the adsorption of Rh-B on UBTL at pH 2.0 and different temperatures.

The analysis of adsorption isotherms at different temperatures by Freundlich and Langmuir models do not give any idea about the adsorption mechanism. Therefore, to predict the adsorption mechanism of the Rh-B dye molecules on the UBTL as chemical or physical, the equilibrium data were also tested with the Dubinin–Raduskevich (D-R) isotherm model [14]. The mathematical expression of the linear form of D-R equation is (4):

$$\ln q_e = \ln q_m - \beta \varepsilon^2 \quad (4)$$

where q_e is the amount adsorbed of dye per unit weight of adsorbent (mol/g), q_m the maximum adsorption capacity (mol/g), C_e is the equilibrium concentration of dye in aqueous solution (mol/L), R is the molar gas constant and T is the temperature (K), β is the activity coefficient related to the mean free energy of adsorption (mol^2/kJ^2) and ε is the Polanyi potential ($\varepsilon = RT \ln(1 + 1/C_e)$) [15]. The D-R isotherm constants, β and q_m can be determined from the slope and intercept, respectively, of the plot of $\ln q_e$ against

ε^2 as shown in Figure 8. The mean free energy of adsorption, E , defined as the free energy change when 1 mole of ion is transferred to the surface of the solid from infinity in solution can be calculated from the β value as given equation (5):

$$E = \frac{1}{\sqrt{2\beta}} \quad (5)$$

The E value gives information about the adsorption type, chemical ion exchange ($E = 8$ – 16 kJ/mol) or physical adsorption ($E < 8$ kJ/mol) [15, 16]. The mean free energy of adsorption, E was recorded between 0.1120 – 0.1166 kJ/mol. This finding implies that physical adsorption may play a role in this removal process.

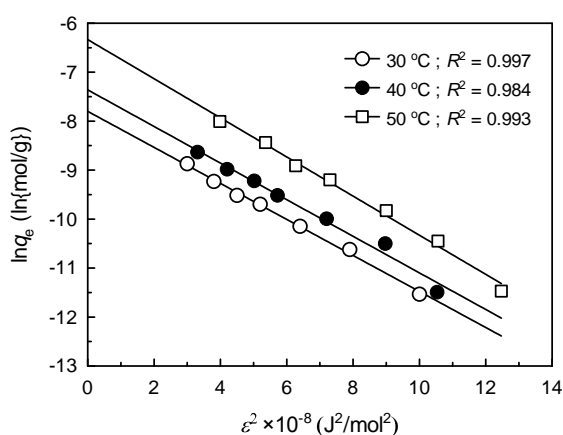


Figure 8. D-R adsorption isotherm of Rh-B on UBTL at pH 2.0.

Separation factor

In order to determine whether the adsorption is favorable or unfavorable, the separation factor, R_L has been calculated using the following equation (6):

$$R_L = \frac{1}{1 + bC_o} \quad (6)$$

where C_o is the initial concentration of Rh-B (mg/L) and b is the Langmuir constant. The values of R_L indicate the nature of the adsorption process to be favorable ($0 < R_L < 1$), unfavorable ($R_L > 1$), liner ($R_L = 1$) or irreversible ($R_L = 0$) [17-18]. The calculated values of R_L for different initial concentrations and at different temperatures were found to be in the range of 0.1 to 0.9 which is in the favorable range (0-1) of adsorption.

Figure 9 shows the variation of separation factor with initial concentration and processing temperature. The gradual decreasing of separation factor with the increase of initial concentration indicating the favorable adsorption at low concentration of Rh-B, and the nature changed from reversible to irreversible with the increasing of dye concentration. Again, the increased of R_L values with increase of temperature suggesting the less favorable adsorption at high temperature.

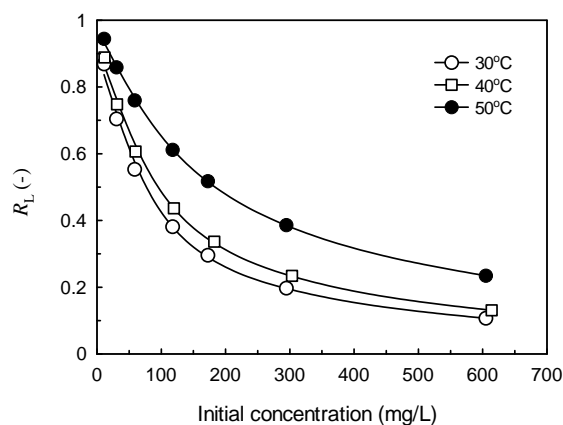


Figure 9. Variation of separation factor with initial concentration of Rh-B at different temperatures.

Adsorption thermodynamics

Thermodynamic parameters (ΔG° , ΔH° and ΔS°) of the adsorption process were calculated from the results of the effect of temperature on adsorption and using following equations (7-8) [5], (9) [19].

$$\left(\frac{d \ln C_e}{d(1/T)} \right)_\theta = \frac{\Delta H^\circ}{R} \quad (7)$$

$$\ln b = \frac{\Delta S^\circ}{R} - \frac{\Delta H^\circ}{RT} \quad (8)$$

$$\Delta G^\circ = -RT \ln b \quad (9)$$

where, θ indicates the fraction of surface coverage, ΔH° is the enthalpy of adsorption, b is Langmuir constant and R is the molar gas constant. For a particular amount adsorbed (70 mg/g), the change of equilibrium concentration with temperature has been calculated from Figure 5. Differential heat of adsorption, ΔH° was calculated from the slope ($= \Delta H^\circ/R$) of the linear plot $\ln C_e$ vs $1/T$ as shown in Figure 10. The positive value of ΔH° (103.8 kJ/mol) for the removal of Rh-B by UBTL from aqueous solution at pH 2.0 shows the endothermic nature of adsorption.

The change of entropy (ΔS°) and free energy (ΔG°) of adsorption at different temperatures were calculated from Eq. (8) and (9), respectively and are presented in Table 2. Positive values of entropy change at different temperatures indicate that the increased randomness at the solid/liquid interface during the adsorption process and suggests good affinity of the Rh-B dye towards the UBTL. Negative values of ΔG° indicate that the adsorption process was spontaneous in nature and confirm the affinity of the adsorbent towards the Rh-B dye at all temperatures studied. Similar thermodynamic findings have also been reported in the literature [19-21].

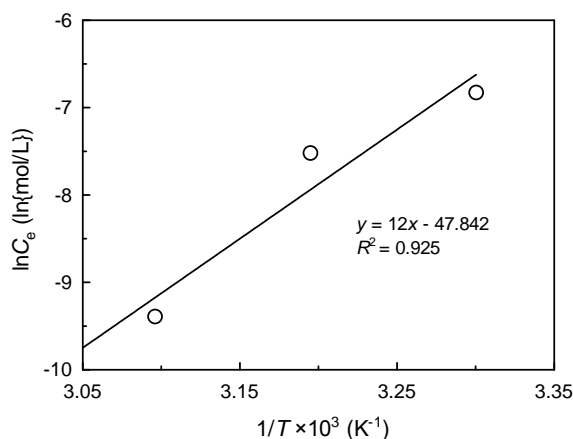


Figure 10. A plot of $\ln C_e$ vs $1/T \times 10^3$ for adsorption of Rh-B on UBTL at pH 2.0.

Table 2. Thermodynamic parameters for the adsorption of Rh-B on UBTL at different temperatures

$T \text{ (K)}$	$b \times 10^3 \text{ (L/mol)}$	$\Delta H^\circ \text{ (kJ/mol)}$	$\Delta S^\circ \text{ (J/mol}\cdot\text{K)}$	$\Delta G^\circ \text{ (kJ/mol)}$
303.16	6.609		+ 0.416	- 22.170
313.16	5.172	+103.8	+ 0.403	- 22.264
323.16	2.586		+ 0.387	- 21.113

Effect of pH and adsorption mechanism

The effect of temperature and the values of thermodynamic parameters of the adsorption did not give its concrete mechanism of the process; endothermic nature of adsorption suggested the process is chemical but the values of mean free energy of adsorption at different temperatures obtained from D-R isotherm indicated the process is physisorption. Therefore, to elucidate the actual mechanism of the adsorption of Rh-B on UBTL, further study was carried out to investigate the effect of solution pH on the adsorption. The pH of solution is one of the most important factors controlling the adsorption of solid-liquid interface, because both adsorbed molecules and adsorbent particles may have functional groups which are affected by the concentration of hydronium ions (H_3O^+) in the solution and which are involved in the molecular adsorption process at the active sites of adsorbent. Figure 11 shows that the adsorption of Rh-B on UBTL surface decreases with increase the solution pH. This effect can be explained from the viewpoint of surface characteristics of UBTL. The estimated zero point charge pH, pH_{ZPC} of UBTL is 4.2 [5]. Since Rh-B is an amphoteric dye, having number of benzene rings and act as an anionic species in acidic solution, when the pH was increased more than 4.2 the surface of UBTL became negative and because of this there was a repulsive force generated between electron rich negative species of Rh-B and UBTL surface. But as the solution pH was decreased the surface became positive [5] and the electrostatic force

of attraction leading the high amount of adsorption. Figure 12 shows the schematic diagram of the adsorption mechanism of Rh-B on UBTL in acidic media. Again, the endothermic nature of the process is might be due to the fragmentation of large Rh-B molecules during adsorption on UBTL.

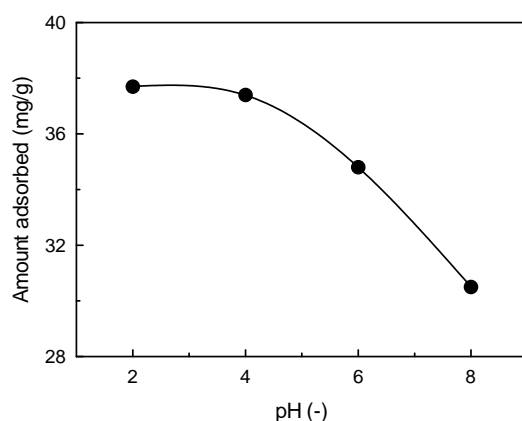


Figure 11. Variation of amount adsorbed with initial pH of solution for at constant concentration and temperature of 30.0 ± 0.5 °C.

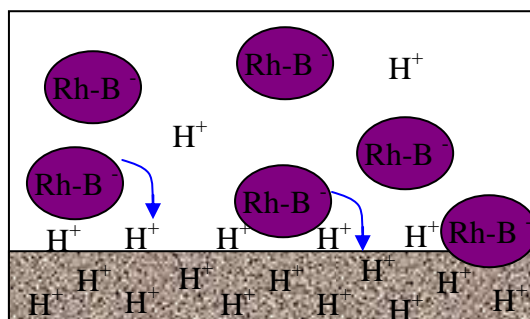


Figure 12. Schematic diagram of the adsorption mechanism of Rh-B on UBTL in acidic media (pH 2.0).

Conclusion

The adsorption characteristics of used black tea leaves for Rhodamine B were investigated by equilibrium study. The adsorption capacity was evaluated by constructing adsorption isotherm at different temperatures using four hours of pre-equilibrium time where maximum adsorption occurred. All isotherms obtained at different temperatures using pre-equilibrium time are well expressed by Dubinin–Raduskevich (D-R) equation as compared with Freundlich and Langmuir models. Freundlich equation is more applicable for the adsorption isotherm at low temperature compared with high temperature. The amount adsorbed obtained from Langmuir isotherm decreases with the increase of temperature which indicated endothermic nature of chemisorption. Again, the small value of mean free energy of adsorption, ($E = 0.112$ kJ/mol) calculated from D-R isotherm suggested that physical adsorption may play a role in this removal process. Finally, the

high amount adsorbed at low pH i.e. acidic solution is suitable for adsorption of Rh-B on UBTL, suggesting specific adsorption of the process. Thermodynamic parameters imply the favorability of the process.

Acknowledgments

The authors would like to thank to the Chairman of Chemistry Department of Dhaka University for providing different facilities during the study. We are also grateful to the Bangladesh Ministry of National Science and Technology for financial support (NST 2008-2009/739/1(21)ES-15) to perform the research.

References and Notes

- [1] Kubin, R. J. *Lumin.* **1983**, *27*, 455. [[CrossRef](#)]
- [2] Slate, D.; Algeo, T. P.; Nelson, K. M.; Chipman, R. B.; Donovan, D. *PLoS Negl. Trop. Dis.* **2009**, *3*, 549. [[CrossRef](#)]
- [3] Sultana, A. [Master's thesis.] University of Dhaka, Bangladesh, 2006.
- [4] Bailey, S. E.; Olin, J. T.; Bricka, R. M.; Adrian, D. D. *Wat. Res.* **1999**, *33*, 2469. [[CrossRef](#)]
- [5] Hossain, M. A. [Doctoral dissertation.] Kanazawa University, Kanazawa, Japan, 2006.
- [6] Hossain, M. A.; Kumita, M.; Michigami, Y., Shegeru, M. *J. Chem. Eng. Jpn.* **2005**, *38*, 402. [[CrossRef](#)]
- [7] Islam, T. S. A.; Begum, H. A.; Hossain, M. A.; Rahman, M. T. *J. Bangla. Acad. Sci.* **2009**, *33*, 167. [[Link](#)]
- [8] Bedmar, A. P.; Araguas, A. Detection and prevention of leaks from dams. Netherlands: Taylor & Francis, 2002.
- [9] Harler, C. R. Tea Manufacture. New York: Oxford University Press, 1972.
- [10] Hossain, M. A.; Kumita, M.; Michigami, Y.; Mori, S. *Adsorption* **2005**, *11*, 555. [[CrossRef](#)]
- [11] Freundlich, H. M. F. *Z. Phys. Chem.* **1906**, *57*, 385.
- [12] Langmuir, I. *J. Am. Chem. Soc.* **1918**, *40*, 1361. [[CrossRef](#)]
- [13] Banat, F.; Al-Bashir, A. B.; Al-Asheh, S.; Hayajneh, O. *Environ. Pollution* **2000**, *7*, 391. [[CrossRef](#)]
- [14] Dubinin, M. M.; Radushkevich, L. V. *Proc. Acad. Sci. USSR. Phys. Chem. Sect.* **1947**, *55*, 331.
- [15] Hobson, J. P. *J. Phys. Chem.* **1969**, *73*, 2720. [[CrossRef](#)]
- [16] Hasany, S. M.; Chaudhary, M. H. *Appl. Radiat. Isotope.* **1996**, *47*, 467. [[CrossRef](#)]
- [17] Vadivelan, V.; Kumar, K. V. *J. Colloid Interf. Sci.* **2005**, *286*, 90. [[CrossRef](#)]
- [18] Weber, T. W.; Chakravorti, R. K. *J. Am. Inst. Chem. Eng.* **1974**, *20*, 228. [[CrossRef](#)]
- [19] Aksakal, O.; Uzun, H. *J. Hazard. Mater.* **2010**, *181*, 666. [[CrossRef](#)]

- [20] Wang, B. E.; Hu, Y. Y.; Xie, L.; Peng K. *Bioresource Technol.* **2008**, 99, 794. [[CrossRef](#)]
- [21] Akar, T.; Tosun, I.; Kaynak, Z.; Ozkara, E.; Yeni, O.; Sahin, E. *N. J. Hazard. Mater.* **2009**, 166, 1217. [[CrossRef](#)]

Alum promoted synthesis of 2H-indazolo[2,1-b]phthalazinetrione derivatives in water

Balaji R. Madje^{a*}, Jagdish V. Bharad^a, Milind B. Ubale^a and Murlidhar S. Shingare^b

^aDepartment of Chemistry, Vasantao Naik Mahavidyalaya, Aurangabad-431003, India.

^bDepartment of Chemistry, Dr. Babasaheb Ambedkar Marathwada University, Aurangabad-431 004, India.

Received: 04 August 2012; revised: 06 September 2012; accepted: 07 September. Available online: 16 September 2012.

ABSTRACT: A new and efficient synthesis of 2H-indazolo[2,1-b]phthalazine-1,6,11(13H)-trione derivatives from the three-component condensation reaction of phthalhydrazide, dimedone, and aromatic aldehydes using alum [KAl(SO₄)₂.12H₂O] as catalyst was performed in aqueous media. The features of this procedure are mild reaction conditions, good to excellent yields, short reaction times and operational simplicity.

Keywords: alum; aqueous media; indazolo[2,1-b]phthalazinetrione; phthalhydrazide; dimedone

Introduction

Literature survey reveals that multicomponent reactions have emerged as an efficient and powerful tool in modern synthetic organic chemistry due to their valued features such as atom economy, straightforward reaction design, and the opportunity to construct target compounds by the introduction of several diversity elements in a single chemical event. Also the purification of products yielded from multicomponent reactions are simple as well as all the organic reagents employed gets consumed and are incorporated into the target compound [1]. The search for multicomponent reaction has paved a considerable attention for the use of phthalazine derivatives which has gained importance during recent year, which may be attributed to their wide range of pharmacological and biological activities [2]. They possess anticonvulsant [3], cardiotonic [4], and vasorelaxant [5] activities. Recently, many researchers has reported synthetic

* Corresponding author. E-mail: balumadje@yahoo.com

methods for the synthesis of 2*H*-indazolo [2,1-*b*]phthalazine-triones by using *p*-TSA [6], silica sulphuric acid [7], silica supported polyphosphoric acid [8], Mg(HSO₄)₂ [9], TMSCl [10], H₂SO₄ in H₂O-EtOH or ionic liquid [11], H₃PW₁₂O₄₀/IL [12], H₄SiW₁₂O₄₀ [13], and (PMA) – SiO₂ [14]. However, these methods have certain drawbacks, which may be attributed to the hazardous nature [6-11], high costly [8-14], long reaction times [7], highly corrosive and difficult to handle [7, 8, 10, 11] material used and also low yield [9, 14].

Organic synthesis in aqueous media is rapidly gaining importance in view of the fact that the use of many toxic and volatile organic solvents contributes to pollution. Since the pioneering studies by Breslow [15] on Diels–Alder reactions, there have been profound research activities in the development of organic reactions in aqueous media offering key advantages such as rate enhancement and insolubility of the final products, which facilitates their isolation by simple filtration. Also, in the context of green chemistry, aqueous media is acting as a stepping stone in the greener synthesis of bioactive heterocyclic compounds. In this respect, the development of water-tolerant catalysts has rapidly become an area of intense research.

Alum (KAl(SO₄)₂.12H₂O) was found to be effective in the synthesis of *cis*-isoquinolic acids [16^a], mono- and disubstituted 2,3-dihydroquinazolin-4(1*H*)-ones [16*b*], dihydropyrimidines via Biginelli reaction [16*c*], coumarins [16*d*], 1,3,4-oxadiazoles [16*e*], dibenzoxanthenes [16*f*], 1,5-benzodiazepines [16*g*], trisubstituted imidazoles [16*h*], mono and bis(spiro-2-amino-4*H* pyran)[16*i*] etc. However, there are no examples of the use of alum as a catalyst for the synthesis of 2*H* indazolo[2,1-*b*]phthalazinetrione derivatives. The present work reveals the study of alum as a catalyst for synthesis of 2*H* indazolo[2,1-*b*]phthalazine-trione derivatives in aqueous media.

Material and Methods

All chemicals were purchased from Merck, Aldrich and used without further purification. Products were characterized by comparison of spectroscopic data (IR, ¹H NMR, mass) and melting points with authentic samples. The ¹H NMR spectra were recorded on a Mercury plus Varian in CDCl₃ at 400 MHz instrument using TMS (0.00 ppm) as an internal standard. IR spectra were recorded on a JASCO FT-IR 460plus spectrophotometer. All the compounds were solid and solid state IR spectra were recorded using the KBr disk technique. Mass spectra were recorded on a Shimadzu GC–MS–QP 1000PX. Melting points were determined apparatus. The products were purified by column or thick layer chromatography techniques.

General procedure for the synthesis of 2*H*-indazolo[1,2-*b*]phthalazine-trione derivatives (4*a*-*m*)

Mixtures of benzaldehyde (12 mmol), dimedone (10 mmol) and phthalhydrazide

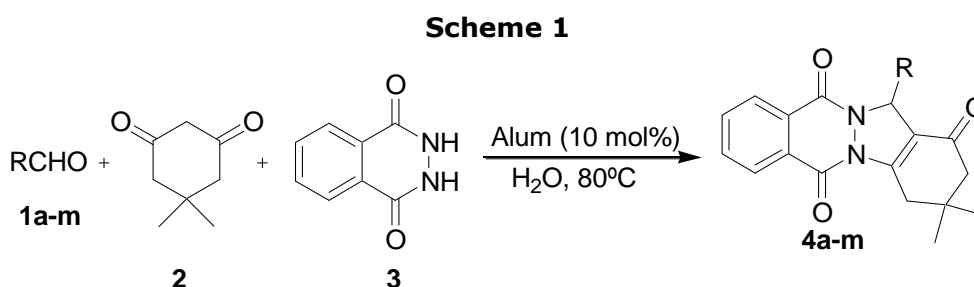
(10 mmol) were stirred in the presence of alum (10 mol %) in water (10 mL) for 5 min. at room temperature; the temperature were then raised to 80 °C for appropriate time (Table 2). Completions of the reaction were indicated by TLC (mobile phase: n-hexane / ethyl acetate 80:20). After completion of the reaction, the mixture were cooled, diluted with water (2 × 10 mL), stirred for 5 min., and the resulting solid product were then purified by recrystallization procedure in aqueous EtOH (25%). The products were characterized by IR, ¹H NMR and mass spectral data and by comparison with the melting points of reported compounds.

Spectral data of representative compounds

(4a): IR (KBr, cm⁻¹): 3028, 2960, 1663, 1618, 1470, 1423, 1361, 1308, 1274, 1147, 1075, 1027, 755, 699. ¹H NMR (400 MHz, CDCl₃): δ = 1.20 (s, 3H), 1.22 (s, 3H), 2.34 (s, 2H), 3.28 (dd, J = 1.7, 18.5 Hz, 1H), 3.45 (d, J = 18.6 Hz, 1H), 6.48 (s, 1H), 7.32-8.37 (m, 9H) ppm; MS, m/z (%): 372 (M⁺,15), 295 (100), 104 (84), 76 (67).

Results and Discussion

In continuation of the previous work on the applications of cheap, easily available and ecofriendly catalyst for the development of new synthetic methodologies [17], in present study report a simple and efficient alum catalyzed synthesis of 2*H*-indazolo[2,1-*b*]phthalazinetrione derivatives has been reported. The transformation involves the condensation reaction of benzaldehyde dimedone and phthalhydrazide in aqueous media at 80 °C temperature (Scheme 1).



In the initial reaction condition, the reaction of benzaldehyde **1a**, dimedone **2** and phthalhydrazide **3** were selected as standard model reaction to optimize the reaction conditions. The reaction were first carried out in water in the absence of alum, no product could be detected at room temperature and reflux temperature even after 4 hours (Table 4 compound **4a**). To determine the optimal catalyst loading required, the reaction were repeated with varying amounts of alum (Table 1). A maximum yield of 94% was obtained with 10 mol% of alum at 80 °C in water. Further increase in catalyst loading 15% or 20% did not have any significant effect on the yield of product. Whereas decreasing the amount of catalyst decreased yields (Table 1, Entry 1 and 2).

Table 1. Optimization of molar ratio of catalyst for the model reaction

Entry	Mole%	Yield/% ^a
1	0	-
2	5	62
3	10	94
4	15	94
5	20	93

^aYields refer to isolated products**Table 2.** Effect of temperature on yield and reaction time

Entry	Temp. (°C)	Reaction time (min)	Yield (%) ^a
1	25	120	trace
2	40	120	45
3	60	120	78
4	80	10	94
5	80	60	94
6	90	10	94
7	100	10	93

^aYields refer to isolated products

To fine the optimum reaction temperature, 25 °C, 40 °C, 60 °C, 80 °C, 90 °C and 100 °C, resulting in the isolation of **4a** in trace, 45%, 78%, 94%, 94%, and 93% yields (Table 3) respectively. Thus, 10 mol% of alum and a reaction temperature at 80 °C were optimal reaction conditions.

Table 3. Comparison of the results of alum in the reaction of benzaldehyde, dimedone and phthalhydrazide with those of other catalysts reported in the literature

Entry	Catalyst (loading)	Reaction condition	Time (min.)	Yield (%)
1	Alum (10 mol%)	H ₂ O, 80°C	5	94
2	<i>p</i> -TSA (30 mol%)	Solvent-free, 80°C	10	86 [6]
3	Silica-SO ₃ H (6.5 mol%)	Solvent-free, 100°C	8	87 [7]
4	Mg(HSO ₄) ₂ (10 mol%)	Solvent-free, 100°C	10	85 [9]
5	PPA-SiO ₂ (5 mol%)	Solvent-free, 100°C	8	92 [8]
6	PMA-SiO ₂ (5 mol%)	Solvent-free, 80°C	30	85 [14]
7	H ₂ SO ₄ (15 mol%)	[bmim][BF ₄] 80°C	30	89 [11]
8	H ₃ PW ₁₂ O ₄₀ (3 mol%)	IL, r.t.	10	90 [12]
9	H ₄ SiW ₁₂ O ₄₀ (1 mol%)	Solvent-free, 100°C	16	92 [13]

With this exciting result, the method was extended this method to a number of aromatic aldehydes to investigate its scope and generality. Aromatic aldehydes, including those bearing electron-withdrawing groups (such as Cl, F, Br and NO₂) or electron-donating groups (such as CH₃, OCH₃) were treated with dimedone and phthalhydrazide catalyzed by alum at 80 °C in water. The corresponding 2*H*-indazolo[2,1-*b*]phthalazinetrione derivatives (**4a-m**) were formed within short reaction times in excellent yields and confirmed by IR, ¹H NMR, Mass spectroscopic analysis. The results are summarized in Table 4.

Table 4. Alum catalyzed synthesis of 2*H*-indazolo[1,2-*b*]phthalazine-trione derivatives (**4a-m**)^a

Compound ^b	R	Time (min)	Yield (%) ^c	M. P. (°C)	
				Found	Reported
4a	C ₆ H ₅	4 h at r.t.	-	-	-
4a	C ₆ H ₅	4 h at reflux	-	-	-
4a	C ₆ H ₅	6	94	204-206	204-206 [6]
4b	4-MeC ₆ H ₄	10	85	226-228	227-229 [6]
4c	2-MeC ₆ H ₄	15	90	242-244	241-243 [8]
4d	4-Cl C ₆ H ₄	5	95	260-262	262-264 [6]
4e	3-Cl C ₆ H ₄	10	90	207-209	204-206 [8]
4f	2-Cl C ₆ H ₄	6	88	264-266	264-266 [6]
4g	4-Br C ₆ H ₄	8	92	262-264	265-267 [6]
4h	4-F C ₆ H ₄	10	88	220-222	217-219 [6]
4i	4-NO ₂ C ₆ H ₄	6	94	218-220	223-225 [6]
4j	3-NO ₂ C ₆ H ₄	8	90	270-272	270-272 [6]
4k	2,4-(Cl) ₂ C ₆ H ₃	6	92	220-222	219-221 [8]
4l	4-OH, 3-OMe C ₆ H ₃	8	94	248-250	250-252 [8]
4m	3,4,5-(OMe) ₃ C ₆ H ₂	5	95	230-232	232-234 [8]

^aReaction conditions: aldehyde (10 mmol), dimedone (10 mmol) and phthalhydrazide (10 mmol) were stirred in the presence of alum (10 mol%) in H₂O (10 mL) at 80 °C temperature.

^bCompounds were characterized by IR, ¹H NMR, mass spectroscopy and compared with reported data.

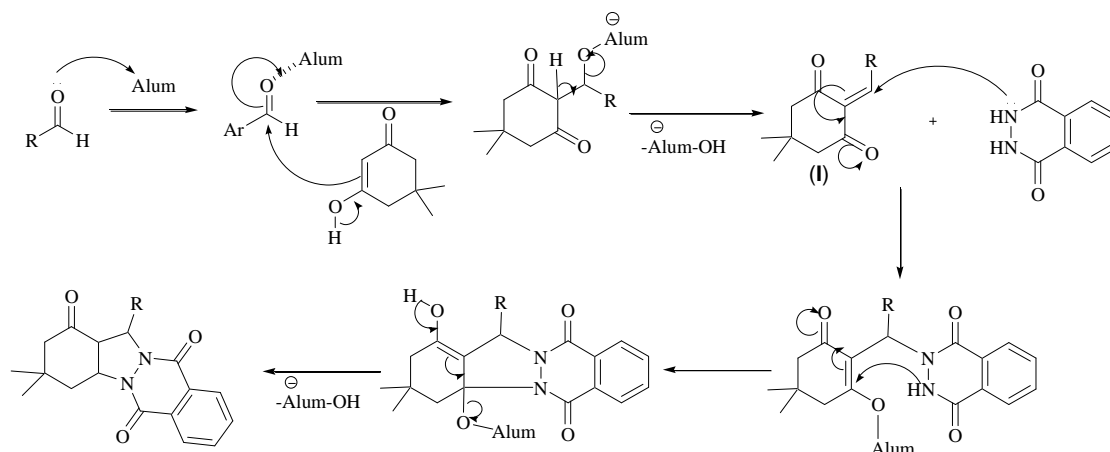
^cIsolated yield.

Alum acts as an effective catalyst with respect to reaction times and yields, when compared with catalyst known to facilitate this transformation, as shown for the condensation reaction of benzaldehyde, dimedone and phthalhydrazide (Table 3).

A process we propose that alum activates the aldehyde by binding with the oxygen atom [12a], ultimately enhancing the electrophilicity of the aldehyde, leading to a decrease in reaction time. The proposed mechanism of the alum catalyzed transformations is shown in Scheme 2. As reported in the literature the Knoevenagel type coupling of arylaldehyde with active methylene compound, dimedone give 2-benzylidene-5,5-dimethylcyclohexane-1,3-dione (I) [18]. Then, the subsequent 1,4-

conjugate addition of phthalhydrazide to the intermediate (I) followed by cyclization affords the corresponding products.

Scheme 2. Proposed mechanism for the synthesis of 2*H*-indazolo[1,2-*b*]phthalazine-triones.



Conclusion

In conclusion, we have developed convenient, alum catalyzed, one pot synthetic protocol for the synthesis of 2*H*-indazolo[2,1-*b*] phthalazinetrione derivatives in aqueous media. The alum is commercially available and inexpensive. The time required for the completion of the reaction is reduced, and yields of the products are increased.

Acknowledgments

The authors are thankful to Principal and the Management of Vasant Rao Naik Mahavidyalaya, Aurangabad for the technical support in this research work.

References and Notes

- [1] (a) Zhu, J.; Bienayme, H.; Eds.; Wiley-VCH: Weinheim, 2005. (b) Basso, A.; Banfi, L.; Riva, R.; Guanti, G. *J. Org. Chem.* **2005**, *70*, 575. [[CrossRef](#)] (c) Ramon, D. J.; Yus, M. *Angew. Chem.* **2005**, *44*, 1602. [[CrossRef](#)] (d) Domling, A. *Chem. Rev.* **2006**, *106*, 17. [[CrossRef](#)]
- [2] (a) Al'-Assar, F.; Zelenin, K. N.; Lesiovskaya, E. E.; Bezhan, I. P.; Chakchir, B. A. *Pharm. Chem. J.* **2002**, *36*, 598. [[CrossRef](#)] (b) Jain, R. P.; Vederas, J. C. *Bioorg. Med. Chem. Lett.* **2004**, *14*, 3655. [[CrossRef](#)] (c) Carling, R. W.; Moore, K. W.; Street, L. J.; Wild, D.; Isted, C.; Leeson, P. D.; Thomas, S.; O'Conner, D.; McKernan, R. M.; Quirk, K.; Cook, S. M.; Atack, J. R.; Waftord, K. A.; Thompson, S. A.; Dawson, G. R.; Ferris, P.; Castro, J. L. *J. Med. Chem.* **2004**, *47*, 1807. [[CrossRef](#)]
- [3] Grasso, S.; DeSarro, G.; Micale, N.; Zappala, M.; Puia, G.; Baraldi, M.; Demicheli, C. *J. Med. Chem.* **2000**, *43*, 2851. [[CrossRef](#)]
- [4] Nomoto, Y.; Obase, H.; Takai, H.; Teranishi, M.; Nakamura, J.; Kubo, K. *Chem.*

- Pharm. Bull.* **1990**, *38*, 2179. [[CrossRef](#)]
- [5] Watanabe, N.; Kabasawa, Y.; Takase, Y.; Matsukura, M.; Miyazaki, K.; Ishihara, H.; Kodama, K.; Adachi, H. *J. Med. Chem.* **1998**, *41*, 3367. [[CrossRef](#)]
- [6] Sayyafi, M.; Seyyedhamzeh, M.; Khavasi, H. R.; Bazgir, A. *Tetrahedron* **2008**, *64*, 2375. [[CrossRef](#)]
- [7] Shaterian, H. A.; Ghashang, M.; Feyzi, M. *Appl. Catal. A.*, **2008**, *345*, 128. [[CrossRef](#)]
- [8] Shaterian, H. R.; Hosseinian, A.; Ghashanh, M. *ARKIVOC* **2009**, (ii), 59. [[Link](#)]
- [9] Shaterian, H. R.; Khorami, F.; Amirzadeh, A.; Doostmohammadi, R.; Ghashang, M. *J. Iran. Chem. Res.* **2009**, *2*, 57-62. [[Link](#)]
- [10] Nagarapu, L.; Bantu, R.; Mereyala, H. B. *J. Heterocycl. Chem.* **2009**, *46*, 728. [[CrossRef](#)]
- [11] Khurana, J. M.; Magoo, D. *Tetrahedron Lett.* **2009**, *50*, 7300. [[CrossRef](#)]
- [12] Razieh, F.; Hamid, A.; Nahid, F. *The Open Catalysis Journal*, **2010**, *3*, 14. [[CrossRef](#)]
- [13] Wang, H-J.; Zhang, X-N.; Zhang, Z-H. *Monatsh Chem* **2010**, *141*, 425. [[CrossRef](#)]
- [14] Gowravaram, S.; Chitti, S.; Avula, R.; Yadav, J. S. *Helv. Chim. Acta* **2010**, *93*, 1375. [[CrossRef](#)]
- [15] (a) Breslow, R. *Acc. Chem. Res.* **1991**, *24*, 159. [[CrossRef](#)] (b) Breslow, R. *Acc. Chem. Res.* **2004**, *37*, 471. [[CrossRef](#)]
- [16] (a) Azizian, J.; Mohammadi, A. A.; Karimi, A. R.; Mohammadizadeh, M. R. *J. Org. Chem.* **2005**, *70*, 350. [[CrossRef](#)] (b) Dabiri, M.; Salehi, P.; Otokesh, O.; Baghbanzadeh, M.; Kozehgary, G.; Mohammadi, A. A. *Tetrahedron Lett.* **2005**, *46*, 6123. [[CrossRef](#)] (c) Azizian, J.; Mohammadi, A. A.; Karimi, A. R.; Mohammadizadeh, M. R. *Appl. Catal. A. General* **2006**, *300*, 85. [[CrossRef](#)] (d) Dabiri, M.; Baghbanzadeh, M.; Kiani, S.; Vakilzadeh, Y. *Monatsh. Chem.* **2007**, *138*, 997. [[CrossRef](#)] (e) Dabiri, M.; Baghbanzadeh, M.; Bahramnejad, M. *Monatsh. Chem.*, **2007**, *138*, 1253. [[CrossRef](#)] (f) Dabiri, M.; Baghbanzadeh, M.; Nikchek, M. S.; Arzroomchilar, E. *Bioorg. Med. Chem. Lett.* **2008**, *18*, 436. [[CrossRef](#)] (g) Mahajan, D.; Nagvi, T.; Sharma, R. L.; Kapoor, K. K. *Aust. J. Chem.* **2008**, *61*, 159. [[CrossRef](#)] (h) Mohammadi, A. A.; Mivechi, M.; Kefayati, H. *Monatsh. Chem*, **2008**, *139*, 935. [[CrossRef](#)] (i) Karimi, A. R.; Seelaghatpour, F. *Synthesis* **2010**, *10*, 1731. [[CrossRef](#)]
- [17] (a) Madje, B. R.; Ubale, M. B.; Bharad, J. V.; Shingare, M. S. *S. Afr. J. Chem.* **2010**, *63*, 36. [[Link](#)] (b) Madje, B. R.; Ubale, M. B.; Bharad, J. V.; Shingare, M. S. *S. Afr. J. Chem.* **2010**, *63*, 158. [[Link](#)] (c) Madje, B. R.; Shelke, K. F.; Sapkal, S. B.; Kakde, G. K.; Shingare, M. S. *Green Chem. Lett. Rev.* **2010**, *3*, 269. [[CrossRef](#)] (d) Shelke, K. F.; Sapkal, S. B.; Sonar, S. S.; Madje, B. R.; Shingate, B. B.; Shingare, M. S. *Bull. Korean Chem. Soc.* **2009**, *30*, 1057. [[CrossRef](#)]
- [18] (a) Kumar, A.; Maurya, R. A. *Tetrahedron* **2007**, *63*, 1946. [[CrossRef](#)] (b) Kaupp, G.; Naimi-Jamal, M. R.; Schmeyers, J. *Tetrahedron* **2003**, *59*, 3753. [[CrossRef](#)] (c) Quiroga, J.; Mejía, D.; Insuasty, B.; Abonía, R.; Nogueras, M.; Sánchez, A.; Cobo, J.; Low, J. N. *Tetrahedron* **2001**, *57*, 6947. [[CrossRef](#)]

Review

Chalcones: compounds possessing a diversity in applications

Urmila Berar

Department of Applied Science of University Institute of Engineering and Technology of the Kurukshetra University, Kurukshetra, India.

Received: 19 May 2012; revised: 03 July 2012; accepted: 08 July. Available online: 19 September 2012.

ABSTRACT: Chalcones are a class of α,β -unsaturated carbonyl compounds that form the central core for a variety of naturally occurring biologically active compounds. They exhibit tremendous potential to act as a pharmacological agent. Besides their various pharmacological activities, chalcones have been explored for different optical applications including second harmonic generation materials in non-linear optics, fluorescent probe for sensing different molecules.

Keywords: chalcones; pharmacological agent; optical properties; fluorescent probe

Introduction

Substituted chalcones are of particular interest for various studies because of their vital role as precursor in the biosynthesis of flavanoids abundantly available in plant kingdom. These bichromophoric molecules separated by a keto-vinyl chain are very useful as substrate for the synthesis of biologically very important heterocyclic compounds like cyclohexenone derivatives and pyrazoline derivatives. The scope of introducing variations in the structure of chalcones by changing various substituents has created an interest of scientists of different fields. Besides the different traditional methods used for synthesizing these molecules such as base catalyzed (NaOH, KOH, Ba(OH)₂) and acid catalyzed (including Lewis acids) condensation processes in the presence of suitable solvent, many new eco-friendly methods like use of ultrasonic radiations [1], microwave assisted [2], solvent free synthesis by grinding [3] etc. have been developed. The crucial interest of scientists in studying these molecules lies in their vast diversity in applications. Besides being important as starting material for synthetic

* Corresponding author. E-mail: urmila81@rediffmail.com

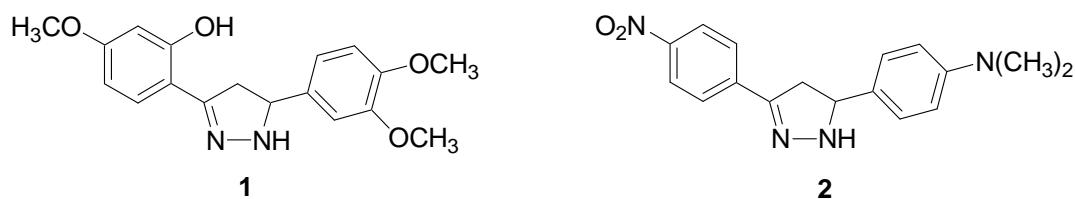
purpose, they are being explored as a new class of non-azo dyes [4], as a pharmacological agent exhibiting a large number of activities out of which antioxidant [7-9], antibacterial [10-12], antifungal [13-15], anticancer and anti-inflammatory [16-18] and antidepressant [20, 21] activities have been reported here. In addition, some photo physical properties of these substances such as non-linear optical properties [23, 24] and their use as fluorescent probe [22] have also been mentioned.

PHARMACOLOGICAL ACTIVITIES

Antioxidant activity

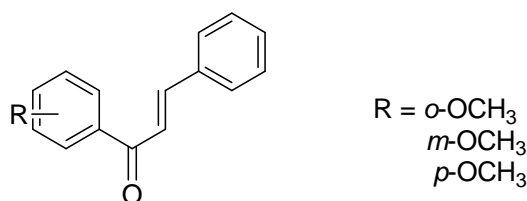
Antioxidants are the compounds that prevent the oxidative damage, induced by free radicals and reactive oxygen species, which is responsible for many pharmacological events such as cancer and ageing etc. Chalcones, in many cases, serve as active participant in plant defense mechanisms to counteract the reactive oxygen species to reduce the destruction at molecular level and the damage caused by microorganisms, insects and herbivores [5]. The antioxidant activity of these compounds is related with various mechanisms like metal ion chelation, free radical consumption, transfer of an electron or hydrogen atom, singlet oxygen quenching and acting as substrate for radicals like hydroxide and superoxides [6].

A lot of research has been carried out to study the free radical scavenging by synthetic chalcones. On the same path, Tan Nhut Doan et al. [7] synthesized a series of allylic chalcones and pyrazolic chalcones. They examined these chalcones and related compounds for their antioxidant properties by using 1,1-biphenyl-2-picrylhydrazyl (DPPH) radical scavenging method. Vitamin C was chosen as reference compound (97.92%). Out of the eight tested samples, the two 2-(5-(3,4-Dimethoxyphenyl)-4,5-dihydro-1H-pyrazol-3-yl)-5-methoxyphenol (**1**) and N,N-Dimethyl-4-(3-(4-nitrophenyl)-4,5-dihydro-1H-pyrazol-5-yl)-benzamine (**2**) exhibited the highest DPPH scavenging activity (89.64% and 89.27%, respectively) whereas the chalcones which were the precursor for these compounds did not show any activity. These results reflect that the presence of pyrazole ring was playing a role to exhibit this activity.



Nurettin Yayli et al. [8] studied the three simple methoxy chalcones for their superoxide radical scavenging activities by using a very common method in which xanthine as the substrate of xanthine oxidase was utilized to produce the superoxide radicals which were then consumed in the presence of antioxidants. The rest of the

radicals were then determined by the reaction with NBT (nitroblue tetrazolium salt) spectrometrically. The results expressed as the concentration of test sample giving 50% reduction in the absorbance of control at 560 nm clearly reflected the effect of position of methoxy group on their potential to scavenge superoxide radicals. One of these chalcones having methoxy group at ortho-position was found to be most active antioxidant (IC_{50} 0.623 mg/mL) even more active than the reference compound (Butylated hydroxytoluene IC_{50} 1.839 mg/mL). The order of the superoxide radical scavenging activity of these three chalcones followed the order *o*-methoxy chalcone (IC_{50} 0.623 mg/mL) > *m*-methoxy (IC_{50} 2.708 mg/mL) > *p*-methoxy (IC_{50} 4.343 mg/mL). These results offer interesting synthetic possibilities to synthesize more potent antioxidants.

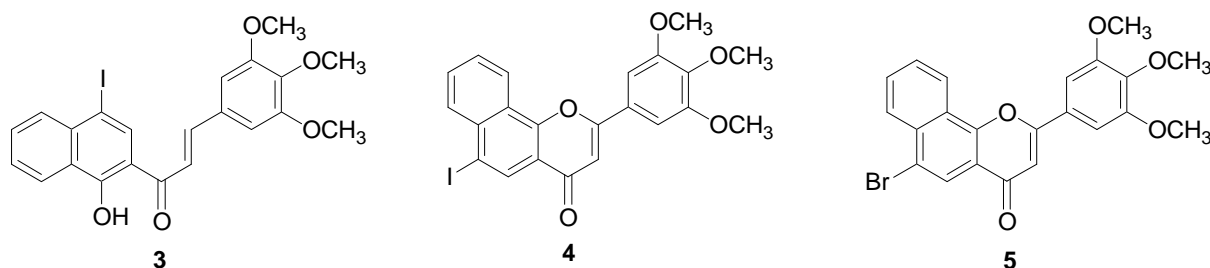


In order to explore the effect of various substituents present in two aromatic rings of chalcone molecules on their antioxidant activities, Ruby John Anto et al. [9] examined about thirty three chalcones and chalcones related compounds. They tested these compounds for superoxide radical scavenging activity and lipid peroxidation inhibition. Most of the chalcones except those substituted with -Cl was found to scavenge superoxide radicals. The compound 1-(2'-Hydroxy-5'-methylphenyl)-3-phenylprop-2-en-1-one (IC_{50} 10.5 μ g/mL) was found to be most active superoxide radical scavenger. The dihydroxy chalcones (1-(2'-hydroxyphenyl)-3-(2-hydroxyphenyl)prop-2-en-1-one, IC_{50} 4.0 μ g/mL) exhibited the highest lipid peroxidation inhibiting activity. One another chalcone substituted with 2'-OH and 4'-OCH₃ (IC_{50} 8.8 μ g/mL) proved to be very efficient in inhibition of lipid peroxidation. The compounds which were structurally similar to the chalcones, only those having methyl group were active superoxide scavengers while as lipid peroxidation inhibitor, only unsubstituted compounds and their dimethyl derivatives were found active. From the study, it reveals that the *o*- and *p*-substitution by electron donating groups may increase the antioxidant activities of chalcones which can open up a way to the more active and efficient synthetic antioxidants.

Antibacterial activity

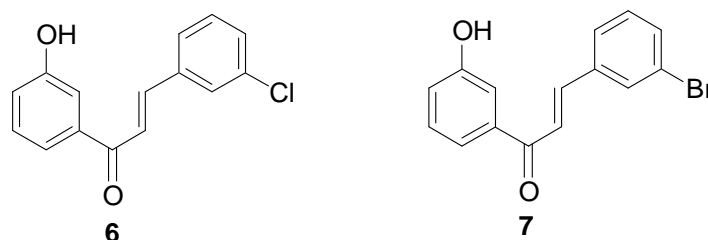
Synthesis of various novel chalcones and their corresponding flavones containing naphthyl moiety was carried out by Sainath B. Zangade et al. [10]. The chalcones were synthesized by using the conventional Claisen-Schmidt condensation method. All the compounds were subjected to antibacterial activity test against *Pseudomonas auriginosa*

(Pa) and *Staphylococcus aureus* (Sa) using cup-plate agar diffusion method. They used antibiotic streptomycin (zone of inhibition Pa= 30 and Sa= 28 mm) as standard antibiotic and 5% DMF as solvent control. Most of the tested compounds showed significant bactericidal behavior but the compounds 1-(1'-hydroxy-4'-iodonaphthyl)-3-(3,4,5-trimethoxyphenyl) prop-2-en-1-one (**3**), (zone of inhibition Pa=27 and Sa=30 mm), its corresponding flavone **4**, (zone of inhibition Pa=28 and Sa=26 mm) and another flavone substituted with bromine instead of iodine group, (**5**), (zone of inhibition Pa=29 and Sa=26 mm) were found to be most active antibacterial agents at concentration of 100 µg/mL. The findings of this vigorous study suggested that the increase in halo substitution in the basic nucleus enhances the inhibition of bacterial growth significantly.



To explore the antibacterial activity of differentially substituted chalcones, Farzana Latif Ansari et al. [11] synthesized two sets of chalcones using conventional and microwave assisted synthesis methods. The set-I chalcones were having two phenyl rings substituted with a variety of groups like hydroxyl, methoxy, halogens, nitro etc. at different positions whereas the set-II chalcones were containing one heterocyclic ring such as pyridinyl, pyrrolyl, furanyl, thienyl and indolyl. They tested all these compounds for their in vitro bactericidal action against six bacterial strains i.e. *B. bronchiseptica*, *M. leuteus*, *P. picketti*, *E. coli*, *E. aerogenes* and *S. setubal* following agar well-diffusion method. Cefixime was used as a standard drug (zone of inhibition 31 and 34 mm respectively). The study revealed that all the tested compounds were active only against *B. bronchiseptica* with a zone of inhibition ranging from 9.5-18.5 mm in diameter. The findings suggested that chalcones bearing electron withdrawing halogen groups like bromo- and chloro- groups {3-(3-bromophenyl)-1-(3'-hydroxyphenyl)prop-2-en-1-one, (**6**) and 3-(3-chlorophenyl)-1-(3'-hydroxyphenyl)prop-2-en-1-one} (**7**), showed the greatest antibacterial activity (zone of inhibition 18.5 and MIC values 0.2 and 0.3 mg/mL respectively) whereas compounds with more polar and electron withdrawing nitro-groups were least active. The hydroxyl and methoxy substituted chalcones showed moderate activity. From the analysis, order of bactericidal activity for various chalcones had been found X > OH > OCH₃ > NO₂. Most active bactericidal chalcones were also found to have high value of hydrophobicity constant, octanol- water partition coefficient and molar volumes with exception of -OCH₃ substituted chalcones. The influence of

heterocyclic ring on antibacterial activity was reflected by the results obtained for set-II chalcones. Only compounds with thiophene moiety were found active bactericidal except nitro substituted chalcones. These studies also strengthened their earlier hypothesis that nitro group attenuates the bactericidal effect. The results could prove fruitful in designing the synthesis of various chalcones possessing high antibacterial activity.

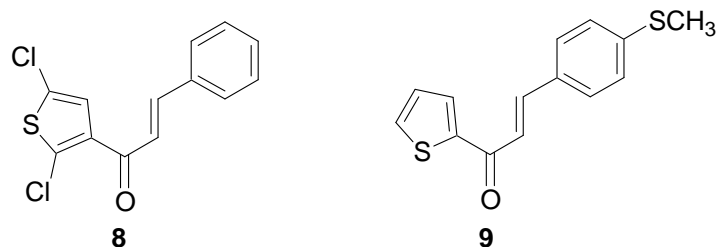


QSAR analysis on a set of thirty three synthesized chalcones tested for their antibacterial activity against human pathogenic gram +ve bacteria, *Bacillus pumilis* was performed by Y. Rajendra Prasad et al. [12]. They used DMSO as solvent and ampicillin as standard antibacterial agent. Three descriptors used to generate QSAR model were ADME weight, HOMO energy and Kappa 2 index. Results of the study suggested that high value of HOMO energy decreases the activity. Electron donating groups provide electrons which can delocalize in the π -space of benzene thus increasing energy of HOMO whereas electron withdrawing groups like halogens will increase bactericidal potential. On other hand, high values of ADME weight and Kappa 2 index showed a positive effect on inhibition of bacterial growth. Designing the chalcone derivatives bearing electron withdrawing substituent on the ring and with high degree of binding linearity with groups those results in high molecular weights increases antibacterial activity against *Bacillus pumilis*.

Antifungal activity

V. Tomar et al. [13] synthesized some novel chalcones containing piperazine or 2,5-dichlorothiophene moiety and evaluated their antimicrobial activities. All these compounds were screened for their antibacterial as well as antifungal potential against various bacterial strains and particularly three fungi *Candida albicans*, *Candida kusei* and *Candida glabrata*. Comparing the results as zone of inhibition and MIC values of tested chalcones with the standard drug fluconazole (29 mm and 50 $\mu\text{g}/\text{mL}$ for each), most of the compounds were showing significant activity against all the three chosen fungi. One chalcone carrying 2,5-dichlorothiophene moiety and unsubstituted phenyl ring (**8**) was found to be most potent antifungal agent with zone of inhibition of 26 mm for each strain and MIC values 2.22, 3.17 and 4.65 $\mu\text{g}/\text{mL}$, respectively. It was even more active than the standard one. Other two compounds with piperazine moiety were highly active agents possessing zone of inhibition and MIC values comparable with that of the most active chalcone in this study. From this analysis, it was also found that compounds

substituted with electron negative nitro group were less active towards the inhibition of fungal growth.

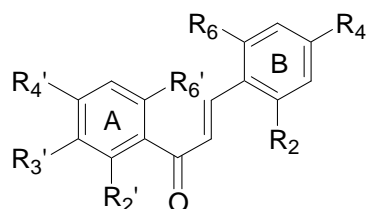


Presence of sulphur in chalcones either as a part of heteroaromatic ring (thiophene moiety) or a part of side chain group i.e. thiomethyl group influences the antifungal activity of chalcones was analysed by Seema Bag group [14] by synthesizing two series of α,β -unsaturated compounds, one with thiophene moiety and other with phenyl ring substituted with thiomethyl group. The second half part of the compounds was a phenyl ring having various substitutions. All the compounds were screened against both fluconazole resistant as well as fluconazole sensitive strains of *Candida albicans* (NCIM 3446 and ATCC 10231 respectively). The vigorous analysis of results of two series samples confirmed the perception as the chalcone having both unsubstituted thiophene moiety and *p*-thiomethyl substituted phenyl ring in the same molecule (**9**) was found to be the most active fungal growth inhibitor (IC_{50} 05 $\mu\text{g/mL}$ for both strains) when compared to the standard fluconazole (IC_{50} 100 and 20 $\mu\text{g/mL}$ respectively). Bromo group on thiophene moiety reflected a negative effect in activity. Among first series compounds, maximum activity was reported for *p*-fluoro substitution (IC_{50} 08 and 05 $\mu\text{g/mL}$, respectively). Antifungal activity decreased with increase in bulk of halogen attached. Also the presence of heavier phenyl group or nitro reduced the activity of chalcones. On the other hand, introducing methoxy group on *p*-position or hydroxyl on any position proved helpful in enhancing the antifungal activity.

P. M. Gurubasavaraza Swamy et al. [15] synthesized and then analysed a group of chalcones and their derivatives bearing hydroxyl benzofuran moiety for their antifungal activity against *Candida albicans* and *Aspergillus flavus* according to cup plate method using DMF as solvent control and griseofulvin as standard drug for comparison. Amongst the series of eleven compounds examined, 1-(3-hydroxybenzofuran-2-yl)-3-(4-methoxyphenyl)prop-2-en-1-one was found to exhibit highest activity almost equal to standard chosen {zone of inhibition at 100 $\mu\text{g/mL}$ 22 mm (tested chalcone) and 24 mm (griseofulvin) for the two strains each}. Comparative study of results reflected that the improvement in antifungal activities of chalcones may be achieved by incorporating hydroxyl and other electron releasing groups at proper positions in the aromatic rings and avoiding nitro group substitution.

Anticancer and anti-inflammatory activities

Ahcene Boumendjel et al. [16] developed a set of fifty nine chalcones (especially methoxylated and some hydroxylated derivatives) by Claisen-Schmidt condensation of required acetophenone with various substituted benzaldehydes. The prepared chalcone series was subjected to test their in vitro antimitotic activities against K562 leukemia cells stained with propidium iodide at a concentration of 10 μM for 24 h. The distribution of the total population in various phases (G0/G1, S, and G2/M) was determined by flow cytometry. Vincristine (VCR) was selected as reference compound. Amongst the screened chalcones, four compounds, (**10-13**) were found showing even higher cell cycle arrest in G2/M phase than the standard one whereas the other two, (**14** and **15**) were showing equal potential than reference chosen. Using MTT assay, a set of eleven different human and murine cell lines (like MCF7, N2A, NIH3T3, SW48, HNO150, HCT116, Messa, CEM, K562, RL, L1210) representing various solid tumors and hematological malignancies was exposed to the selected chalcones **11**, **12** and **13** for further analyzing their cell growth inhibition tendency. The IC_{50} concentration values in μM (drug concentration required to induce 50% loss of cell viability with reference to untreated cell after 24 h incubation) reflected compound, (**12**) as the most potent against almost all type of cell lines.



		G2/M arrest (%)	Clog P
10 ,	$\text{R}_2' = \text{R}_4' = \text{OCH}_3$, $\text{R}_2 = \text{R}_4 = \text{R}_6 = \text{OCH}_3$	86	3.87
11 ,	$\text{R}_2' = \text{R}_6' = \text{OCH}_3$, $\text{R}_2 = \text{R}_6 = \text{OCH}_3$	78	3.88
12 ,	$\text{R}_2' = \text{R}_6' = \text{OCH}_3$, $\text{R}_2 = \text{R}_4 = \text{R}_6 = \text{OCH}_3$	84	3.87
13 ,	$\text{R}_2' = \text{R}_4' = \text{R}_6' = \text{OCH}_3$, $\text{R}_2 = \text{R}_4 = \text{R}_6 = \text{OCH}_3$	86	3.83
14 ,	$\text{R}_3' = \text{R}_4' = \text{OCH}_3$, $\text{R}_2 = \text{R}_4 = \text{R}_6 = \text{OCH}_3$	72	3.52
15 ,	$\text{R}_2' = \text{OCH}_3$, $\text{R}_4' = \text{NH}_2$, $\text{R}_2 = \text{R}_4 = \text{R}_6 = \text{OCH}_3$	74	2.95

The thorough analysis of data for in vitro antimitotic activities revealed that optimum value of lipophilic character (C log P) to show significant inhibition of cell growth was around 4 (as in the case of most effective chalcones found in test). As this character changed, by replacing methoxy group on ring A by ethoxy or methyl groups, activity was found to be reduced (might influencing the cell permeation required for cell growth inhibition). Also the dimethoxylation and trimethoxylation of the two phenyl rings proved significant for antimitotic behavior of various chalcones although the substitution pattern on ring B influenced the activity less than ring A. One of the highly active chalcones, (**12**), was further subjected to in vivo studies to test toxicity level in healthy animals and was found to be nontoxic up to the maximum tested dose level (1 mg/Kg) thus representing a group of very good anticancer agents.

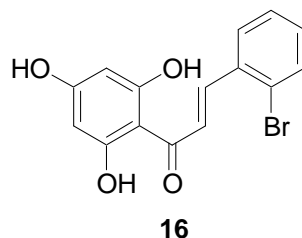
A new series of quinolinyl and chloroquinolinyl chalcones was synthesized by Vijay Kotra et al. [17] to study the effect of quinoline moiety present in chalcones on their anticancer and anti-inflammatory activities (as evident from the literature, two entities i.e. quinoline and chalcone both exhibits anticancer activities alone). They screened selected chalcones for their in vitro anticancer potential on RAW cell lines using MTT assay which was based on the appearance of highly colored blue formazan product by mitochondrial reduction of yellow MTT tetrazolium dye and noted the results as % inhibition of cell growth. Among the eight tested compounds, 3-(4-chlorophenyl)-1-(3-methyl-1-phenyl-2-naphthyl)prop-2-en-1-one exhibited the highest 103 % inhibition. Three more compounds named 1-(3-methyl-1-phenyl-2-naphthyl)-3-(2-thienyl)prop-2-en-1-one, 1-(7-chloro-3-methyl-1-phenyl-2-naphthyl)-3-(2-furyl)prop-2-en-1-one and 1-(7-chloro-3-methyl-1-phenyl-2-naphthyl)-3-(2-thienyl)prop-2-en-1-one were found to show significant anticancer activity (101.59, 100.20 and 100.14% inhibition, respectively). Anti-inflammatory activity of ten chalcones were also evaluated in albino rats of either sex weighing between 200-250 g using carrageenan induced acute paw edema method. Indomethacin was taken as standard for comparison. Mostly the chalcones possessing high anticancer activity were found to exhibit appreciable reduction in paw edema (which is beneficial for cancer treatment) up to 81.78 % at a concentration level of 20 mg/Kg as compared to the standard (82 %, 10 mg/Kg).

Babasaheb P. Bandgar et al. [18] synthesized a large number of chalcones by reacting differentially substituted acetophenones with 2,4-dimethoxybenzaldehyde and 3,4,5-trimethoxybenzaldehydes using Claisen-Schmidt condensation and analyzed their anticancer and anti-inflammatory activities. Anticancer activity of the chalcones was determined against five human cancer cell lines responsible for renal cell carcinoma, pancreatic carcinoma, non-small cell lung carcinoma and colon carcinoma. Flavopiridol (700 nM) and Gemcitabine (500 nM) were taken as standard. Results of the anticancer activity of chalcones at 10 μ M concentration revealed that nitro substitution at *p*-position of ring A increased the cell inhibition tendency of chalcone up to 100% as compared to the references chosen which seemed surprising as some compounds containing nitro group are supposed to exhibit carcinogenic and mutagenic behavior. The substitution in 3,4,5-trimethoxychalcones on ring A affected their anticancer activity considerably (ranging from 50-95 %) in the order of OCH₃ > OH > Cl > Br. Also from the study, it was found that increase in number of methoxy groups increased the anticancer activity. These chalcones were also analyzed for their anti-inflammatory activities in terms of TNF- α and IL-6 inhibitory activity. All 3,4,5-trimethoxy chalcones showed 90-100% inhibition at 10 μ M concentration as compared to reference dexamethasone (73% inhibition of TNF- α and 84 % of IL-6 at 1 μ M concentration) and 2,4-dimethoxychalcones. Many of the tested chalcones showing anti-inflammatory activities were also possessing anticancer

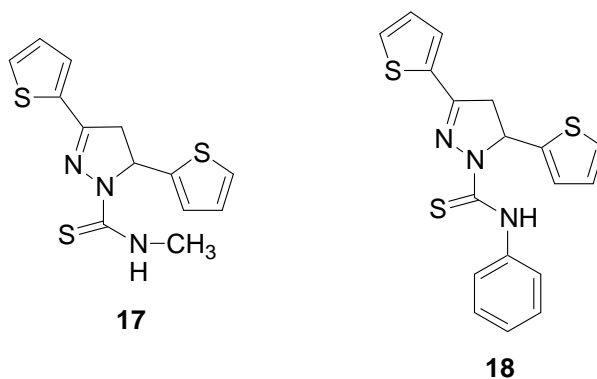
activities.

Antidepressant activity

Drugs available for curing depression, a very serious behavioral problem related with brain which may even induce suicidal characteristics, are associated with several undesirable side effects. So there is an urgent unavoidable need for more efficient antidepressants with minimum intolerable side effects. Inspired from the fact that a hydroxyl chalcone obtained by central ring opening of naturally existing flavonoid, Apigenin [19] (bearing antidepressant activity) was found to possess antidepressant activity, Xin Sui [20] et al. synthesized a series of 2', 4', 6'-trihydroxy chalcones and evaluated them for their antidepressant activity in male Kunming mice (20-24 g, local breed) by using forced swimming test (FST) and tail suspension test (TST). Fluoxetine was taken as reference for comparing the results. One of the tested compound, 3-(2-bromophenyl)-1-(2', 4', 6'-trihydroxyphenyl)prop-2-en-1-one (**16**) (10 mg/Kg) was found to be most active antidepressant with a significant decrease in duration of immobility (period of immobility = 69.4 s and for reference it was 57.4 s at same dose level). Results revealed the effect of nature of various substituents and their position in ring B on antidepressant activity of different chalcones.



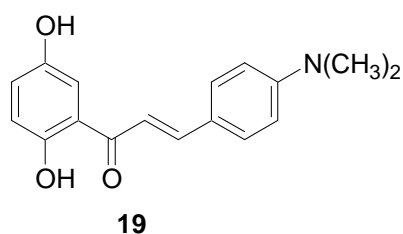
Various chalcones {1-(2-Thienyl)-3-phenyl/(2-thienyl)prop-2-en-1-ones} were used by Zuhail Ozdemir et al. [21] to prepare a set of 3-(2-thienyl)pyrazoline derivatives in order to study their antidepressant effects on local breed albino mice using Porsolt's behavioral despair test i.e. forced swimming test (FST). They compared the results with tranylcypromin sulfate, an antidepressant drug. Among the analyzed, compounds with 2-thienyl moiety at 5-position of pyrazoline ring except one were found to decrease the duration of immobility up to appreciable extent. Two derivatives, 1-*N*-methylthiocarbamoyl-3,5-di-(2-thienyl)-2-pyrazoline (**17**) and 1-*N*-phenylthiocarbamoyl-3,5-di-(2-thienyl)-2-pyrazoline (**18**) exhibited highest activity as antidepressant with duration of immobility 43 sec and 48 sec (for standard drug chosen, observed immobility period was of 57 sec at same dose level of 10 mg/Kg). Data reflected that the introduction of a thienyl moiety at 5-position of pyrazoline ring improved the antidepressant activity of chalcones.



AS FLUORESCENT PROBE

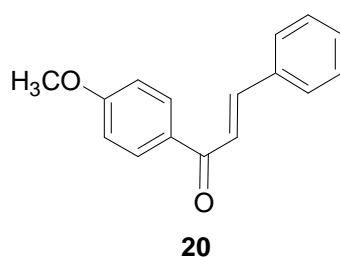
The substances which exhibit variation in the fluorescence characteristics under influence of external environment at molecular level and also nontoxic to human body can act as fluorescent probe. Chalcones have been found to be biologically active species. They also show absorbance and fluorescence behavior in UV-Vis region which might be more pronounced when both electron donating and electron withdrawing substituent present in the molecule results in effective intramolecular charge transfer (ICT) process.

The effect of polarity of solvent on absorbance and emission characteristics of a particular chalcone named 4'-dimethyl-2,5-dihydroxychalcone (**19**) was studied by Zhicheng Xu et al. [22] by using steady-state absorption and fluorescent spectrum in various non-polar and polar solvents like carbon tetrachloride, diethyl ether, tetrahydrofuran, acetone, dimethyl formamide, dimethyl sulfoxide, ethanol and methanol. They analyzed the fluorescence quantum yields and also the difference in dipole moment values of the molecule in ground and excited state by plotting a curve between Stokes shifts versus the orientation polarizability. Larger difference in dipole moment values ($\Delta\mu = 6.5$ D) revealed that atomic charges were redistributed in higher energy state due to the charge transfer from dimethyl amino group (electron donating) to carbonyl moiety (electron withdrawing species). Minor changes in the absorbance pattern of the target molecule were observed in different solvent environment whereas a significant bathochromic shift was found for fluorescence. That was attributed to large extent of solvation of molecule in excited state than in ground state. As the polarity of the solvent was increased, the emission maximum shifted to higher wavelength (solvents from CCl₄ to DMSO, values from 488 nm to 533 nm). But in protic solvents although with higher polarity, smaller λ_f values (529 nm & 530 nm for ethanol and methanol respectively) were noted due to intermolecular H-bonding between the solvent and -N(CH₃)₂ that decreased the availability of lone pair of electrons for charge transfer process.

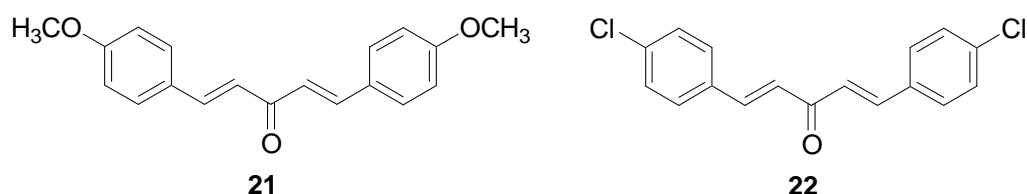


AS NON-LINEAR OPTICAL MATERIAL

The crystals of compounds exhibiting non-linear optical behavior can be used in wide range of optical applications like optical parametric generation and amplification (OPG, OPA), laser harmonic generation, frequency conversion (SFG, DFG), eye and sensor protection etc. The inorganic crystalline substances like potassium di deuterium phosphate (KDP), lithium iodate (LiIO_3), lithium triborate (LBO), beta barium borate (BBO), potassium titanyl phosphate (KTP) etc. have been utilized for this purpose extensively. But recently a large no of organic crystals have also been found to be capable of showing second and third order non-linear optical properties. Chalcones being very easy to be synthesized, easy crystal growth, excellent non-linear optical behavior created an interest of J. Indra et al. [23] to synthesize a chalcone molecule 1-(4-methoxyphenyl)-3-(phenyl)-2-propen-1-one (**20**), cream white solid with molecular formula $\text{C}_{16}\text{H}_{14}\text{O}_2$, molecular weight 238 and melting point $109\text{ }^\circ\text{C}$ using Claisen-Schmidt condensation process. The maximum absorption wave length for the target was found to be 326 nm from the absorption spectra in UV region of electromagnetic spectrum. The power technique using neodymium-doped yttrium-aluminum-garnet (Nd: YAG) laser with 13 mJ/s power was used to determine the second harmonic generation conversion efficiency of the sample which was found to be comparable with that of urea.



John Kiran et al. [24] synthesized two chalcone compounds named *p*-methoxy dibenzylidene acetone (PDBA) (**21**) and *p*-chlorodibenzylidene acetone (CDBA) (**22**) by the familiar method. The PDBA pale- yellow crystal with superior surface quality having maximum dimension of $12 \times 7 \times 1.3\text{ mm}^3$ and the CDBA crystal with somewhat lower surface quality and $13 \times 8 \times 2\text{ mm}^3$ size were grown by using slow evaporation solution technique. Both crystals (with cutoff wavelengths of 440 and 450 nm) did not exhibit any absorbance in visible and IR regions of electromagnetic spectrum.



As the second harmonic generation capacity of PDBA and CDBA were found to be significantly high than the standard chosen i.e. urea (15.5 and 4.5 times), these compounds were further examined for their non-linear optical (NLO) properties. Second order NLO coefficients (d coefficients) were determined by Standard Maker fringe technique and it was revealed that these coefficients of targeted molecules were much larger than those of most frequently used crystal materials as LiB_3O_5 , KTiOPO_4 etc. The NLO properties of PDBA were more pronounced than CDBA which might be due to the presence of electron donating methoxy group on phenyl ring. These crystals were also superior to the common NLO crystals in their bulk threshold damage values which were determined as 8.2 and 7.2 GW/cm^2 at 1064 nm (for LBO, KTP & KDP, values are >0.90 , >2.4 and $>0.2.4$ GW/cm^2 respectively) and 4.6 and 1.4 GW/cm^2 at 532 nm (for LBO, KTP and KDP, values are >0.22 , >2.0 and >8.0 GW/cm^2 respectively) using 9ns and 8ns laser pulses. In view of this chalcone compounds may prove to be very efficient as NLO materials.

Conclusion

From this review, it can be revealed that chalcones and their analogs exhibit a variety of pharmacological activities and they can be further studied for their efficient use as an active biological agent. Chalcones also show a very good second harmonic generation capability and can be explored as non-linear optical material.

Acknowledgments

The author is thankful to Director, UIET, Kurukshetra University for utilizing the facilities of text and e-journal access in institute and university library.

References and Notes

- [1] Chtourou, M.; Abdelhédi, R.; Frikha, M. H.; Trabelsi, M. *Ultrason. Sonochem.* **2009**, *17*, 246. [[CrossRef](#)]
- [2] (a) Abdel-Aziz, H. A.; Al-Rashood, K. A.; ElTahir, K. E. H.; Ibrahimca, H. *S. J. Chin. Chem. Soc.* **2011**, *58*, 863. [[CrossRef](#)] (b) Kakati, D.; Sarma, J. C. *Chemistry Central Journal* **2011**, *5*, 1. [[CrossRef](#)]
- [3] (a) Rateb, N. M. ; Zohdi, H. F. *Synth. Commun.* **2009**, *39*, 2789. [[CrossRef](#)] (b)

- Rajendra, K.; Saini, K.; Choudhary, S. A.; Joshi, Y. C.; Joshi, P. *E-Journal of Chemistry* **2005**, *2*, 224. [[CrossRef](#)]
- [4] Sharma, B.; Agrawal, S. C.; Gupta, K. C. *International J. ChemTech. Research* **2010**, *1*, 25.
- [5] Vaya, J.; Belinky, P. A.; Aviram, M. *Free Radical Bio. Med.* **1997**, *23*, 302. [[CrossRef](#)]
- [6] Robards, K.; Prenzlere, P. D.; Tucker, G.; Swatsitang, P.; Glover, W. *Food Chem.* **1999**, *66*, 401. [[CrossRef](#)]
- [7] Doan, T. N.; Tran, D. T. *Pharmacology and Pharmacy*, **2011**, *2*, 282. [[CrossRef](#)]
- [8] Yayli, N.; Ucuncu, O.; Yasar, A.; Gok, Y.; Kucuk, M.; Kolayli, S. *Turk J. Chem.* **2004**, *28*, 515. [[Link](#)]
- [9] Anto, R. J.; Sukumaran, K.; Kuttan, G.; Rao, M. N. A.; Subbaraju, V.; Kuttan, R. *Cancer Letters*, **1995**, *97*, 33. [[CrossRef](#)]
- [10] Zangade, S. B.; Vibhute, A. Y.; Chavan, S. B.; Vibute, Y. B. *Der Pharmacia Letter* **2011**, *3*, 20. [[Link](#)]
- [11] Ansari, F. L.; Baseer, M.; Iftikhar, F.; Kulsoom, S.; Ullah, A.; Nazir, S.; Shaukat, A.; Haq, I.; Mirza, B. *ARKIVOC* **2009**, (x), 318. [[Link](#)]
- [12] Prasad, Y. R.; Kumar, P. R.; Smiles, D. J.; Babu, P. A. **2008**, *ARKIVOC*, (xi), 266. [[Link](#)]
- [13] Tomar, V.; Bhattacharjee, G.; Kamaluddina, Kumar, A. *Bioorg. Med. Chem. Lett.* **2007**, *17*, 5321. [[CrossRef](#)]
- [14] Bag, S.; Ramar, S.; Degani, M. S. *Med. Chem. Res.* **2009**, *18*, 309. [[CrossRef](#)]
- [15] Swamy, P. M. G.; Agasimundin, Y. S. *Rasayan J. Chem.* **2008**, *1*, 421. [[Link](#)]
- [16] Boumendjel, A.; Bocard, J.; Carrupt, P. A.; Nicolle, E.; Blanc, M.; Geze, A.; Choisnard, L.; Wouessidjewe, D.; Matera, E. L.; Dumontet, C. *J. Med. Chem.* **2008**, *51*, 2307. [[CrossRef](#)]
- [17] Kotra, V.; Ganapaty, S.; Adapa, S. R. *Indian J. Chem., Sect B: Org. Chem. Incl. Med. Chem.* **2010**, *49*, 1109.
- [18] Bandgar, B. P.; Gawande, S. S.; Bodade, R. G.; Totre, J. V.; Khobragade, C. N. *Bioorg. Med. Chem.* **2010**, *18*, 1364. [[CrossRef](#)]
- [19] Yi, L. T.; Li, J. M.; Li, Y. C.; Pan, Y. *Life Sciences*, **2008**, *82*, 741. [[CrossRef](#)]
- [20] Sui, X.; Quan, Y. C.; Chang, Y.; Zhang, R. P.; Xu, Y. F.; Guan, L. P. *Med. Chem. Res.* [[CrossRef](#)]
- [21] Ozdemir, Z.; Kandilci, H. B.; Gumusel, B.; Calis, U.; Bilgin, A. A. *Arch. Pharm. Chem. Life Sci.* **2008**, *341*, 701. [[CrossRef](#)]
- [22] Xu, Z.; Bai, G.; Dong, C. *Spectrochim. Acta Part A*, **2005**, *62*, 987. [[CrossRef](#)]
- [23] Indra, J.; Karat, P. P.; Sarojini, B. K. *J. Cryst. Growth*, **2002**, *242*, 209. [[CrossRef](#)]
- [24] Kiran, A. J.; Kim, H. C.; Kim, K.; Rotermund, F.; Ravindra H. J. *Appl. Phys. Lett.* **2008**, *92*, 113307. [[CrossRef](#)]

A tutorial for molecular dynamics simulations using Amber package

Marcos Vinícius R. Garcia^{*a}, Wivirkins N. Marciela^a, Roberto da Silva Gomes^b e Marcos Serrou do Amaral^a

^aCentro de Ciências Exatas e Tecnologia, Universidade Federal de Mato Grosso do Sul, UFMS, Cidade Universitária s/n, Postal Code: 79070-900, Campo Grande, MS, Brazil.

^bSynthesis and Transformations of Organic Molecules Laboratory (SINTMOL), Centro de Ciências Exatas e Tecnologia, Universidade Federal de Mato Grosso do Sul, UFMS, Av. Senador Filinto Muller, 1555, Cidade Universitária, Postal Code: 79074-460, Campo Grande, MS, Brazil.

Received: 04 June 2012; revised: 24 July 2012; accepted: 27 August 2012. Available online: 21 September 2012.

ABSTRACT: *In this paper we present a tutorial for performing molecular dynamics calculations utilizing Amber package. Through it we explain the function of each step in a theoretical work of MD, thus enabling the application of acquired knowledge to other systems without many difficulties. For this tutorial, we simulated by MD and analyzed various geometrical and structural parameters for doxycycline, a potent antimicrobial agent.*

Keywords: *doxycycline; QM/MM; educational; cluster*

Introduction

AMBER is a package of computer programs whose function is to allow users to perform simulations of molecular dynamics (MD) with chemical structures of many types, such as: organic and inorganic molecules and biomolecules [1]. The term "AMBER" is also sometimes used to refer to empirical force fields [2].

Neither individual program of the AMBER package performs all steps of the MD, but together they offer a complete procedure, being a powerful framework for many common calculations.

The set of programs provides the option of running simulations QM/MM (quantum mechanics/molecular mechanics), where part of the system can be treated by quantum

* Corresponding author. E-mail: mvrifon@gmail.com

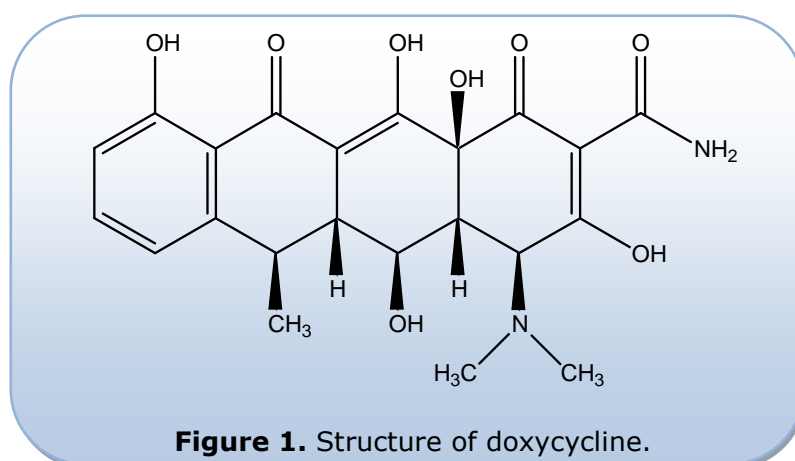
mechanics (QM).

The advantage of the QM/MM simulation is in fact supporting the gas phase and buffer (with hundreds of atoms) using semi-empirical methods. The AMBER package has tools that allow the correction of the system volume by multiplication of the box solvation with explicit solvent. Moreover it has the extensive chemical structures can be used as solvent of the system.

This package consists of several programs, including:

- **Leap:** used to prepare the system for the simulation programs;
- **Antechamber:** automates the process of parametrization;
- **Sander:** central simulation program and has facilities for energy minimization and molecular dynamics with a wide variety of options;
- **Ptraaj:** used to perform analysis of simulation results.

In this tutorial, we use the doxycycline (Fig. 1), derived from the oxytetracycline, because presents high power antibiotic and high degree of liposolubility. It is highly stable in normal human serum. Basically bacteriostatic, has antimicrobial action activated by inhibiting protein synthesis. The compound is used against a wide variety of Gram-positive and Gram-negative bacteria and other microorganisms [3].



PREPARATION OF THE FILES TO MOLECULAR DYNAMIC SIMULATION

We use two auxiliary programs Ghemical [4] and Gaussian03 [5]) to prepare the solute to start the procedures by AMBER package.

Creating a directory

Firstly is necessary creating a directory on the machine where the calculations will

be performed. We will do all the steps remotely (using the tool for remote user), this requires access to the central directory to be used by the terminal command:

```
ssh user@<remote machine name>
```

After accessing the machine where the calculations are performed, we will create and enter into the directory that stores data about the calculation. To create it, the command is **mkdir**, and how the name is "doxycycline", we have:

```
mkdir doxycycline
```

To open the execution command we use the command **cd**

```
cd doxycycline
```

Into the directory, having the file of the optimized coordinates of the drug by classical mechanics, the process of preparation and simulation of the chosen system can be done. The procedure was divided in stages or steps in order to facilitate understanding.

Optimization the geometry of the structure

1st Step

We perform the optimization of the geometry using quantum calculations at the HF/6-31G(d,p) theory level, in order to obtain the geometry of lowest energy.

In this theory, the base set used for the calculations is divided generally for "a-bcG(d,y)", and each letter corresponds to a variable used in each part of the model, where "a" represents the number of Slater primitive (STO) necessary to describe the valence shell, "b" and "c" represents the number of Gaussians primitive (GTO) required for each STO involved and the "x" and "y" means the polarization [5].

To prepare the compound for this stage is necessary converts the format file of the coordinates (.gpr to .gau), in order to start the calculations by Gaussian03. The command that contains this function runs as follows "babel":[6]

```
babel -igpr doxycycline.gpr -ogau doxycycline.gau
```

Then the input file for calculating the Gaussian03 (doxycycline.gau) is edited by adding a header that indicates the type of calculation used and the theory will add the following data, which indicates a geometric optimization:

```
%chk=doxiciclina.chk
```

```
#P HF/6-31G(d,p) opt test
```

With the file ready, we start the calculations in the Gaussian03 using a simple command, as below:

```
nohup g03 < doxycycline.gau > doxycycline.log &
```

Where *doxycycline.gau* represents the input file with initials coordinates and *doxycycline.log* is the output file that will contains geometric data and physical conformation of the best energy obtained. The "&" permits the machine to be used while the calculations are performed.

We can follow the calculations from the command **less**, thus the calculation can be followed in real time. At the end of the *doxycycline.log* output file, we need to have the following term: "Normal termination of Gaussian 03".

With this result, begin to prepare our system for the main stage of this tutorial, the molecular dynamics simulation. To continue is necessary the conversion of *doxycycline.log* file to pdb format: the starting point for AMBER program. The command will be, as follows:

```
babel -ig03 doxycycline.log -o pdb doxycycline.pdb
```

After conversion, our next step is to edit the file *doxycycline.pdb* using a text editor. We need to withdraw all lines beginning with the term "CONNECT".

2nd Step

To start the simulation for MD, the system is prepared with the compound in aqueous solution.

Using the AMBER package some important files are generated, for example, *doxycycline.prmtop* that contains the parameters of the structure and *doxycycline.inpcrd*, the initial coordinates.

Into Amber Package exists a diverse set of solvents. For this simulation we use SPC/E water model [7] as a solvent and treated without interactions between the electronic density of atoms of the same structure.

The files that Amber package needs are obtained through three programs: antechamber, parmchk and tleap.

Antechamber is designed to build an archive of preparation for the topology of the solute [8], in this case, doxycycline. In combination with DivCon (a semiempirical QM program) calculate partial atomic charges. By default, the force field GAFF is used to describe the solute-solvent interactions, since this option is indicated on the solute with few atoms or represented by small molecule [9]. The command used by antechamber is as follows:

```
antechamber -i doxycycline.pdb -fi pdb -o doxycycline.prep -fo prep1 -c bcc
```

In this command each index means:

- i → receive input file
- fi → create a input file (.pdb)
- o → means file of the process result
- fo → format of the file of the process result
- c → indicates the type of atomic charge utilized, in this case, AM1-BCC

The *parmchk* program is a database to parameterization for the calculations of this tutorial and we utilized to create the physico-chemical parameters of solvation box [10]. Using *doxycycline.prep* as input file in the following command:

```
parmchk -i doxiciclina.prep -f prep -o doxy.frcmod
```

The last program used in the preparation of the system is *tleap*. With this program, we obtain the files of initial coordinates (*inpcrd*) and topology (*prmtop*). To open the program is necessary the command line:

```
tleap -s -f leaprc.gaff99SB
```

After opening the program other set of commands is necessary:

```
HOH=SPC  
WAT=SPC  
loadamberparams frcmod.spce  
source leaprc.gaff  
loadAmberParams doxy.frcmod  
loadAmberPrep doxy_bcc.prep  
SYS = loadPdb NEWPDB.PDB  
check SYS  
solvateBox SYS SPCBOX 13.0  
saveAmberParm SYS doxyciclyne.prmtop doxyciclyne.inpcrd  
savePdb SYS system.pdb  
Quit
```

It generates a cubic box, where are the solute and solvent molecules (Fig. 2).

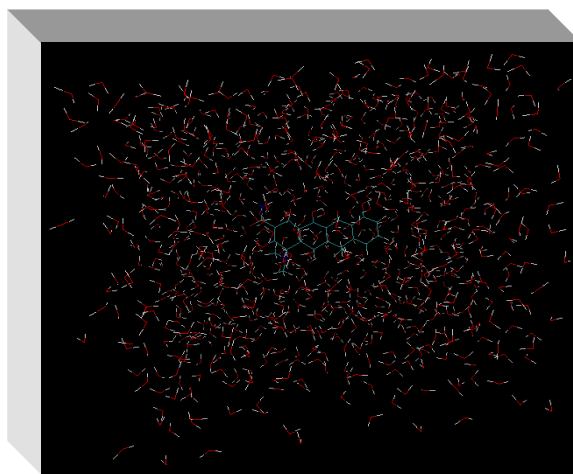


Figure 2. Cubic box with the solute and solvent molecules.

Preparation of the files to molecular dynamic simulation

Simulations using the AMBER package are divided in four steps, and taking a specific function and dependent on each other. The first and second steps are optimization geometries; the third, is MD termalization phase (increase system temperature); and, the latter is MD equilibration. Each of the steps is described below:

Step 1: We performed an energy minimization to relieve steric interactions that could interfere with the dynamics [5].

```

initial minimization with restriction
&cntrl
imin = 1, → to perform (1 = minimization, molecular dynamics = 0).
maxcyc = 30000, → maximum number of cycles
ncyc = 20000, → the logarithm becomes steepest descent conjugate gradient
ntb = 1, → boundary condition with constant volume
          ntr = 1, → restrictions to run position (1 = on, 0 = off)
cut = 10 → cutoff radius in angstroms
/
Hold the solute fixed
500.0 → strength in kcal / mol used to limit the atomic positions.
RES 1 → indicates which residues to be restricted
END
END

```

Scheme 1. Data founded in file *min_1.in* (Step 1).

Step 2: Minimization of the system as a whole, without restrictions [5].

```

Unrestrained minimization
&cntrl
imin = 1,
maxcyc = 25000,
ncyc = 20000,
ntb = 1,
ntr = 0,
cut = 10
/
END

```

Scheme 2. Data founded in file *min_2.in* (Step 2).

Step 3: Restrict Position MD and termalization step. This calculation is carried out starting position to relax the molecules of solvent around solute and heat the system to target temperature. The movements of doxycycline are restricted, so a force is applied in order to maintain the its positions. The relaxation time of the solvent for water is about 10 ps, so should perform at least another 10 ps of dynamics to relax the solvent [5].

25ps MD with position restrained on doxycycline

```

&cntrl
imin = 0,
irest = 0, → 0 = without effect condition to restart the calculation (default)
ntx = 1, → 1= to read the initial coordinates from the file "inpcrd"
ntb = 1,
cut = 10,
ntr = 1,
ntc = 2, → 2=hydrogens bonds are contained
ntf = 2, → 2=hydrogen bonds are omitted in the calculations
tempi = 0.0, → initial temperature of the system
temp0 = 298.0, → equilibrium temperature of the system
ntt = 3, → thermostat scale (1 = Langevin Dynamics)
gamma_ln = 1.0, → collision frequency in ps-1 when ntt = 3
nstlim = 12500, dt = 0.002, → simulation time:n° steps multiplied by integration time
ntpr = 100, ntwx = 500, ntwr = 1000 → the calculated coordinates are archived
/
Keep solute fixed with weak restraints
10.0
RES 1
END
END

```

Scheme 3. Data founded in file *md_1.in*. (Step 3).

Step 4: MD equilibration, without restriction, at desired temperature, should be used 2,000 ps [5]. This value was taken to be only an example for the tutorial.

```

298K constant temp MD
&cntrl
imin=0,
ntb=1,
ntx=5, → 5= to read the initial coordinates from the file "mdcrd"
irest=1, → 1= with effect condition to restart the calculation (default)
cut=10.0,
ntc=2,
ntf=2,
tempi=298.0, → the indicated temperature at end of file md1.out
temp0=298.0,
ntt=3,
gamma_ln=1.0,
nstlim=1000000, dt=0.002,
ntpr=500, ntwx=500,
/
END

```

Scheme 4. Data founded in file *md_2.in*. (Step 4).

We performed the molecular simulation in all steps (energy minimization and molecular dynamics) for the classical force field. This method contains his theory based on molecular mechanics, without taking into account the effect of electronic density

between the atoms of the molecule.

In the case of laboratory have a computational cluster (two or more computers working together to perform a heavy process), should be execute the commands of calculations using the program itself a cluster of computers: **qsub**.

But it becomes necessary to create files to indicate the number of processors to be used and the type of calculation made by the cluster, the following are those along the line of command:

1) *File name: amber_1.qsub*

```
#PBS -N min_1
#PBS -q eternity
#PBS -l nodes=1:ppn=8
cd $PBS_O_WORKDIR
mpiexec sander.MPI -O -i min_1.in -o min1.out -p doxiclina.prmtop -c
doxiciclina.inpcrd -r doxiciclina_min1.rst -ref doxiciclina.inpcrd
```

Command line: *qsub amber_1.qsub*

2) *File name: amber_2.qsub*

```
#PBS -N min_2
#PBS -q eternity
#PBS -l nodes=1:ppn=8
cd $PBS_O_WORKDIR
mpiexec sander.MPI -O -i min_2.in -o min2.out -p doxiclina.prmtop -c doxiciclina_min1.rst -r
doxiciclina_min2.rst
```

Command line: *qsub amber_2.qsub*

3) *File name:amber_3.qsub*

```
#PBS -N md_1
#PBS -q eternity
#PBS -l nodes=1:ppn=8
cd $PBS_O_WORKDIR
mpiexec sander.MPI -O -i md_1.in -o md_2.out -p doxiclina.prmtop -c doxiciclina_min2.rst -r
doxiciclina_md1.rst -x doxiciclina_md1.mdcrd -ref doxiciclina_min2.rst -inf md1.inf
```

Command line: *qsub amber_3.qsub*

4) *File name: amber_4.qsub*

```
#PBS -N md_2
#PBS -q eternity
#PBS -l nodes=1:ppn=8
cd $PBS_O_WORKDIR
mpiexec sander.MPI -O -i md_2.in -o md_2.out -p doxiclina.prmtop -c doxiciclina_md1.rst -r
doxiciclina_md2.rst -x doxiciclina_md2.mdcrd -ref doxiciclina_md1.rst -inf md2.inf
```

Command line: `qsub amber_4.qsub`

In this case, it is necessary to create files to indicate the number of processors that should be used and the type of calculation performed by clusters.

If there are any problems with the laboratory and the calculation, it does not finish as expected, the work done is not lost, you can restart the process from where it left off, publishing a new input file, creating from output file (.rst) in a new input file (.in) using the time necessary to complete the calculation.

ANALYSIS OF DATA OBTAINED BY COMPUTER SIMULATION

Radial Distribution Function $g(r)$

Radial distribution function describes how the density of surrounding matter varies according to a separate point and takes into account the correlations in the distribution of molecules, which arise from the forces they exert on each other [11]:

To start the study of $g(r)$ is necessary to choose which atoms are involved and interacting systems. In this case the region was chosen because of the amide can occur a possible formation of internal hydrogen bonds and solvent molecules.

It is possible to study how the hydrogen atoms of water molecules distribute themselves around the nitrogen atom belonging to the amide group. For this the program will be used and will use the file *rdf.in*:

```
trajin doxiciclina_md1.mdcrd
trajin doxiciclina_md2.mdcrd
radial HOH1.rdf 0.1 15.0 :WAT@H1:LIG1@N
radial HOH2.rdf 0.1 15.0 :WAT@H2:LIG1@N
```

Will run the following command:

```
ptraj doxiciclina.prmtop < rdf.in
```

Two graphical data files are generated, but for analysis we must use only those

with the word "standard" in the name and generate a graphic (Fig. 3) and run the following command using the WYSIWYG 2D plotting tool xmgrace. [12]

```
xmgrace HOH1.rdf_standard.xmgr HOH2.rdf_standard.xmgr
```

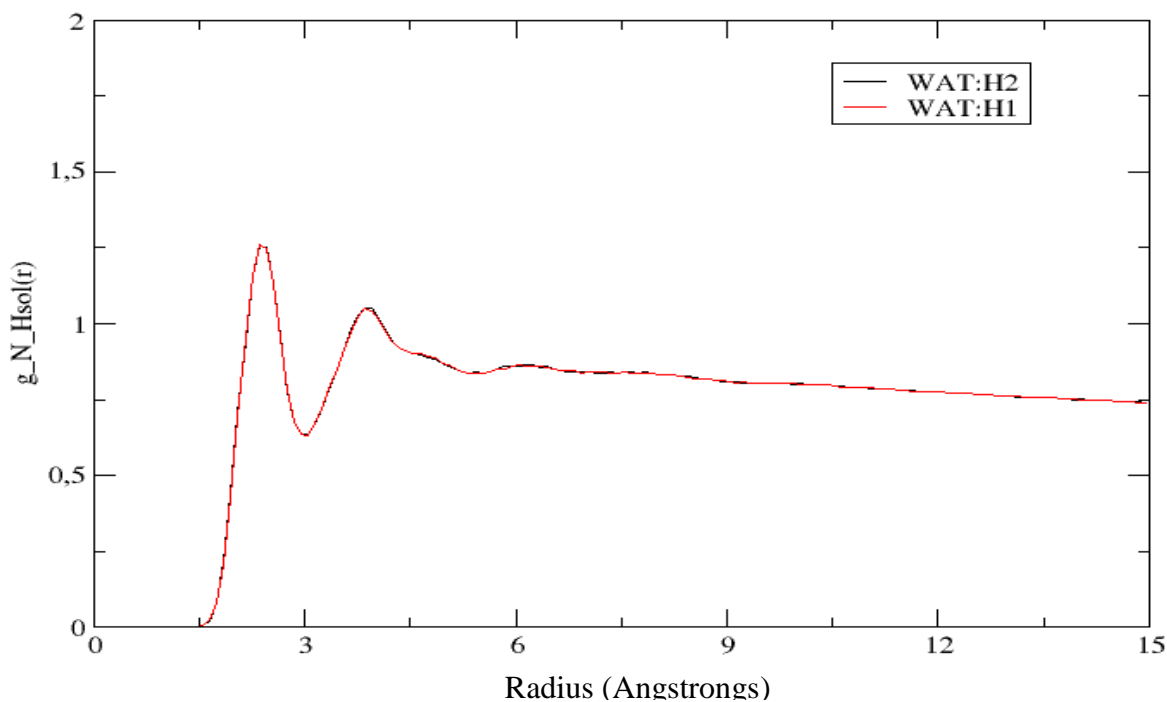


Figure 3. Graphic showing the density distribution of the hydrogen atoms around the nitrogen.

The results offered as occurred in the solvent-solute interactions in the chosen region.

Number of hydrogen bonds

Hydrogen bonds are the key to many phenomena, including the formation and stabilization of secondary structures. Therefore, it is important that the geometry of hydrogen bonds are incorporated as accurately as possible in potential energy functions.

In theoretical chemistry, the study of the number of hydrogen bonds formed by molecular dynamics simulations provides a statistical analysis of the stability of each such interaction. The parameter to be analyzed is the percentage of occupancy (% occupancy) of each, since the stable are those with index up to fifty percent (> 50%). In summary the greater the numerical value of the percentage, the better [13].

The solute-solvent interaction type hydrogen bond between the hydrogens of the water and nitrogen of the amide group can be study, we must use the hbonds.in file:

```
trajin doxiciclina_md1.mdcrd
```

```
trajin doxiciclina_md2.mdcrd
donor LIG1 N N1
acceptor WAT H1 H2
hbond distance 3.0 angle 120 solventneighbor 6 donor LIG1 N N1 acceptor WAT H1 H2 series
hbond
```

Will run the following command:

```
ptraj doxiciclina.prmtop < hbonds.in
```

In this case there was an interaction that lasted long enough to be noticed

3.3 Root-mean-square deviation (RMSD)

This analysis is a major tool of molecular dynamics simulations. It is possible to study the stability, balance and flexibility of the system [14, 15].

There is a link between the number of atoms and the elevation and index RMSD is independent of choosing atoms participate in this analysis. To view this file (fig. 4), we must create and edit file rmsd.in, as below:

```
trajin doxiciclina_md1.mdcrd
trajin doxiciclina_md2.mdcrd
rms first out doxiciclina_rms.dat :1-56 time 1.0
```

Will run the following commands:

```
ptraj doxiciclina.prmtop < rmsd.in
xmgrace doxycycline_rms.dat
```

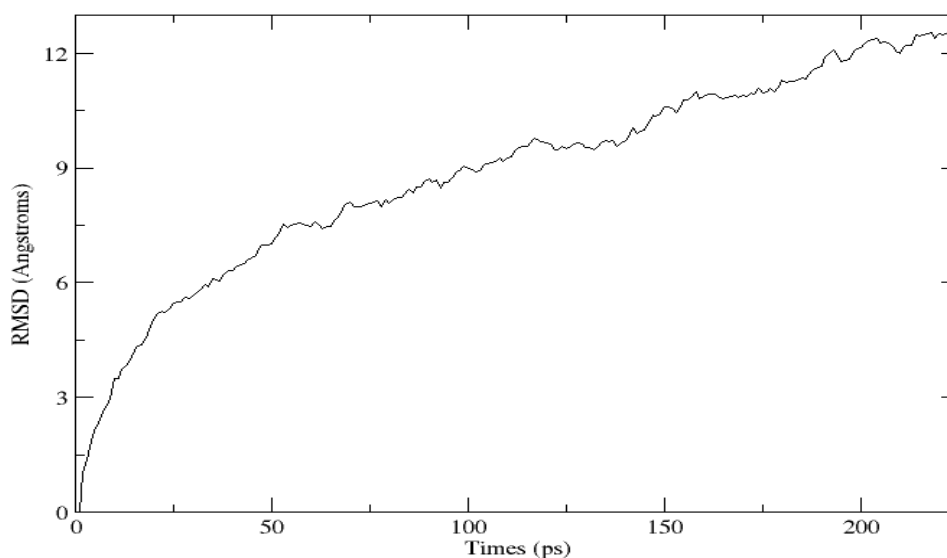


Figure 4. Graphic showing the RMSD data.

Conclusion

We presented a tutorial explaining how to conduct computational simulations for solute-solvent systems by MD. In particular, we addressed the computational resources of the AMBER package. Additionally, we explained how to perform some analysis on the use of this very common computational technique. Thus, we believe that the information given in this work can assist beginners in the application of MD in their computational studies.

Acknowledgments

The authors thank to the Fundação de Amparo à Pesquisa do Estado de Mato Grosso do Sul (FUNDECT) for financial support of this research, the Coordenação de Aperfeiçoamento de Pessoal de Nível Superior (CAPES) for scholarship to R.S.G. (PNPD 022/2012) and for a fellowship to M.V.R.G., the Conselho Nacional de Desenvolvimento Científico e Tecnológico (CNPq) for a fellowship to W.N.M. .

References and Notes

- [1] Case, D. A.; Darden, T. A.; Cheatham III, T. E.; Simmerling, C. L.; Wang, J.; Duke, R. E.; Luo, R.; Merz, K. M.; Pearlman, D. A.; Crowley, M.; Walker, R. C.; Zhang, W.; Wang, B.; Hayik, S.; Roitberg, A.; Seabra, G.; Wong, K. F.; Paesani, F.; Wu, X.; Brozell, S.; Tsui, V.; Gohlke, H.; Yang, L.; Tan, C.; Mongan, J.; Hornak, V.; Cui, G.; Beroza, P.; Mathews, D. H.; Schafmeister, C.; Ross, W. S.; Kollman, P. A. *AMBER 9*, **2006**, University of California, San Francisco.
- [2] Wang, J.; Wolf, R. M.; Caldwell, J. W.; Kollman, P. A.; Case, D. A. *J. Comp. Chem.* **2004**, *25*, 1157. [[CrossRef](#)]
- [3] Ramakrishna, R.; Huang, Y.; Abubucker, S.; Heinz, M.; Crosby, S. D.; Mitreva, M.; G. J. Weil, *J. Biom. Sci.* **2012**, *19*, 21. [[Link](#)]
- [4] Hassinen, T.; Peräkylä, M. *J. Comput. Chem.* **2001**, *22*, 1229. [[Link](#)]
- [5] Frisch, M. J.; Trucks, G. W.; Schlegel, H. B.; Scuseria, G. E.; Robb, M. A.; Cheeseman, J. R.; Montgomery, J. A.; Junior, T. V.; Kudin, K. N.; Burant, J. C.; Millam, J. M.; Iyengar, S. S.; Tomasi, J.; Barone, V.; Mennucci, B.; Cossi, M.; Scalmani, G.; Rega, N.; Petersson, G. A.; Nakatsuji, H.; Hada, M.; Ehara, M.; Toyota, K.; Fukuda, R.; Hasegawa, J.; Ishida, M.; Nakajima, T.; Honda, Y.; Kitao, O.; Nakai, H.; Klene, M.; Li, X.; Knox, J. E.; Hratchian, H. P.; Cross, J. B.; Bakken, V.; Adamo, C.; Jaramillo, J.; Gomperts, R.; Stratmann, R. E.; Yazyev, O.; Austin, A. J.; Cammi, R.; Pomelli, C.; Ochterski, J. W.; Ayala, P. Y.; Morokuma, K.; Voth, G. A.; Salvador, P.; Dannenberg, J. J.; Zakrzewski, V. G.; Dapprich, S.; Daniels, A. D.; Strain, M. C.; Farkas, O.; Malick, D. K.; Rabuck, A. D.; Raghavachari, K.; Foresman, J. B.; Ortiz, J. V.; Cui, Q.; Baboul, A. G.; Clifford, S.; Cioslowski, J.; Stefanov, B. B.; Liu, G.; Liashenko, A.; Piskorz, P.; Komaromi, I.; Martin, R. L.; Fox, D. J.; Keith, T.; Al-Laham, M. A.; Peng, C. Y.; Nanayakkara, A.; Challacombe,

- M.; Gill, P. M. W.; Johnson, B.; Chen, W.; Wong, M. W.; Gonzalez, C.; Pople, J. A. *Gaussian 03, Revision E.01*, Wallingford CT, **2004**.
- [6] Walters, P.; Stahl, M. <http://www.eyesopen.com/babel.html>.
- [7] London South Bank University, <http://www.lsbu.ac.uk/water/models.html>, login in 08/31/2012.
- [8] Case, D. A.; Darden, T. A.; Cheatham III, T. E.; Simmerling, C. L.; Wang, J.; Duke, R.; Luo, R.; Merz, K. M.; Wang, B.; Pearlman, D. A.; Crowley, M.; Brozell, S.; Tsui, V.; Gohlke, H.; Mongan, J.; Hornak, V.; Cui, G.; Beroza, P.; Schafmeister, C.; Caldwell, J. W.; Ross, W. S.; Kollman, P.A. *AMBER 8*, **2004**, University of California: San Francisco.
- [9] Barreiro, E. J.; Rodrigues, C. R. *Quím. Nova* **1997**, *20*, 300. [[CrossRef](#)]
- [10] <http://ambermd.org/antechamber/ac.html>, login in 08/31/2012
- [11] McQuarrie, D.A.; *Statistical Mechanics*, Harper Collins Publishers, **1976**.
- [12] <http://plasma-gate.weizmann.ac.il/Grace/>
- [13] Kerrigan, J. E. (Robert Wood Johnson Medical School, The University of Medicine and Dentistry of New Jersey) AMBER 9.0 Drug/DNA Complex Tutorial.
- [14] Namba, A. M.; Silva, V. B.; Silva, C. H. T. P. *Eclética Química* **2008**, *33*, 13. [[CrossRef](#)]
- [12] Salas, C.; Ene, L.; Ojeda, N.; Soto, H.; *Bosque* **2010**, *31*, 179. [[Link](#)]